

# Dynamical phase transitions in the collisionless pre-thermal states of isolated quantum systems: theory and experiments

Jamir Marino,<sup>1</sup> Martin Eckstein,<sup>2</sup> Matthew S. Foster,<sup>3,4</sup> and Ana Maria Rey<sup>5,6</sup>

<sup>1</sup>*Institut für Physik, Johannes Gutenberg-Universität Mainz, D-55099 Mainz, Germany*

<sup>2</sup>*Department of Physics, University of Erlangen-Nürnberg, 91058 Erlangen, Germany*

<sup>3</sup>*Department of Physics and Astronomy, Rice University, Houston, Texas 77005, USA*

<sup>4</sup>*Rice Center for Quantum Materials, Rice University, Houston, Texas 77005, USA*

<sup>5</sup>*JILA, National Institute of Standards and Technology,*

*and Department of Physics, University of Colorado, Boulder, CO 80309*

<sup>6</sup>*Center for Theory of Quantum Matter, University of Colorado, Boulder, CO 80309*

(Dated: January 26, 2022)

We overview the concept of dynamical phase transitions in isolated quantum systems quenched out of equilibrium. We focus on non-equilibrium transitions characterized by an order parameter, which features qualitatively distinct temporal behaviour on the two sides of a certain dynamical critical point. Dynamical phase transitions are currently mostly understood as long-lived prethermal phenomena in a regime where inelastic collisions are incapable to thermalize the system. The latter enables the dynamics to sustain phases that explicitly break detailed balance and therefore cannot be encompassed by traditional thermodynamics. Our presentation covers both cold atoms as well as condensed matter systems. We revisit a broad plethora of platforms exhibiting pre-thermal DPTs, which become theoretically tractable in a certain limit, such as for a large number of particles, large number of order parameter components, or large spatial dimension. The systems we explore include, among others, quantum magnets with collective interactions,  $\phi^4$  quantum field theories, and Fermi-Hubbard models. A section dedicated to experimental explorations of DPTs in condensed matter and AMO systems connects this large variety of theoretical models.

## CONTENTS

I. Introduction	1
II. Dynamical phase transitions and the Landau-Ginzburg paradigm	3
A. Fully-connected Ising model in transverse field	3
B. Long-range interactions	5
C. $O(\mathcal{N})$ models in the large $\mathcal{N}$ limit	5
III. Exactly solved dynamics in Richardson-Gaudin models via the Lax spectral method	8
A. BCS superfluids and Richardson-Gaudin	9
B. The Lax spectral method	10
1. Isolated roots and phases I, II, III	10
C. A simple example	12
1. Phases I and II	12
2. Quench-generated Floquet phase III	13
D. Fluctuation phenomena	14
E. Topological features	14
IV. Dynamical phase transitions in infinite dimensions	16
A. The Hubbard model in infinite dimensions	16
B. DPTs related to non-thermal symmetry breaking	17
C. DPTs between pre-thermal phases at short-time	19
V. Experimental Observation	21
A. DPTs in Condensed Matter Systems	21

## B. DPTs in Cold Atom Experiments

22

## VI. Conclusions

27

## VII. Acknowledgements

27

## References

27

## I. INTRODUCTION

Dynamical phase transitions occur whenever the observables of an isolated quantum system feature distinct qualitative temporal behavior as a function of a control parameter measuring the deviation of the system from equilibrium. In this review, we are interested in a particular class of dynamical phase transitions (DPTs) which are characterized by an order parameter that features non-analytic behavior at the non-equilibrium critical point separating distinct dynamical phases [1]. The DPTs we discuss here manifest during the so called pre-thermal stage of dynamics of a quantum many body system [2–4]. The notion of pre-thermalization is broad encompassing high energy physics and condensed matter. A system is said to pre-thermalize when its observables approach a long-lived quasi-steady state at intermediate times, before inelastic collisions set in and the system reaches thermodynamic equilibrium. In this regard, the behaviour of the order parameter witnessing the DPT will manifest after a transient where non-universal effects attributed to microscopic details of the model, such as lattice properties, or short-time inhomogeneous de-

phasing, have faded away.

Pre-thermalization is mostly studied in the context of small interaction quenches that can result in a long, perturbative, window of the dynamics, where the quasi-particles of some pre-quench integrable model are weakly deformed and still free to scatter elastically [5–11]. Interactions renormalise the energy of these excitations, and only at later times they induce inelastic processes responsible for the redistribution of energy and for the eventual equilibration. Accordingly, we will refer to pre-thermalization as a *collisionless regime*, which is a short-hand to describe that inelastic collisions are still weak and ineffective.

In order to access DPTs, one can perform quenches in Hamiltonian parameters. In the last years this is becoming accessible in AMO and to some extent also in condensed matter experiments. Up to date the main focus has been on DPTs that take place in some limit such that interactions can still be treated non-perturbatively at the expense of solving dynamics which are mean-field like, gaussian or semi-classical. The study of DPTs in this regime is the central topic of this review. We will revisit a broad plethora of systems exhibiting collisionless behaviour within a long lived pre-thermal window, enabled by taking a large intrinsic parameter in the system such as the number of particles ( $N$ ) – in Sec. II A or III B, and the number of components of a field ( $\mathcal{N}$ ) – in Sec. II C. Further, some aspects of DPTs beyond the collisionless regime can be studied in a controlled manner in limit of infinite dimensions, which is reviewed in Sec. IV.

The focus on a non-equilibrium order parameter which characterizes the DPT, distinguishes the subject of this review from the notion of dynamical transitions explored in the context of Loschmidt echoes [12–14]. We will also not review the broad topic of non-thermal fixed points in cold atoms [15–19] (see [20] for a review), which although appear akin to a pre-thermal phenomenon, exhibits a different mechanism from the large  $N$ ,  $\mathcal{N}$ , or  $d$  pre-thermal states discussed in this review.

Regarding its experimental observation, broadly speaking, non-equilibrium dynamical phases are observed in much wider contexts than their equilibrium counterparts. They are relevant for a variety of disciplines beyond AMO and condensed matter physics, including chemistry, biology and even sociology [21]. For example, non-equilibrium critical phenomena have been seen in, polymers, colloidal gels, molecular glasses and spin glasses as they are cooled down below a critical temperature, “glassy transition point,” at which the system’s evolution slows down so much that it falls out of equilibrium [1]. Lasers also show dynamical transitions, where the light emitted by an array of atoms changes abruptly from incoherent to extremely coherent when the input power (the control parameter in this case) exceeds a certain threshold [21]. Another example are liquid layers, where the heat transport changes from conduction to convection when the temperature-gradient between the

lower and the upper surfaces of the liquid is increased above a critical point [22]. Finally, different dynamical phases occur in the population dynamics or ecology when two interacting ‘kinds’ of species, the predator and the prey, start to feature a perpetual cyclic pattern when the food supply for one species is maintained at or beyond a certain limit [23]. Similar behavior is seen in chemical reactions where a chemical instability triggers oscillatory patterns in which the colour of the reactants changes periodically from red to blue and vice versa [24]. Although it is clear that in any of these situations the concepts of temperature, and thermal equilibrium, do not have a clear meaning, all of them share the fact that the familiar notion of the order parameter, introduced by Landau for a description of second order phase transitions, can be used to describe the distinct change of behavior of the system as an external control parameter is varied. This is profitable since it allows to treat disparate systems at a macroscopic level with similar concepts and mathematical tools, and allow us to make fascinating analogies between them invoking the concept of universality.

Nevertheless, a key point shared by all the systems described in the above paragraph is that they belong to the realm of non-equilibrium open systems, and therefore their dynamics are fundamentally irreversible [21]. A more restricted scenario, which is the one discussed in this review, deals with evolution under fully unitary, coherent and reversible dynamics. Under this context experimental observations of non-equilibrium phase transitions have remained more elusive. Only in the recent years new opportunities in many-body physics have been opened up thanks to the increased degree of control and ability to synthesize, manipulate, and detect ultra cold atomic systems as well as new developments in THz pump-probe experiments. The novel experimental capabilities are stimulating new methods to benchmark and understand DPTs in general, and they are leading to exciting investigations of non-equilibrium behaviors.

The review is structured as follows. In Sec. II A and Sec. III B we present the dynamics of exactly solvable fully-connected spin models in the limit of large number of spins,  $N \rightarrow \infty$ . The associated DPTs include the Ising universality class and Richardson-Gaudin magnets. In Sec. II B we discuss different dynamical behaviours associated to interactions which are not all-to-all, but decay spatially in a power law fashion. In Sec. II C, we consider the limit of large number of components ( $\mathcal{N}$ ) of a  $\phi^4$  field theory. This serves as an instructive toy model to show how Gaussian fluctuations can modify the physical picture of Secs. II A and III B. In Sec. IV we consider DPTs arising in strongly correlated systems in the large dimensionality limit  $d \rightarrow \infty$ , where an exact solution is possible within dynamical mean field theory (DMFT); interestingly the model studied in this limit exhibits ergodic behaviour and eventually thermalizes, allowing to inspect aspects of DPTs beyond pre-thermalization. Emphasis is placed on the similarities between the DPTs observed in this class of models and those discussed in

Sec. II A. Finally, Sec. V discusses the experimental platforms where DPTs have been observed from solid state to cold atoms. This section serves as further connector among the other three theory sections.

## II. DYNAMICAL PHASE TRANSITIONS AND THE LANDAU-GINZBURG PARADIGM

The Landau-Ginzburg description of thermal equilibrium phase transitions is one of the cornerstones of criticality and universality [25] in a vast plethora of systems [26] including soft matter (e.g. liquid-gas critical points), condensed matter (e.g. magnets, superfluidity, and superconductivity), as well as applications to cosmology [27]. Together with a systematic inclusion of thermal or quantum fluctuations via a renormalization group analysis, Landau-Ginzburg theory lays the foundations of critical phenomena in equilibrium statistical mechanics [28–30]. Given its success in explaining equilibrium [31] and relaxational dynamics of classical [32] and open quantum systems [33–35], it was not surprising to witness in the last decade a surge of works exploring dynamical phase transitions after a quench, which can be understood via an effective  $\phi^4$ -field theory description. Our review will therefore start considering those DPTs which possess an effective description in terms of a double well picture of the energy landscape of the underlying physical model.

We will first consider a fully connected spin model (the Lipkin-Meshkov-Glick model [36–48]) which is exactly solvable through a mean-field analysis in the thermodynamic limit (Sec. II A). Its dynamical phases can be understood using a double well picture, providing the simplest analytically tractable instance of a dynamical critical point.

In Sec. II C, we will then consider the dynamics of a field theory with an  $\mathcal{N}$ -component scalar order parameter [28], which in the  $\mathcal{N} \rightarrow \infty$  limit admits an exact solution in terms of Gaussian fluctuations self-consistently coupled to the motion of the order parameter. The leading  $1/\mathcal{N}$  correction controls non-integrable scattering among different modes and therefore the disappearance of the pre-thermal plateau where the DPT of the field theory can occur. This is analogous to the effect of  $1/N$  corrections (where now  $N$  is the system size) on the DPTs of LMG and Richardson models discussed in Secs. II A and III, and it merges with the unifying theme of this review: DPTs occur in collisionless non-equilibrium states of dynamics [3–5, 7, 27, 49–52]. When collisions due to non-linearities set in, these pre-thermal states are destabilized and the system is attracted towards a thermal fixed point where only equilibrium phase transitions can occur (if permitted by dimensionality and symmetries). A further example of this phenomenology will be provided in Sec. IV, where DPTs are obtained in strongly correlated systems through an exact dynamical mean field treatment valid in the  $d \rightarrow \infty$  limit (here  $d$  are the physical

dimensions).

### A. Fully-connected Ising model in transverse field

In this section, we consider a class of quantum Ising systems with spins  $s$  on a  $d$ -dimensional lattice, interacting via a ferromagnetic coupling,  $J_{|\mathbf{r}-\mathbf{r}'|}$ , and subject to a transverse magnetic field pointing along the  $z$  direction

$$H = - \sum_{\mathbf{r}, \mathbf{r}'} J_{|\mathbf{r}-\mathbf{r}'|} \hat{\sigma}_{\mathbf{r}}^x \hat{\sigma}_{\mathbf{r}'}^x - g \sum_{\mathbf{r}} \hat{\sigma}_{\mathbf{r}}^z. \quad (1)$$

Here the sums run over  $r = 1, 2, \dots, N$ , with  $N$  the total system size. In Eq. (1),  $\hat{\sigma}_{\mathbf{r}}^\alpha$  are the operators corresponding to the normalized spin components in the  $\alpha = x, y, z$  direction. For concreteness we consider in the following the  $s = 1/2$  case, although most of the results remain qualitatively unchanged for arbitrary spin length  $s$ . The parameter  $g$  is the Larmor frequency induced by the transverse field. This class of systems is of importance for experimental realizations of DPTs in trapped ions [54], cavity QED systems [55], and neutral atoms arrays [56], as we discuss in Sec. V.

For all-to-all interactions  $J_{|\mathbf{r}-\mathbf{r}'|} = \lambda/N$ , for all  $\mathbf{r}, \mathbf{r}'$ , the Hamiltonian in Eq. (1) corresponds to the infinite-range or fully-connected Lipkin-Meshkov-Glick (LMG) model [36–48]

$$\hat{H} = - \frac{\lambda}{N} \sum_{i,j=1}^N \hat{\sigma}_i^x \hat{\sigma}_j^x - g \sum_{i=1}^N \hat{\sigma}_i^z, \quad (2)$$

where each of the  $N$  spins interacts with all the others with the same ferromagnetic coupling strength  $\propto \lambda$ . The  $1/N$  scaling of the coupling  $\lambda$  in Eq. (2) is adopted to make the energy extensive in the thermodynamic limit (notice that this scaling is not always satisfied in experimental implementations, e.g. cavity QED systems, see Sec. V). As  $N \rightarrow \infty$  the mean-field approximation becomes exact for the Hamiltonian (2), and therefore the model is solvable in the thermodynamic limit: the properly normalized commutation relations of these collective spin operators,  $\hat{\sigma}^\alpha \equiv \sum_{i=1}^N \hat{\sigma}_i^\alpha / N$ , approach the classical limit for  $N \rightarrow \infty$ . In fact, these operators have a spectrum in  $[-1, 1]$  and they satisfy

$$[\hat{\sigma}^\alpha, \hat{\sigma}^\beta] = \frac{1}{Ns} i \epsilon^{\alpha\beta\gamma} \hat{\sigma}^\gamma, \quad (3)$$

which can be used to define an effective Planck's constant  $\hbar_{\text{eff}} \equiv (N/2)^{-1}$ . This property is instrumental to investigate the corrections to the  $N \rightarrow \infty$  limit via a semi-classical expansion in inverse powers of  $N$ . Such corrections include [53] wavepacket spreading with deviations from the classical trajectory on Ehrenfest time scales  $\propto \mathcal{O}(\sqrt{N})$ , recurrences on times  $\sim \mathcal{O}(N)$  and tunnelling events between the two ferromagnetic minima on time scales  $\propto \mathcal{O}(e^{cN})$ .

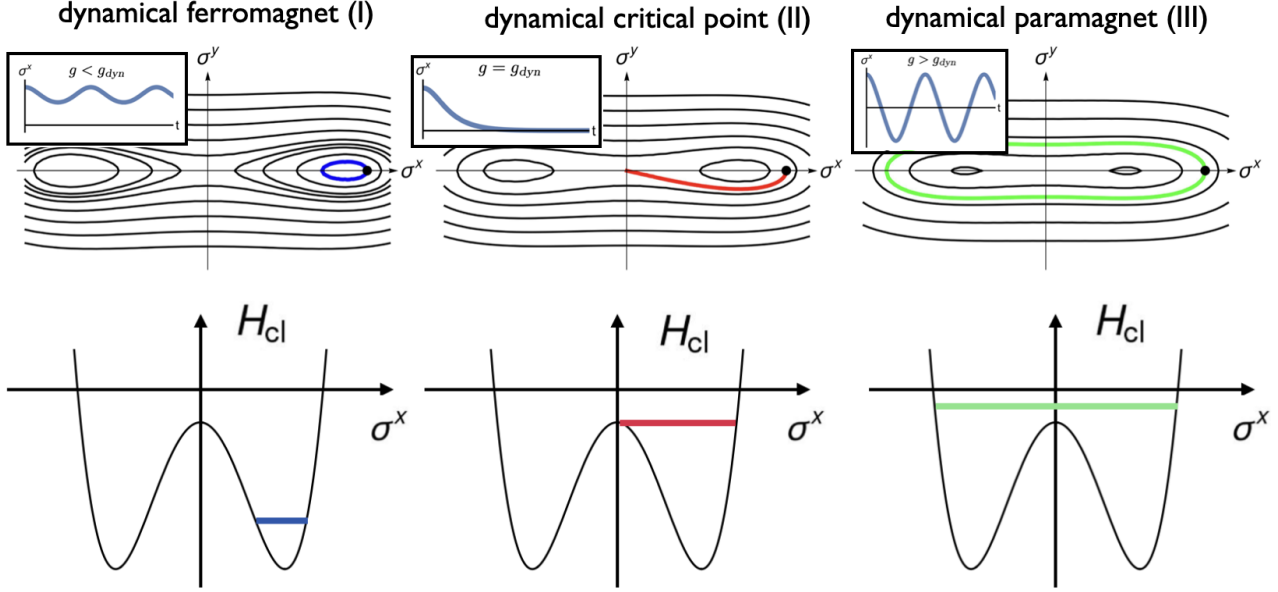


FIG. 1. Upper row: Quantum quench of the transverse field in the LMG model: dynamical ferromagnetism (I) with oscillations around a non-vanishing value of  $\sigma^x$ ; critical relaxation (II) at the dynamical critical point; dynamical paramagnetism (III) with persistent oscillations around a zero mean value. Lower row: energy  $H_{cl}$  of the collective classical spin configuration,  $\vec{\sigma}$ , as a function of the magnetization  $\sigma^x$ . For the dynamical ferromagnet the energy of the initial state (cf. main text) is not sufficiently large to escape the minima of the potential (blue line); for the paramagnetic phase the energy is above the double-well barrier (green line), and therefore the orbit of the magnetization can encircle both minima and average out to zero over long time windows. The figure is adapted from Ref. [53].

From Eq. (3), it results that, for  $N \rightarrow \infty$ , the model can be exactly solved in terms of a classical, continuous spin  $\vec{\sigma}$  of normalized length  $\rho$ , by neglecting the above mentioned finite  $N$  effects which require exact diagonalization or a semi-classical approximation to be observed [57]. The three-dimensional vector  $\vec{\sigma} = \rho(\sin \theta \cos \varphi, \sin \theta \sin \varphi, \cos \theta)$  is a classical spin whose phase space is the surface of a Bloch sphere of radius  $0 < \rho \leq 1$ , with polar,  $\theta$ , and azimuth angles,  $\varphi$ . The LMG model then reduces to the classical Hamiltonian

$$\begin{aligned} \mathcal{H}_{cl}(\vec{\sigma}) &= -\lambda(\sigma^x)^2 - g\sigma^z = \\ &= -\lambda\rho^2 \sin^2 \theta \cos^2 \varphi - g\rho \cos \theta. \end{aligned} \quad (4)$$

For ferromagnetic interactions the system exhibits an equilibrium zero-temperature phase transition from a paramagnetic ground state with  $\langle \hat{\sigma}^x \rangle = 0$  for  $g > g_{cr} \equiv 2\lambda$ , to a pair of ferromagnetic ground states with  $\langle \hat{\sigma}^x \rangle_{\pm} = \pm m \neq 0$  for  $g < g_{cr}$ , characterized by the spontaneous breaking of the  $\mathbb{Z}_2$ -symmetry. These two ferromagnetic minima can be derived from the Bloch sphere representation of Eq. (4) and they are given by  $(\theta^*, \varphi = 0)$  and  $(\theta^*, \varphi = \pi)$  with  $\cos \theta^* = g/g_{cr}$ . Accordingly, the value of the order parameter is  $\sigma^x = \pm \rho \sin \theta^* = \pm \rho \sqrt{1 - (g/g_{cr})^2}$ , where we have kept  $\rho$  fixed since the total spin length of the system is conserved.

The associated classical energy landscape of the collective spin  $\vec{\sigma}$  (along the plane  $\sigma^y = 0$ ) is portrayed

in Fig. 1 as a function of the magnetization  $\sigma^x$  for the ferromagnetic phase  $g < g_{cr} = 2\lambda\rho$ . At equilibrium and in the thermodynamic limit, the degenerate ground state wave-functions of the collective spin are localized at the two classical minima respectively, and  $\vec{\sigma}$  behaves like a classical particle at rest at the bottom of one of the two wells.

DPTs in the LMG model have been studied extensively in the last decades [58–65]. We now overview the dynamical phase diagram summarized in Fig. 1, primarily following Ref. [53] for the sake of concreteness. The non-equilibrium evolution of  $\langle \vec{\sigma}_i(t) \rangle$  is given by the classical equations of motion associated to the Hamiltonian in Eq. (4),  $\dot{\sigma}^\alpha = \{\sigma^\alpha, \mathcal{H}_{cl}\}$ , where the evolution is given in terms of Poisson brackets.

We prepare the spin chain in a ferromagnetic ground state of the Hamiltonian Eq. (4) with transverse field  $g_0 < g_{cr} = 2\lambda\rho$ . This choice of initial state is instrumental to illustrate the archetypal features of the dynamical phase diagram, and it corresponds to a quantum quench of the transverse field  $g$ . We prepare the spin chain in the ground state of the hamiltonian  $H(g_0)$  at  $t = 0$ , and then abruptly vary the transverse field up to the value  $g$  so that the evolution at times  $t > 0$  would occur under the Hamiltonian  $H(g)$ .

For a quench,  $H(g_0) \rightarrow H(g)$ , with  $g < g_{dyn} \equiv (g_0 + g_{cr})/2$ , the energy of the system remains below the

barrier that separates the two ferromagnetic sectors. Indeed, the value of  $g_{\text{dyn}}$  can be determined [61, 66] by equating the energy of the initial state with the height of energy 'hill' separating the two minima in Fig. 1. Correspondingly, the spin will precess within the starting ferromagnetic sector (trajectory I in Fig. 1). As the strength of the quench increases, the precession period increases, until for  $g \rightarrow g_{\text{dyn}}$  it takes an infinite time to complete one cycle, and the unstable point at the top of the energy barrier is approached exponentially (trajectory II in Fig. 1). For deep quenches above this threshold,  $g > g_{\text{dyn}}$ , the energy of the system is larger than the energy barrier separating the two minima of the double well. The orbit of the collective spin encircles both minima, such that the symmetry is restored after taking time-averages, and the average magnetization,  $\overline{\sigma^x}$ , vanishes (trajectory III in Fig. 1). Indeed, the time-average

$$\overline{\sigma^x} = \lim_{T \rightarrow \infty} \frac{1}{T} \int_0^T dt \sigma^x(t), \quad (5)$$

as a function of the post quench value, acts as a dynamical order parameter, and it vanishes abruptly at the dynamical critical value  $g_{\text{dyn}}$ .

This dynamical critical point therefore separates a *dynamical ferromagnetic phase* with  $\overline{\sigma^x} \neq 0$  from a *dynamical paramagnetic phase* with  $\overline{\sigma^x} = 0$ . The singularity of the equilibrium order parameter upon approaching the critical point is algebraic,  $\overline{\sigma^x} \sim (g_{\text{dyn}} - g)^\beta$ , with critical exponent  $\beta = 1/2$ ; on the contrary, the non-equilibrium order parameter  $\overline{\sigma^x}$  discussed here displays a logarithmic singularity at the dynamical critical point.

Similar dynamical mean-field pictures hold also for infinite dimensional Bose-Hubbard systems [61], Jaynes-Cummings hamiltonians [61], or for the evolution of classical  $\phi^4$ -field theories [67, 68] (see also the following Section II C). The DPTs occurring in these models can be all explained with a classical cartoon for their energy landscape after a quench, as done here for the LMG model. In Section II C, we review a model where the effects of Gaussian fluctuations on top of the evolution of a classical order parameter are instead crucial to characterize the onset of the DPT.

## B. Long-range interactions

DPTs beyond the exact mean-field behaviour of the LMG model can be also inspected considering long-range couplings  $J_{|\mathbf{r}-\mathbf{r}'|} \propto |\mathbf{r}-\mathbf{r}'|^{-\alpha}$  in Eq. (1) (see Refs. [69, 70]). For  $\alpha \leq 3$ , the model describes, for instance, trapped ions simulators (cf. Sec. V for experimental observations of the DPT in a chain of trapped ions with  $0.8 \lesssim \alpha \lesssim 1$ ). The resulting non-equilibrium phase diagram can be derived using a MPS time-dependent variational principle [71]. Equipped with long-range interactions, the quantum spin model in Eq. (1) interpolates from the LMG limit ( $\alpha = 0$ ) to the short-range Ising model in

transverse field ( $\alpha \rightarrow \infty$ ), and it therefore offers a precious angle to analyze the interplay of dimensionality and interactions range in the formation of a dynamical critical point [72–78] (see also Sec. IV in this regard). In particular, the authors of Ref. [69] have considered dynamics in one dimension starting from a fully polarized state along the  $\hat{x}$ -direction, unveiling a DPT for all values of  $\alpha \leq 2$ . This critical value of  $\alpha$  is the same for supporting a thermal phase transition in equilibrium long-range interacting spin chains [45, 79–81]. An important difference with the LMG case, stands in the fact that the model is now not integrable, neither can its dynamics be mapped to classical equations of motion. As a consequence, the order parameter decays because of inhomogeneous dephasing [82–84] towards a vanishing or non-vanishing expectation value depending on the dynamical phase (paramagnetic or ferromagnetic), rather than exhibiting long-lived orbits as in the LMG model. This is a generic feature expected for quantum many-body systems whose dynamics cannot be simply described with the motion of a collective mode. Once again in agreement with the statistical mechanics of equilibrium long-range systems [45, 79–81], the order parameter decays always to zero for  $\alpha > 2$ , regardless of the post quench values of  $g$ , since the critical point flows into the universality class of short-range Ising chains. This is consistent with the expectation that a one dimensional model cannot support a phase transition at finite energy density, regardless where this results from a temperature or from the energy injected with a quantum quench [85].

Furthermore, for  $\alpha < 1$ , the order parameter acquires again the persistent oscillatory behaviour if the thermodynamic limit is taken before the long-time asymptotics. This is again explained by recalling that long-range Ising models with  $\alpha < 1$  fall into the universality class of the LMG model [45, 79–81]. It is therefore in the window  $1 < \alpha < 2$  that a genuine quantum many body dynamical transition is observed. Upon changing the dimensionality, these two thresholds are expected to change with the qualitative picture remaining unaltered.

Interestingly, dynamical transitions monitored by the cusps of the Loschmidt echo occur at any  $\alpha$  (cf. Ref. [69]), showing that these two notions of dynamical criticality describe qualitatively different physics.

This section finds its natural experimental counterpart in Sec. V where realizations of DPTs in long-range interacting systems are discussed in detail.

## C. $O(\mathcal{N})$ models in the large $\mathcal{N}$ limit

In this Section we discuss a prototypical example illustrating the richness of non-equilibrium phase transition of isolated systems beyond mean-field. The model we review allows for an exact treatment of quantum fluctuations. It is furthermore iconical as it deals with the quantum dynamics of a Landau-Ginzburg theory, and it might therefore offer a prototypical model for DPTs in

more complex non-integrable quantum many-body systems. We consider a  $\mathcal{N}$ -component bosonic order parameter  $\hat{\Phi} = (\hat{\phi}_1, \hat{\phi}_2, \dots, \hat{\phi}_{\mathcal{N}})$  in  $d$  spatial dimensions, with an  $O(\mathcal{N})$ -invariant Hamiltonian [28]

$$\hat{H}(r, u) = \int d^d \mathbf{x} \left[ \frac{1}{2} \hat{\Pi}^2 + \frac{1}{2} (c \nabla \hat{\phi})^2 + \frac{r}{2} \hat{\phi}^2 + \frac{u}{4! \mathcal{N}} (\hat{\phi}^2)^2 \right], \quad (6)$$

where  $\hat{\Pi} = \partial_t \hat{\Phi}$  is the  $\mathcal{N}$ -component momentum canonically conjugated to  $\hat{\Phi}$ , and  $r$  and  $u$  parametrise respectively the mass term and the strength of the non-linearity (for quantum quenches of fermionic variants of this model in the context of DPTs, see Refs. [86, 87]). The requirement of invariance under rotations of the  $O(\mathcal{N})$  group is the reason for the appearance of scalar products only,  $\hat{\Pi}^2$  and  $\hat{\phi}^2 = \hat{\Phi} \cdot \hat{\Phi} = \sum_{i=1}^{\mathcal{N}} \hat{\phi}_i^2$ , in the Hamiltonian (6). The field theory in Eq. (6) is customarily taken as an effective continuum description of a microscopic model [85] (with spin, fermionic or bosonic degrees of freedom) and it therefore requires an ultraviolet momentum cutoff  $\Lambda$ , which is usually the inverse of the lattice spacing. Upon varying  $\mathcal{N}$ , Eq. (6) describes the Ising ( $\mathcal{N} = 1$ ) and Heisenberg ( $\mathcal{N} = 3$ ) models, or the Bose-Hubbard at the particle-hole symmetric point ( $\mathcal{N} = 2$ ), to mention a few [85].

The success in modeling dynamical phase transitions with the field theory (6) resides in a closure at the Gaussian level of its hierarchy of equations of motion. Specifically, at  $\mathcal{N} \rightarrow \infty$  the evolution of the state of the  $O(\mathcal{N})$  model is fully characterized by the dynamics of the two point functions self-consistently coupled to the evolution of  $\langle \hat{\Phi} \rangle$ , with higher order correlation functions parametrically suppressed in powers of  $1/\mathcal{N}$ . The large- $\mathcal{N}$  limit has allowed to extrapolate several qualitative features of the equilibrium thermal phase diagram of the  $O(\mathcal{N})$  model to finite values of  $\mathcal{N}$  and  $d$  (see [28, 85]). Specifically, in the limit  $\mathcal{N} \rightarrow \infty$ , quartic interactions in Eq. (6) decouple at leading order which amounts to the formal substitution  $(\hat{\phi}^2)^2 \sim \langle \hat{\phi}^2 \rangle \hat{\phi}^2$ . In field theoretical language this corresponds to a Hartree-Fock approximation [88, 89]. Here, we have used the fact that, if the  $O(\mathcal{N})$  symmetry of the initial state is not broken, the average  $\langle \hat{\phi}_a \hat{\phi}_b \rangle$  of two generic components of  $\hat{\Phi}$  vanishes unless  $a = b$ . Its non-vanishing value is independent of  $a$  and equal to the fluctuation  $\langle \hat{\phi}^2 \rangle$  of a generic component of the field.

In diagrammatic language, the large- $\mathcal{N}$  limit amounts to retaining only tadpole corrections to  $r$  and ‘candy’ (RPA) diagram corrections to  $u$  [90]. The dynamics of the field components are therefore equivalent to a time-dependent quadratic Hamiltonian with an effective mass,  $r_{\text{eff}}(t)$ , to be self-consistently determined from the expectation value of  $\langle \hat{\phi}^2 \rangle$  (see Eq. (7) below). The model becomes then exactly solvable via a time-dependent self-consistent Gaussian ansatz. The large- $\mathcal{N}$  expansion allowed the authors of Refs. [67, 88, 89, 91–95] to disregard thermalizing collisions that are effective at times parametrically large in  $\mathcal{N}/u^2$ , and which dictate equili-

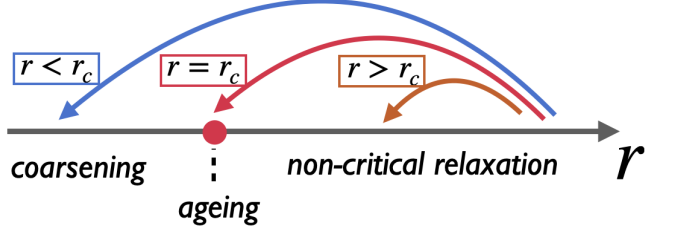


FIG. 2. Sketch of the dynamical phases of the  $O(\mathcal{N} \rightarrow \infty)$  model resulting from a quench with large initial mass ( $r_0 \gg \Lambda^2$ ). The system is quenched above ( $r > r_c$ ), at ( $r = r_c$ ), or below ( $r < r_c$ ) the dynamical critical point; in the latter case dynamics display ageing. This dynamical critical point separates non-critical relaxation (a dynamically disordered phase) from coarsening (a dynamically ordered phase).

bration. DPTs emerge in such a collisionless pre-thermal regime [3, 4, 27, 96] (cf. with Sec. II), as we will also emphasize later in Sec. III.

The typical quench protocol used to probe the dynamical phase diagram of this model consists in preparing the system in the ground state of the non-interacting Hamiltonian  $\hat{H}(r_0, 0)$ , and then letting the dynamics evolve with  $\hat{H}(r, u)$  at later times. Exact solvability in the  $\mathcal{N} \rightarrow \infty$  limit allows us to elucidate the role of fluctuations in the formation of the dynamical critical point. The time-dependent effective mass,  $r_{\text{eff}}(t)$ , dressed by Gaussian fluctuations reads

$$r_{\text{eff}}(t) = r + \frac{\mathcal{N} + 2}{6\mathcal{N}} u \int \frac{d^d p}{(2\pi)^d} \langle \hat{\phi}_{\mathbf{p}}(t) \hat{\phi}_{-\mathbf{p}}(t) \rangle. \quad (7)$$

with  $\hat{\phi}_{\mathbf{p}}$  the Fourier transform of the field. The right hand side of Eq. (7) reaches a steady state value as a result of inhomogeneous dephasing of the oscillating factors with frequencies depending on the momenta  $\mathbf{p}$  in the integrand. When the post-quench value of the mass  $r$  is tuned to a critical value  $r_c(r_0, u)$  such that it cancels the contribution from the fluctuations integral in (7), the stationary value of the effective mass  $r^* \equiv r_{\text{eff}}(t \rightarrow \infty)$  vanishes and, consequently, the spatial correlation length  $\xi = (r^*)^{-1/2}$  diverges, thus signalling the onset of a dynamical critical point. Following Ref. [93], we can evaluate the behaviour of the effective asymptotic mass  $r^*$  for small deviations in the post-quench value,  $\delta r$ , from the dynamical critical point  $r_c$ , finding

$$r^* = \delta r - \frac{u}{24} r^* \int_0^\Lambda \frac{p^{d-3} dp}{(2\pi)^d} \frac{(p^2 + r_0)^{1/2}}{(p^2 + r^*)}, \quad (8)$$

with  $\Lambda$  the ultraviolet momentum cutoff, typically related to inverse lattice spacing of the microscopic model from which the field theory is derived. For  $d > 4$  the integral in Eq. (8), which encodes the role of fluctuations, converges upon tuning  $r^* \rightarrow 0$  (close to criticality). For  $2 < d < 4$  the integral is instead the leading term, implying the scaling  $r^* \sim (\delta r)^{2/(d-2)}$ . This yields a correlation length  $1/\xi^* \sim \sqrt{r^*}$ , with a static critical exponent

$\nu = 1/(d - 2)$ . For  $d \geq 4$  we find the mean field exponent  $\nu = 1/2$  since, as we just discussed, fluctuations are RG irrelevant. This upper and lower critical dimension for the DPT of the  $O(\mathcal{N} \rightarrow \infty)$  model are the same for thermal equilibrium thermal phase transitions [85, 96]. Although Eqs. (7) and (8) are structurally analogous to equilibrium thermal transitions, the fluctuation corrections to the bare mass are quantitatively different, resulting in a different location for the critical point in the thermal and non-equilibrium cases.

In order to explore the nature of the different dynamical phases, we assume to prepare the system with a given initial mass,  $r_0$ , and consider different post quench values of  $r$ . We will focus in the following on the asymptotic  $t \rightarrow \infty$  value of the effective mass,  $r^*$ , on its real-time scaling features and on momentum-resolved correlation functions. Fig. 2 provides a graphical summary of the three dynamical phases and of their properties. We will be primarily following Ref. [89] in our exposition.

(i) For  $r > r_c(r_0, u)$ , the system undergoes a non-critical relaxation characterized by a finite value of the correlation length and correlation time, and by a vanishing value of the order parameter. This is the *dynamically disordered phase*. The symmetric correlation function  $C_{\mathbf{p}}(t, t') = -i/\{\hat{\phi}_{\mathbf{p}}(t), \hat{\phi}_{-\mathbf{p}}(t')\}$  displays oscillations with asymptotic period set by  $\sim (r^*)^{-1/2}$ .

(ii) For quenches to the *critical point*,  $r \rightarrow r_c(r_0, u)$ , slow modes are characterized by aging dynamics, where the symmetric correlation function acquires the scaling form  $C_{\mathbf{p}}(t, t') \propto (tt')^\theta$  for  $t \gg t'$  and  $p \rightarrow 0$ , with a non-equilibrium universal exponent  $\theta = d/4$  in  $2 < d < 4$  (see Refs. [89, 97]). This is the analog of the ageing exponent occurring in non-equilibrium classical systems quenched close to critical temperature [98, 99]; in contrast, in the case discussed here, the system acts as its own bath because isolated from the environment. The phenomenon is called ageing because the characteristic relaxation time-scale is the age of the system itself, i.e. the time,  $t$ , elapsed after the quench. As in its classical counterpart, ageing denotes a dynamical regime where correlation functions break time-translational invariance in a universal fashion [94]. Indeed, the exponent  $\theta$  does not depend on microscopic details, rather it is dictated by dimensionality, symmetries and conservation laws, as in conventional theory of critical phenomena. Remarkably, the value of the exponent  $\theta$  cannot be related to the equilibrium ones  $\nu, \eta, z$ , etc. The absence of a gap and therefore of a characteristic timescale at criticality, implies that each mode has a typical relaxation time scale of order  $\sim 1/p$ . Therefore the ageing window is expected to extend for each mode within  $1/\Lambda \lesssim t \lesssim 1/p$ , and for well separated times  $t \ll t'$ . For  $t \lesssim 1/\Lambda$ , non-universal effects due to the microscopic details of the model will set in.

Concerning the steady state forming after deep quenches  $r_0 \gg \Lambda^2$ , the infrared modes equilibrate at the effective temperature  $T_{\text{eff}} \simeq \sqrt{r_0}$ . Notice however that this does not imply that the system has thermalized to a

Gibbs state [88]; on the contrary, higher momenta have occupations that violate equipartition of energy. The fact that in the presence of a finite energy density low momenta modes effectively thermalize, while higher momentum tails do not satisfy detailed balance, is a general feature of non-equilibrium phase transitions, present also in driven-open systems [100].

For small initial masses  $r_0 \ll \Lambda^2$ , the system undergoes a dynamical crossover around a time scale  $\sim 1/r_0$ , from a regime where dynamical scaling is characterized by a ‘quantum’ ageing exponent  $\theta'$  into a regime ruled by the effectively thermal exponent  $\theta$  we have just discussed. This additional ageing exponent  $\theta'$  corresponds to an unstable pre-thermal fixed point [101] whose canonical scaling properties are akin to a zero-temperature quantum critical point (the lower and upper critical dimensions are the same in the equilibrium and non-equilibrium case,  $1 < d < 3$ ).

(iii) Finally, for  $r \leq r_c(r_0, u)$ , the time-dependent effective mass decays with a universal  $\sim 1/t^2$  behaviour on long time scales, as it also happens for quenches at the dynamical critical point (below the upper critical dimension  $d < 4$ ). For  $d \geq 4$ , this decay turns into  $\sim t^{-(d-2)}$  as it can be predicted from dimensional analysis. However, in this regime with  $r < r_c(c_0, r_0, u)$ , the system exhibits coarsening [88, 89, 92], and correlation functions are characterized by a form of dynamical scaling distinct from the ageing typical of the critical point. Coarsening is caused by the formation of growing domains with different values of the order parameter, similarly to the phenomenon of spinodal decomposition [102]. It occurs for quenches starting from a symmetric ground state,  $r_0 > r_c$ . Physically, one expects that the system globally remains in a symmetric state with vanishing order parameter, however, the symmetry can be broken within spatial domains which appear separated by walls. Within each of them, the order parameter,  $\hat{\phi}$ , acquires the value of one of the two different  $Z_2$ -symmetry broken phases [102–104]. The average linear extension of the ordered domains increases with time, until a specific domain possibly prevails over the others, establishing the equilibrium state. However, the size of domains grows algebraically and actual equilibrium is reached only asymptotically. This lack of an intrinsic length scale in the system affects the equal-time two-point correlation functions which scale as  $C_{p=0}(t, t) \sim t^\gamma$  with  $\gamma = d - 1$ .

We finally remark that the dynamical phases of the  $O(\mathcal{N} \rightarrow \infty)$  model remain qualitatively unaltered [105] when the value of the mass is continuously ramped at a sufficiently fast speed from  $r_0$  to  $r$ , rather than suddenly quenched between the same two values. More precisely, when the duration of the ramp is finite, the critical properties associated to the dynamical transition are qualitatively the same as in the sudden quench scenario, while as the ramp is infinitely slow the equilibrium quantum phase transition at zero temperature is eventually recovered.

### III. EXACTLY SOLVED DYNAMICS IN RICHARDSON-GAUDIN MODELS VIA THE LAX SPECTRAL METHOD

In this Section, we review a class of all-to-all interacting spin exchange models of the Richardson type whose evolution under a quantum quench is solved exactly by a version of self-consistent mean field theory [106]. The solution reveals different dynamical phases of an order parameter, which can decay to zero (“phase I”) [107, 108], assume a non-equilibrium steady-state value (“phase II”) [109], or even exhibit persistent oscillations (“phase III,” a *self-generated Floquet phase* [107]). Although these dynamical phases of matter may carry some resemblance to those resulting from quenches of LMG-type models (cf. Sec. II A above), this Section aims at emphasising their markedly different origin which results from the classical and quantum integrability of Richardson magnets.

The order parameter for this class of models can be defined via

$$\Delta \equiv -G \sum_i s_i^- . \quad (9)$$

This is an equal-weight sum of spin-1/2 lowering operators in an  $N$ -spin system. It plays the role of the BCS pairing gap in applications to quenched superfluids and superconductors (see below).

Fig. 3 shows the quench phase diagram for a system exhibiting phases I, II, and III. In this figure, ground-state order-parameter values for the pre- ( $\Delta_i$ ) and post-quench ( $\Delta_f$ ) Hamiltonian label the vertical and horizontal axes, so that any point in the phase diagram away from the diagonal line is a quench. In this particular system (a quenched  $p + ip$  superfluid), the ground state exhibits a topological transition at a certain value of the order parameter  $\Delta_i = \Delta_f = \Delta_{QCP}$ . This extends to a line in the quench phase diagram, separating nonequilibrium phases characterized by different winding numbers  $W$ .

The models described in this section can be realized in a collisionless (prethermalization) regime for a range of physical systems, as will be discussed in Sec. V, including

- Far-from equilibrium dynamics in solid-state superconductors, following excitation by an intense subgap (terahertz) pulse [114–120],
- Quenches in central-spin type problems (Gaudin magnets), or synthetic spin-1/2 magnets with infinite-range interactions realized in ultracold fermionic atoms in a trap [121] and cavity QED systems [122],
- Ultracold fermionic superfluids, with different pairing symmetries (such as  $s$ -wave or  $p$ -wave) where a quench corresponds (e.g.) to a change in the strength of the attractive interactions responsible for pairing, as could be accomplished by tuning a Feshbach resonance [107–110, 123–125]. The approach has been extended to multicomponent superconductors with competing orders [126].

- Quenches in topological superfluids, such as a chiral  $p + ip$  system that can host circulating Majorana edge modes [110, 111, 127].

All of these systems can be approximately described by a Hamiltonian of Richardson-Gaudin type [128–130], which is both classically and quantum mechanically integrable. Quantum integrability implies that the many-body spectrum can be obtained from the Bethe ansatz [128–136]. Instead, here we focus on the thermodynamic (infinite-system-size) limit, where self-consistent mean field theory can become exact [107, 109, 137, 138]. In this case, the system resides in a pure BCS-type state at all times (with time-dependent coherence factors), and the dynamics of generic observables (Green’s functions) can be computed exactly by exploiting the *classical integrability*.

This section is organized as follows. First, we will describe how the Richardson-Gaudin spin model emerges from the description of a BCS superfluid. We will then illustrate how the dynamical phase diagram can be obtained using the “Lax spectral method” [109, 110,

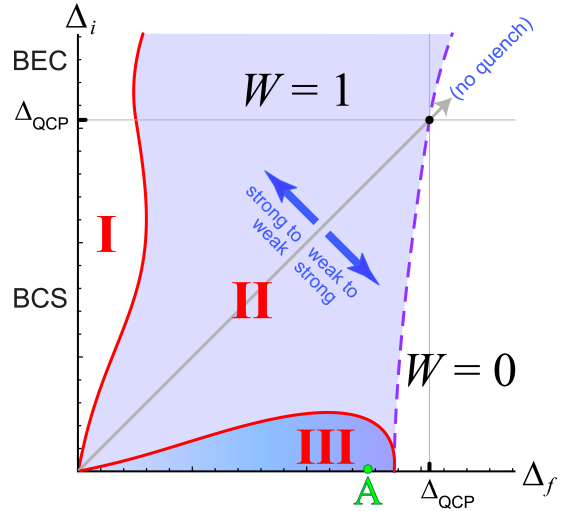


FIG. 3. Quench phase diagram for a 2D  $p + ip$  fermion superfluid, from Refs. [110, 111]. Here  $\Delta_i$  ( $\Delta_f$ ) denotes the ground-state BCS order parameter in the pre- (post-)quench Hamiltonian. Any point with  $\Delta_i \neq \Delta_f$  corresponds to a quench, while the line  $\Delta_i = \Delta_f$  denotes the ground state.  $\Delta_i$  ( $\Delta_f$ ) is associated to an attractive BCS pairing interaction strength  $G_i$  ( $G_f$ ), assumed to change instantaneously at the time of the quench. The subsequent dynamics of  $\Delta(t)$  fall into three different phases I, II, III, described in the text. Phase III is a self-generated Floquet phase, which in the case of a  $p + ip$  superfluid exhibits topological edge states, see Fig. 4. In this figure,  $W = 1$  ( $W = 0$ ) indicates topological (trivial) domains of phase II. The region with  $W = 1$  hosts Majorana edge states, even for quenches that start from the trivial BEC phase ( $\Delta_i > \Delta_{QCP}$ ).  $\Delta_{QCP}$  denotes the ground-state topological quantum phase transition between BCS and BEC phases [112, 113]; the dashed purple line is its nonequilibrium extension.

123, 137, 138], which exploits the classical integrability and the simplifications that occur in the thermodynamic limit. For a particularly simple class of initial conditions (different from the usual assumption of a BCS-ground initial state), we show explicitly how the solution method works, giving the dynamical phases I, II, III described above, and we will outline how to compute generic observables. Sec. III D gives an overview of fluctuation phenomena beyond the scope of mean-field dynamics, including quenches from an initial normal Fermi liquid state [139–146]. Finally, we summarize a few key features of quench-induced dynamical topological phase transitions [110, 111, 127].

We limit the overview in this section to the idealized, thermodynamic limit for integrable Richardson-Gaudin models. Time and length scales for observing this physics in ultracold Fermi gases and THz-driven superconductors are discussed later in Sec. V A.

### A. BCS superfluids and Richardson-Gaudin

Consider a spin-1/2 Fermi gas in  $d$  spatial dimensions, with local, attractive interactions. The Hamiltonian is

$$\begin{aligned} H &= \sum_{\sigma \in \uparrow, \downarrow} \int d^d \mathbf{r} c_\sigma^\dagger(\mathbf{r}) \left( -\frac{1}{2m} \nabla^2 \right) c_\sigma(\mathbf{r}) \\ &\quad - G \int d^d \mathbf{r} c_\uparrow^\dagger(\mathbf{r}) c_\downarrow^\dagger(\mathbf{r}) c_\downarrow(\mathbf{r}) c_\uparrow(\mathbf{r}) \\ &= \sum_{\mathbf{k}, \sigma} \varepsilon_k c_{\mathbf{k}\sigma}^\dagger c_{\mathbf{k}\sigma} \\ &\quad - G \sum_{\mathbf{k}, \mathbf{k}', \mathbf{q}} c_{\mathbf{k} + \frac{\mathbf{q}}{2}\uparrow}^\dagger c_{-\mathbf{k} + \frac{\mathbf{q}}{2}\downarrow}^\dagger c_{-\mathbf{k}' + \frac{\mathbf{q}}{2}\downarrow} c_{\mathbf{k}' + \frac{\mathbf{q}}{2}\uparrow}, \quad (10) \end{aligned}$$

where the second equality expresses the Hamiltonian in terms of momentum modes in a finite volume. Here  $\varepsilon_k = k^2/2m$  is the kinetic energy, and  $G > 0$  denotes a local, spin-singlet pairing interaction strength. The fermion creation and annihilation operators satisfy canonical anticommutation relations,  $c_{\mathbf{k}\sigma} c_{\mathbf{k}'\sigma'}^\dagger + c_{\mathbf{k}'\sigma}^\dagger c_{\mathbf{k}\sigma} = \delta_{\mathbf{k}, \mathbf{k}'} \delta_{\sigma, \sigma'}$ , where  $\sigma, \sigma' \in \{\uparrow, \downarrow\}$  label the spin.

Inspired by the solution to the Cooper problem that gives a minimal bound-state energy for a two-electron pair with zero center-of-mass momentum, we drop interaction terms in Eq. (10) with nonzero  $\mathbf{q}$ . The resulting “reduced BCS Hamiltonian” [150] can be expressed in terms of Anderson pseudospins [151]

$$\begin{aligned} S_{\mathbf{k}}^+ &\equiv c_{\mathbf{k}\uparrow}^\dagger c_{-\mathbf{k}\downarrow}^\dagger, & S_{\mathbf{k}}^- &\equiv c_{-\mathbf{k}\downarrow} c_{\mathbf{k}\uparrow}, \\ S_{\mathbf{k}}^z &\equiv \frac{1}{2} (n_{\mathbf{k}\uparrow} + n_{-\mathbf{k}\downarrow} - 1), \end{aligned} \quad (11)$$

where  $n_{\mathbf{k}\sigma} \equiv c_{\mathbf{k}\sigma}^\dagger c_{\mathbf{k}\sigma}$ . Simplifying notation by labeling single-particle levels with  $i, j \in \{1, \dots, N\}$  instead of

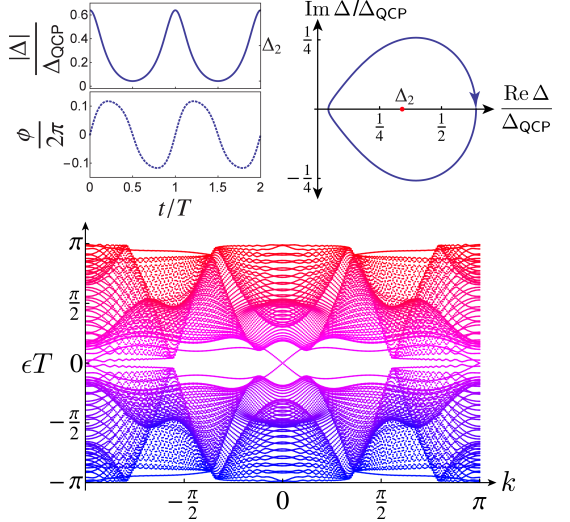


FIG. 4. Self-generated Floquet phase III for a sufficiently large weak-to-strong quench in the model described in Fig. 3 [111, 127]. A Floquet phase is a dynamical state of matter characterized by parameters that oscillate periodically in time [147]. Floquet systems can exhibit topological features [112, 148] such as protected edge states at the sample boundary, even when the undriven system is topologically trivial [149]. The top left shows the periodic (but strongly anharmonic) amplitude and phase of the order parameter  $\Delta(t)$ , while the top right depicts its orbit in the complex plane. On the bottom, diagonalization of a lattice-regularized strip shows Floquet-Majorana edge states (crossing in the center gap) for this particular quench, marked “A” in Fig. 3. Majorana edge modes will appear only in a fermionic superfluid or superconductor with a physical boundary.

momenta, the reduced  $s$ -wave BCS Hamiltonian is

$$H = \sum_{i=1}^N 2\varepsilon_i S_i^z - G \sum_{i,j=1}^N S_i^+ S_j^-. \quad (12)$$

This “Richardson” Hamiltonian [128, 129] is similar to the Dicke model, which features all-to-all coupling of the in-plane spin components, but here each spin is subject to a potentially different Zeeman field  $2\varepsilon_i$ . The all-to-all coupling is a necessary, but not sufficient condition for integrability [142]; integrable variants can describe  $p$ -wave and other pairings [131–136].

Using the SU(2) algebra of the pseudospins, the Heisenberg equations of motion are

$$\dot{\vec{S}}_i = \vec{S}_i \times \vec{B}(\varepsilon_i), \quad (13a)$$

$$\vec{B}(\varepsilon_i) \equiv -2\varepsilon_i \hat{z} - \Delta(\hat{x} + i\hat{y}) - \Delta^*(\hat{x} - i\hat{y}), \quad (13b)$$

where the BCS order parameter was defined in Eq. (9).

In the thermodynamic limit  $N \rightarrow \infty$ , the expectation of  $\Delta$  in an initial BCS pure state becomes a classical observable (Ehrenfest’s theorem). Then,  $\langle \vec{S}(t) \rangle \equiv \vec{s}(t)$  satisfies the equation of motion for a classical spin in an external field. The usual BCS ground-state equation

[150] obtains by aligning each spin to its own magnetic field [151]. The total particle number is encoded in the conserved  $S^z \equiv \sum_i s_i^z$ ; its value can be fixed by adding this to the field  $\vec{B}$  with a chemical potential.

## B. The Lax spectral method

### 1. Isolated roots and phases I, II, III

The Lax spectral method [109, 110, 123, 137, 138] simplifies the dynamics for the classical spins, generated by the BCS Hamiltonian in Eq. (12). The idea is that the all-to-all coupling in this model leads to a reduction of the collective dynamics, such that the time evolution of  $\Delta(t)$  can be determined by solving an emergent few-spin problem. This can be understood as a sort of exact renormalization group: the effective few-spin problem is governed by a “Lax reduced” Hamiltonian of precisely the same form as Eq. (12), but with  $M < N$  spins and renormalized parameters. The parameters of the reduced model can be determined from the  $N$ -spin quench via the integrability. Specifically, these obtain from the roots of a certain spectral polynomial, defined below.

Here, we detail the Lax construction for the  $s$ -wave Hamiltonian in Eq. (12) [109, 123, 137, 138]. A similar construction for a  $p+ip$  superconductor can be found in [110]. See Refs. [130–136] for the general classification of Richardson-Gaudin models.

We define the Lax vector and its norm,

$$\vec{L}(u) \equiv \sum_{i=1}^N \frac{\vec{s}_i}{u - \varepsilon_i} - \frac{\hat{z}}{G}, \quad L_2(u) \equiv \vec{L} \cdot \vec{L}(u), \quad (14)$$

where  $u$  is an arbitrary parameter. The spins can be taken to satisfy classical Poisson brackets  $\{s_i^a, s_j^b\} = \delta_{ij}\epsilon^{abc}s_i^c$ . Then Eq. (12) implies that the Lax vector satisfies the same equation of motion as the spins,

$$\dot{\vec{L}}(u) = \vec{L}(u) \times \vec{B}(u). \quad (15)$$

The Lax norm is conserved. Moreover, it is easy to check that  $\{L_2(u), L_2(v)\} = 0$  for any  $u, v$ . Using this fact and the explicit expression for the Lax norm, one can identify a set of  $N$  independent conserved quantities. These are Hamiltonians of central-spin type (“Gaudin magnets”),

$$H_i \equiv \vec{s}_i \cdot \left[ -\frac{\hat{z}}{G} + \sum_{j \neq i} \frac{\vec{s}_j}{\varepsilon_i - \varepsilon_j} \right], \quad \{H_i, H_j\} = 0 \quad \forall i, j. \quad (16)$$

Up to an additive constant, the BCS Hamiltonian is the particular combination

$$H = -G \sum_i 2\varepsilon_i H_i + G(S^z)^2. \quad (17)$$

From the conserved Lax norm, we define an order  $2N$  spectral polynomial in the parameter  $u$ ,

$$Q_{2N}(u) \equiv G^2 \prod_{i=1}^N (u - \varepsilon_i)^2 L_2(u). \quad (18)$$

To see how a small number of degrees of freedom can govern the dynamics, we trade the spins for an alternative set of “separation variables,” defined as follows. Eqs. (14) and (9) imply that

$$L^-(u) \equiv L^x(u) - iL^y(u) = -\frac{\Delta}{G} \frac{\prod_{\alpha=1}^{N-1} (u - u_\alpha)}{\prod_{j=1}^N (u - \varepsilon_j)}. \quad (19)$$

The  $N - 1$  zeroes of this equation  $\{u_\alpha\}$  are complicated functions of the  $\{\varepsilon_i\}$ , the precise form of which we do not need. By considering the  $d/dt [L^-(u(t))]$  for a possibly time-dependent  $u(t)$ , we can derive the equations of motion for these separation variables [137],

$$\dot{u}_\alpha = 2i \frac{\sqrt{Q_{2N}(u_\alpha)}}{\prod_{\beta \neq \alpha} (u_\alpha - u_\beta)}. \quad (20)$$

The reduction to fewer degrees of freedom is best illustrated by an example. Using the spin configuration that solves the BCS equations in the ground state, one can explicitly show that the spectral polynomial in Eq. (18) possesses  $N - 1$  doubly-degenerate zeroes along the real  $u$ -axis. Since  $L_2(u) = L^+(u)L^-(u) + [L^z(u)]^2$ , any such zero  $u_0$  also satisfies  $L^-(u_0) = 0$ . In other words, the  $N - 1$  separation variables  $\{u_\alpha\}$  are static, and confined to the real axis [Eq. (20)]. In addition,  $Q_{2N}(u)$  possesses a complex-conjugate pair of zeroes  $\{u_1, u_1^*\}$  that encode the BCS ground-state order parameter  $\Delta_0$  (which we take to be real). For a particle-hole symmetric  $\varepsilon_i$  spectrum, one simply finds that  $u_1 = i\Delta_0$ .

Consider the case of a quench, wherein some initial pure state undergoes evolution according to the BCS Hamiltonian in Eq. (12). The initial state must be expressible as a configuration of the  $N$  pseudospins (a pure BCS state), but is otherwise arbitrary [152]. Feeding this initial spin configuration into the spectral polynomial [using the Lax vector in Eq. (14)], one can characterize the state of the system in terms of the pattern of zeroes for  $Q_{2N}(u)$ , which is conserved. For finite  $N$  and a generic initial state, one finds  $N$  complex conjugate pairs of zeroes, implying that all separation variables  $u_\alpha$  evolve nontrivially according to Eq. (20). Despite the integrability of these equations, explicit results are only available for small  $N$  in terms of hyperelliptic functions [137, 138].

In the thermodynamic  $N \rightarrow \infty$  limit, however, for certain classes of initial conditions the situation simplifies dramatically. In particular, for quenches that evolve an initial weakly paired BCS or strongly paired BEC ground state (characterized by coupling  $G_i$ ) according to a post-quench Hamiltonian with  $G \equiv G_f \neq G_i$ , one finds that only three possible dynamical phases appear. These are

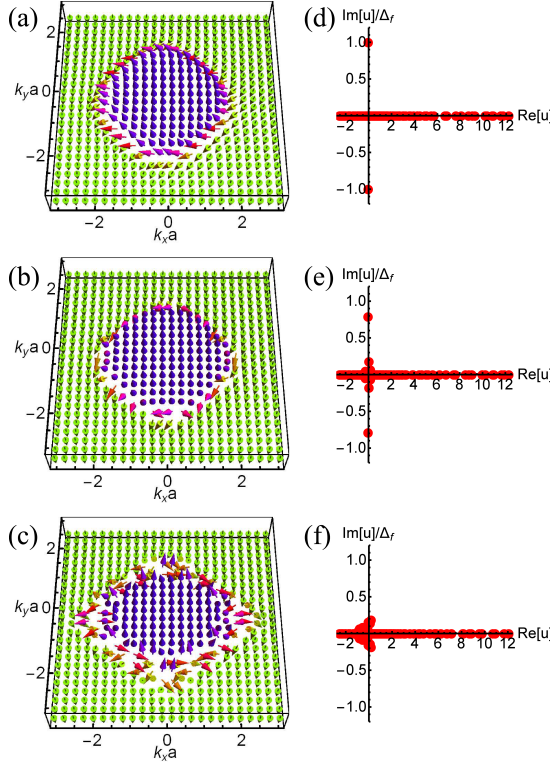


FIG. 5. This figure shows the Anderson pseudospin texture for a model 2D  $s$ -wave superconductor, following a “quench” induced by a subgap electromagnetic pulse [119], see also Refs. [116–118, 120]. This work was inspired by the results of the experiment by Matsunaga et al. [114], depicted in Fig. 9 and reviewed in Sec. V A, below. The Anderson pseudospin textures and the Lax roots of the spectral polynomial are depicted immediately after the application of an intense THz pulse. (a), (b), and (c) are the spin textures after light exposure, corresponding to the roots shown in (d), (e), and (f) respectively. The pair of roots away from the real axis are called isolated roots, and these encode the key properties of the BCS state. The system is a quarter-filled square lattice tight-binding model with 24-by-24 sites (the system is chosen to be small for the purpose of this illustration). Panels (a) and (d) correspond to a very weak pump energy, (b) and (e) to an intermediate pump energy, and (c) and (f) to a strong pump. The isolated roots  $u_1^\pm \simeq \pm i\Delta_\infty$  for the deformed spin textures encode the asymptotic value of  $\Delta(t \rightarrow \infty) = \Delta_\infty$  in the phase II pre-thermalization plateau. The main effect of the THz field quench is to twist Anderson pseudospins near the Fermi energy in the  $x$ - $y$  plane; more intense pulses produce more disordered twist patterns, and push the isolated roots towards the real axis. For strong pulses (c,f), the isolated roots merge with the real axis and the system enters phase I [107, 108] with  $\Delta_\infty = 0$ , see Fig. 6.

termed phase I, II, and III, and correspond respectively to zero, one, and two isolated pairs of roots of the spectral polynomial [107–109]. The remaining roots merge into a branch cut along the real axis, and thus correspond to a continuum of “frozen” separation variables. The separation between isolated and remaining roots is illustrated

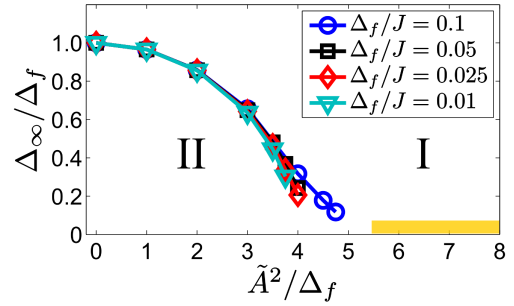


FIG. 6. Theoretical prediction for the nonequilibrium phase diagram of an  $s$ -wave BCS superconductor subject to an ultra-short ( $\simeq$  monocycle) THz pulse with center frequency  $\omega \simeq \Delta$ , from Ref. [119], described in Fig. 5. The 2D square lattice has linear size  $L = 1000$  at quarter filling. Values of  $\Delta_\infty$  are extracted from the isolated Lax roots corresponding to the spin configuration immediately after cessation of the pump pulse. We plot  $\Delta_\infty$  as a function of the peak pulse intensity  $\tilde{A}^2$ , with different values of  $\Delta/J$  ( $J$  is the hopping strength). As illustrated in Fig. 5, more intense pulses produce larger deformations of the pseudospins along the Fermi surface, leading to a suppression of the asymptotic BCS gap  $\Delta_\infty$ .

for a finite system in Fig. 5. The physics of phases I–III are as follows (see also the example phase diagrams in Fig. 3 and 6.)

- In phase I, there are no isolated roots, and  $\Delta(t) \rightarrow 0$  in the long-time limit. This occurs for large strong-to-weak quenches,  $G_f \ll G_i$  [108], and corresponds to an effective zero-spin problem. In a superconductor quenched to phase I, the optical conductivity or Meissner response would appear indistinguishable from a normal metal [119]. Anomalous coherences persist however, encoded in the dephased precession of Anderson pseudospins; schemes for detecting these are discussed in [153–156], see Sec. IV B. Phase I could be accessed in a solid-state superconductor subject to a sufficiently strong subgap THz pulse, as illustrated in Figs. 5 and 6.
- In phase II there is one pair of isolated roots, corresponding to an effective one-spin problem. Phase II describes small quenches, and smoothly connects to the ground-state configuration (no quench).  $\Delta(t)$  asymptotes to a nonequilibrium, steady-state value  $\Delta_\infty$ . For quenches entirely in the weak-pairing BCS regime, the approach to this prethermalized value takes a universal form [109, 157],

$$\Delta(t) \simeq \frac{\alpha}{\sqrt{t}} \cos(2\Delta_\infty t + \phi_0) + \Delta_\infty, \quad (21)$$

for some constants  $\alpha, \phi_0$ . The value of  $\Delta_\infty$  is precisely determined by the isolated roots of the spectral polynomial for the  $N \rightarrow \infty$  spin system. Decaying oscillations at frequency  $2\Delta_\infty$  were observed in the THz pump-probe experiment Ref. [114], see Fig. 9 and Sec. V A.

- In phase III, there are two pairs of isolated roots, corresponding to an effective two-spin problem. This occurs for sufficiently large weak-to-strong quenches, and connects in a somewhat intricate way to a quench starting from a normal (unpaired) Fermi liquid state [106, 139, 140], (see Sec. III D, below). The isolated roots of the spectral polynomial in the thermodynamic limit determine the parameters of this two-spin problem, leading to an effective equation of motion for  $\Delta(t)$ . The solution can always be expressed in terms of elliptic functions, and thus corresponds to a *quench-generated Floquet phase* [107, 123], as illustrated in Fig. 4 for a  $p + ip$  superfluid quench [110, 111, 127]. Heating is a potential difficulty with driven Floquet systems [147], but the quench-induced phase III dynamics could evade this problem. By contrast, a numerical study of quenches in a nodal  $d$ -wave superconductor did not exhibit phase III, which is damped out due to excited gapless quasiparticles [158]. This  $d$ -wave reduced BCS model is not of Richardson-Gaudin type, due to the form of the interaction coupling.

### C. A simple example

#### 1. Phases I and II

In this subsection, we illustrate the Lax spectral method for the model in Eq. (12). In order to keep the analysis as simple as possible, instead of a BCS (or BEC) initial Anderson pseudospin configuration, we consider a fully  $x$ -polarized initial state [159]. In fact, this initial state was used in a recent ultracold fermionic atoms experiment [121] to probe the phase I to phase II DPT (see Sec. V).

$$\vec{s}_i = (1/2)\hat{x}, \quad \forall i \in \{1, \dots, N\}. \quad (22)$$

The spectral polynomial [Eq. (18)] is

$$Q_{2N}(u) = \left[ \prod_{i=1}^N (u - \varepsilon_i)^2 + \left( \frac{G}{2} \right)^2 P_{N-1}^2(u) \right], \quad (23a)$$

where

$$P_{N-1}(u) \equiv \prod_{i=1}^N (u - \varepsilon_i) \left[ \sum_{j=1}^N \frac{1}{u - \varepsilon_j} \right]. \quad (23b)$$

Assume that the single-particle energies reside in the bounded interval  $-2J \leq \varepsilon_i \leq 2J$ . Then, for  $G \ll 2J$ ,  $Q_{2N}(u)$  possesses  $2N$  zeroes that appear in complex conjugate pairs close to each of the  $N$  bare real energies  $\{\varepsilon_i\}$ . On the other hand, for  $G \gg 2J$ ,  $2(N-1)$  zeroes appear close to the  $N-1$  real zeroes of  $P_{N-1}(u)$ . Thus there must be an additional, isolated pair.

To take the thermodynamic  $N \rightarrow \infty$  limit, we consider a simple 1D cosine band  $\varepsilon \rightarrow 2J \cos(k)$ , with  $|k| \leq \pi$ .

The Lax norm evaluates to

$$L_2(u) = (L\nu_0)^2 \left[ \frac{\pi^2}{(u/J)^2 - 4} + \frac{1}{g^2} \right], \quad g = \nu_0 L G, \quad (24)$$

where  $\nu_0 = 1/(2\pi J)$  is the density of states at the band center and  $L$  is the linear system size. The roots are  $u_1^\pm = \pm J \sqrt{4 - (\pi g)^2}$ . There is a dynamical phase boundary at  $g_c \equiv 2/\pi$ : for  $g < g_c$ , the isolated roots are real and merge with the continuum branch cut—this is phase I. For  $g > g_c$ , the isolated roots are purely imaginary, and we have phase II.

For phase II, the Lax reduced problem corresponds to a single collective pseudospin  $\vec{\sigma}$ , with a one-spin BCS Hamiltonian [compare to Eq. (12)]

$$H_1 = 2\chi\sigma^z - \frac{|\Delta_\infty|^2}{G}, \quad |\Delta_\infty| = -G|\sigma^-|. \quad (25)$$

Here  $\chi$ ,  $\Delta_\infty$ , and  $\sigma^z$  are all constants that must be determined by the roots of the effective one-spin spectral polynomial,

$$Q_2(u) = (u - u_1^+)(u - u_1^-). \quad (26)$$

Using the isolated roots from the many-body Lax norm in Eq. (24), we find that

$$\Delta_\infty = |u_1^\pm| = 2J\theta(g - g_c) \sqrt{\left(\frac{g}{g_c}\right)^2 - 1}, \quad (27)$$

where  $\theta(x)$  is the unit step function.

It is important to note that not all information about the long-time evolution of the post-quench dynamics is encoded by the isolated roots. In a BCS ground state, each Anderson pseudospin  $\vec{s}_i$  is aligned to its magnetic field  $\vec{B}(\varepsilon_i)$  [Eq. (13b)] (possibly modified by a chemical potential term to fix the density). In phase II, the effective magnetic field is determined by the asymptotic value of the gap  $\Delta_\infty$ ,

$$\vec{B}_\infty(\varepsilon_i) = -2\varepsilon_i \hat{z} - 2\Delta_\infty \hat{x}.$$

However, the steady-state pseudospins will in general exhibit precession around this field at a finite canting angle,

$$\lim_{t \rightarrow \infty} \vec{s}_i(t) = \frac{1}{2} \sqrt{1 - \gamma_i^2} \left\{ \begin{array}{l} \cos[2E_\infty(\varepsilon_i)t] \hat{B}_\infty(\varepsilon_i) \times \hat{y} \\ + \sin[2E_\infty(\varepsilon_i)t] \hat{y} \end{array} \right\} - \frac{\gamma_i}{2} \hat{B}_\infty(\varepsilon_i), \quad (28)$$

where  $E_\infty(\varepsilon_i) \equiv \sqrt{\varepsilon_i^2 + \Delta_\infty^2}$  is the asymptotic steady-state BCS quasiparticle energy. The function  $\gamma_i$  can be computed exactly by evaluating the Lax norm for the precessing solution in Eq. (28), discarding terms that oscillate as  $t \rightarrow \infty$ , and equating this with Lax norm for the pre-quench initial condition; we omit details here, but see Refs. [108, 110, 123]. In phase II, the function  $\gamma_i$  plays

the role of a nonequilibrium distribution function for the quasiparticle spectrum in the asymptotic steady state:

$$-\gamma_i = 1 - 2f_i, \quad (29)$$

where  $f_i$  would take the Fermi-Dirac form in terms of the quasiparticle energies for a system in thermal equilibrium.

Once the gap  $\Delta_\infty$  and the distribution function  $\gamma_i$  are known, generic  $n$ -body steady-state Green's functions (retarded, Keldysh, etc.) can be computed for the evolving pure BCS state. See e.g. Refs. [110, 127, 160] for examples of one-body functions and observables such as rf spectroscopy, tunneling, and time-resolved ARPES, and Ref. [119, 161] for the current-current correlator that determines the optical conductivity and Meissner response of a quenched solid-state superconductor.

## 2. Quench-generated Floquet phase III

Phase III arises for sufficiently large weak-to-strong pairing BCS quenches, see e.g. Figs. 3 and 4. As we review below in Sec. IIID, a special case corresponds to turning on attractive interactions for an initially unpaired, noninteracting Fermi gas ground state. Fluctuations (either quantum or thermal) play a crucial role in the real dynamics of such a quench, because the non-interacting ground state (a fully  $\pm s^z$ -polarized Anderson pseudospin magnet with a sharp domain wall at the Fermi surface) is a metastable stationary state.

Nevertheless, one can use the Lax spectral method to consider the formal limit of  $\Delta_i/\Delta_f \rightarrow 0$ , where  $\Delta_i$  ( $\Delta_f$ ) denotes the prequench (postquench) ground state gap (associated to a pairing strength  $G_i$  or  $G_f$ , respectively). In this limit,  $\Delta(t)$  possesses a soliton solution that grows from zero, reaches a peak, and decays back to zero [106]. The undamped oscillations of  $\Delta(t)$  in phase III can be understood as a train of such solitons [106, 109], and are thus in some sense adiabatically connected to the quench from an initial state with a sharp Fermi step.

Instead of the metastable normal state, here we consider the fully  $s^x$ -polarized initial state in Eq. (22), but now with a pair of sharp domain walls: [159]

$$\vec{s}_i = (1/2)\hat{x}\operatorname{sgn}(\varepsilon_i). \quad (30)$$

As proposed in Ref. [122] such an initial state can be prepared in a cavity QED system. In that work it is discussed how this state can be used to probe phases I, II and III in a controllable setting. See Sec. V. For the 1D cosine band employed above, the Lax norm in the continuum limit evaluates to [cf. Eq. (24)]

$$L_2(u) = (L\nu_0)^2 \left\{ \frac{[\csc^{-1}(u/2J)]^2}{(u/2J)^2 - 1} + \frac{1}{g^2} \right\}. \quad (31)$$

For  $g = 0$ , this has only real roots at  $u = \pm 2J$ . For any  $g > 0$ , two pairs of conjugate isolated roots nucleate into

the complex- $u$  plane. Denote these as  $\{u_1, u_1^*, u_2, u_2^*\}$ . For this particle-hole symmetric example,  $u_2 = -u_1^*$ . In the limit of large  $g$ , one has

$$\left( \frac{u_1}{2J} \right)^2 \simeq \frac{2g^2}{1 - i\sqrt{4g^2 - 1}}. \quad (32)$$

Two pairs of isolated roots corresponds to an effective two-spin problem, with spectral polynomial

$$Q_4(u) = (u - u_1)(u - u_1^*)(u - u_2)(u - u_2^*). \quad (33)$$

Parameterizing the order parameter  $\Delta(t)$  in terms of an amplitude and phase via

$$\Delta \equiv \sqrt{R} \exp(-i\phi), \quad (34)$$

one can solve the two-spin problem to obtain equations of motion in terms of the roots. Details of this calculation can be found elsewhere [106, 110, 123]. The results are

$$\begin{aligned} \dot{R}^2 &= 4(R_+ - R)(R - R_-)(R + \tilde{R}), \\ \dot{\phi} &= c_1 + \frac{c_2}{R}, \end{aligned} \quad (35)$$

where

$$\begin{aligned} R_\pm &\equiv (|\operatorname{Im} u_1| \pm |\operatorname{Im} u_2|)^2, \\ \tilde{R} &\equiv [\operatorname{Re}(u_1 - u_2)]^2, \\ c_1 &\equiv \operatorname{Re}(u_1 + u_2), \\ c_2 &\equiv [\operatorname{Re}(u_1 - u_2)][(\operatorname{Im} u_1)^2 - (\operatorname{Im} u_2)^2]. \end{aligned} \quad (36)$$

In our example [Eqs. (31) and (32)], we define  $u_r \equiv \operatorname{Re} u_1$ ,  $u_i \equiv \operatorname{Im} u_1$ , and  $u_2 = -u_1^*$ . Then the amplitude  $\Delta(t)$  is given by

$$\Delta(t) = 2u_i \operatorname{dn}(2u_i t | M) \simeq 2u_i \cos\left(\frac{2\pi t}{\mathcal{T}}\right), \quad (37)$$

where

$$\begin{aligned} M &= 1 + u_r^2/u_i^2, \\ \mathcal{T} &= \frac{1}{2u_i} [4K(M) + 4iK(1 - M)]. \end{aligned} \quad (38)$$

In Eq. (37),  $\operatorname{dn}(z|M)$  is the Jacobi elliptic function, with  $M$  the “modulo”; the approximate form of  $\Delta(t)$  given by the second equality is a very good approximation, except for very large  $|u_{r,i}|$ . In Eq. (38),  $K(M)$  is the complete elliptic integral of the first kind, and  $M = k^2$ , with  $k$  the elliptic modulus parameter.

We conclude that the  $x$ -polarized “domain wall” initial condition in Eq. (30) gives rise to a self-generated Floquet phase III, where the order parameter is given by the elliptic solution in Eq. (37). The parameters of this solution are determined by the four isolated roots  $\{u_1, u_1^*, -u_1, -u_1^*\}$ , where  $u_1$  is given by Eq. (32) for sufficiently large  $g$ .

Finally, we note that more complicated initial conditions with additional discontinuities can excite three or more pairs of isolated roots. These typically give rise to a self-generated, *quasiperiodic Floquet phase* for  $\Delta(t)$  in the prethermalized regime [109, 162]. These quasiperiodic phases have so far received little attention, and remain an attractive avenue for future work.

## D. Fluctuation phenomena

The reduced BCS Hamiltonian in Eq. (12) is an approximation to the idealized model for a Fermi gas with short-ranged interactions in Eq. (10). Only Cooper pairs with zero center-of-mass (COM) momentum are retained. This has several consequences. Formally, when this model is coupled to an electric field [119], appropriate for THz driving of a solid-state superconductor, the projection to zero-COM pairs breaks gauge invariance. This can be restored by incorporating the vector potential into the pairs, and still gives an effective classical system that can be efficiently simulated numerically [163].

Two more intricate problems are of particular theoretical and experimental interest. These are (1) a quench from the normal Fermi liquid state, either above  $T_c$  or at zero temperature with the pairing interactions turned off, and (2) a quench in a system of size  $L \gg \xi$ , where  $\xi$  is the coherence length. We discuss these in turn.

Quenches in which attractive pairing interactions are switched on from an equilibrium normal state above  $T_c$  have been studied in Refs. [143–146]. In this case, the fluctuation dynamics of the pairing amplitude are overdamped and can be treated classically, while the Keldysh method can be employed to evaluate one- and two-fermion observables (such as the optical conductivity [144, 145, 161]).

By contrast, a quench from a normal system with energy density below  $T_c$  is an extreme limit of a weak-to-strong pairing quench, and thus would be expected to induce the self-generated Floquet phase III (see e.g. Fig. 3). A weak-to-strong BCS quench from a finite-temperature initial paired state, in a system with  $N$  pseudospins, can exhibit  $\mathcal{O}(\sqrt{N})$  oscillation cycles, which can make phase III easily observable for  $N \gg 1$ . This follows from the central-limit theorem [140]. On the other hand, the quench from the normal state would exhibit only  $\mathcal{O}(\ln N)$  oscillations [140]. This would hardly be distinguishable from phase II [Eq. (21)] in an ultracold atom experiment (where  $N$  is not exponentially large, unlike in solid state systems).

More problematic for ultrafast THz quench experiments in solid-state superconductors (discussed below in Sec. V A) is the fact that practical sample sizes typically have linear dimension  $L \gg \xi$ , where  $\xi = \hbar v_F / \pi \Delta$  is the coherence length. It can be shown that phase III is unstable in this case to the spontaneous generation of spatial fluctuations (“Cooper pair turbulence”) [141, 164]. The mechanism is parametric resonance.

Finally, it must be remembered that even Eq. (10) is a significant simplification for both real ultracold Fermi gases and solid-state superconductors. In the case of gases, it neglects the internal degrees of freedom that can lead to losses [165–167], while for a superconductor, it neglects the retarded character of the dynamical pairing interaction, as typically mediated by phonons [150, 168].

## E. Topological features

In an ordinary, *s*-wave fermionic superfluid or superconductor, the BCS and BEC regimes respectively correspond to weak and strong pairing limits. One speaks of the BCS-to-BEC crossover in the zero-temperature quantum phase diagram, as a function of the pairing interaction strength [ $G$  in Eq. (12)] [113]. The BCS regime can be pictured as a gas of weakly bound, strongly overlapping Cooper pairs, while the cartoon for the BEC is a bosonic condensate of tightly bound two-fermion molecules. Since the zero temperature system is fully gapped for any nonzero pairing strength, the BCS and BEC regimes are limits of the same phase.

By contrast, for non-*s*-wave pairing, there is typically a genuine quantum phase transition separating the BCS and BEC regimes. In particular, for 2D  $p+ip$  superfluid, the weak-pairing BCS phase is topologically nontrivial. It means there exists a quantized integer-value winding number  $W$ , which characterizes the phase, that takes a nonzero value. The most important physical consequence of  $W \neq 0$  is the presence of gapless, chiral edge states that circulate around a 2D sample of finite extent [112]. This is a superconducting analog of the quantum Hall effect, except that the circulating edge fermions (called “Majorana fermions”) carry only energy instead of charge. A  $p+ip$  BCS superconductor can also host so-called “Majorana zero modes” in vortex cores; these are non-abelian anyons that could be exploited for topological quantum computation [112, 169].

On the other hand, the strongly paired BEC regime of a 2D  $p+ip$  superfluid is topologically trivial; there are no gapless edge states, and it cannot host Majorana zero modes. This is because topology is encoded in the effective bandstructure for the fermionic quasiparticles of the superfluid, but in the strongly paired BEC, the only low-lying excitations are bosonic molecules. The quantum phase transition separating the BCS and BEC regimes involves a closing of the excitation gap, such that gapless bulk quasiparticles appear precisely at the transition.

Other topologically nontrivial superconductors and superfluids are possible in three dimensions, analogous to the distinct *p*-wave paired  $^3\text{He}$  *B* and *A* phases [170, 171]. The former (latter) is a fully gapped, time-reversal invariant (gapless Weyl, time-reversal breaking) topological superfluid; both are predicted to host gapless two-dimensional Majorana fermion surface fluids.

Because topology and its consequences (e.g., gapless edge and surface states) are *global features* of a quantum phase of matter [148], these are expected to be immune to weak symmetry-preserving perturbations. It is therefore natural to ask which features survive under a *global* quantum quench.

Quench and Floquet dynamics in topological bandstructures is already a vast subject, see e.g. Refs. [147, 149, 172–182]. Here we confine our attention to topological features that emerge in a self-consistent quench, studied for a *p*-wave Richardson-Gaudin model in [110,

[111, 127], see also [142, 183, 184].

The dynamical phase diagram for quenches in the 2D  $p + ip$  Richardson-Gaudin model is shown in Fig. 3. It possesses the same three dynamical phases I, II, III for the order parameter  $\Delta(t)$  discussed above. In this case, the self-generated Floquet phase III is topological, and features chiral Majorana edge states, shown in Fig. 4. These are similar to edge states obtained in equilibrium [112] or under external Floquet driving [149], except that they are induced here by a sufficiently large weak-to-strong pairing quench. It was argued in Ref. [111] that phase III might be realizable in an ultracold Fermi gas, by quenching from an undetectably small (but nonzero) initial gap strength  $\Delta_i$  to an intermediate strength  $\Delta_f \gg \Delta_i$ . Although the latter regime is associated to strong parasitic three-body losses [165–167] that

prevent the adiabatic cooling to an equilibrium topological state, a parameter window with  $\mathcal{T} \ll t_3$  could possibly allow experimental observation of phase III. Here  $\mathcal{T}$  is the period of the Floquet phase, and  $t_3$  is the three-body loss lifetime.

Another key feature of the phase diagram in Fig. 3 is the winding number  $W$ , which takes different values in two regions of phase II. The  $W = 1$  ( $W = 0$ ) region is a topological (trivial) phase II regime. The topological version would host chiral gapless Majorana edge states for a realization in terms of paired fermions, with a sample boundary.

There are different notions of winding numbers that are equivalent in equilibrium, but which must be distinguished for a quench. The winding number  $W$  (Volovik invariant) is defined via [110, 170]

$$W \equiv \frac{\epsilon_{\alpha\beta\gamma}}{3!} \int_{-\infty}^{\infty} d\omega \int \frac{d^2\mathbf{k}}{(2\pi)^2} \text{Tr} \left[ \hat{\mathcal{G}}^{-1} \left( \partial_\alpha \hat{\mathcal{G}} \right) \hat{\mathcal{G}}^{-1} \left( \partial_\beta \hat{\mathcal{G}} \right) \hat{\mathcal{G}}^{-1} \left( \partial_\gamma \hat{\mathcal{G}} \right) \right]. \quad (39)$$

---

Here  $\alpha, \beta, \gamma \in \{\omega, k_x, k_y\}$  and repeated indices are summed. The matrix  $\hat{\mathcal{G}}(\omega, \mathbf{k}) \equiv \hat{G}_R(i\omega, \mathbf{k})$ ; the latter is the analytic continuation of the Fourier transform for the retarded, Bogoliubov-de Gennes Green's function  $\hat{G}_R(t - t', \mathbf{k})$ . In the long-time steady state of phase II, this Green's function is time-translationally invariant and independent of the distribution function  $\gamma_i$  [defined in Eqs. (28) and (29), above]. Because the retarded Green's function encodes information about the *spectrum of excitations* in the phase II steady-state, it is the appropriate topological index to determine the post-quench topology and its consequences (presence or absence of edge states). In Fig. 3,  $\Delta_{\text{QCP}}$  denotes the ground-state topological phase transition between the BCS and BEC regimes; the dashed purple line is its nonequilibrium extension.

By contrast, a different winding number defined to characterize the many-body state of the system does *not* change following a quench in the collisionless, prethermalized regime [110, 172, 173]. This winding number can be defined as [110]

$$Q \equiv 8\pi\epsilon_{abc} \int \frac{d^2\mathbf{k}}{(2\pi)^2} \frac{1}{k} s_{\mathbf{k}}^a \partial_k s_{\mathbf{k}}^b \partial_{\phi_k} s_{\mathbf{k}}^c, \quad (40)$$

where  $k, \phi_k$  are polar coordinates for the momentum plane, and  $a, b, c \in \{1, 2, 3\}$  (again with repeated indices summed). The winding number  $Q$  characterizes the pseudospin texture of the many-body state. For an equilibrium topological BCS state, this is a skyrmion texture with  $Q = W = 1$  [110, 112]. In the BEC state  $Q = W = 0$ , and the texture can instead be deformed to a trivial ferromagnetic one. The unitary evolution under the Richardson-Gaudin Hamiltonian [which neglects

---

center-of-mass spatial fluctuations for the order parameter  $\Delta(t)$ ] prevents a change in  $Q$  for any quench.

The most interesting consequence of the dual winding numbers ( $W, Q$ ) out-of-equilibrium appears for phase II quenches across the topological quantum phase transition, such that  $W \neq Q$ . Then, one can show that consistency between Eqs. (39) and (40) requires a *population inversion* in the occupation of steady-state quasiparticle states. I.e., the distribution function  $-\gamma = 1 - 2f$  [Eqs. (28) and (29)], which has  $\gamma_{\mathbf{k}} = -1$  for all quasiparticle states in either the BCS or BEC ground state, necessarily “winds” to  $\gamma_{\mathbf{k}} = +1$  for  $\mathbf{k} \rightarrow 0$  (the bottom of the parabolic band without pairing). This population inversion has detectable consequences for far-from-equilibrium phase II observables, such as rf spectroscopy or time-resolved ARPES [110, 127]. The takeaway is that, in a far-from equilibrium situation, a topological change ( $W \neq Q$ ) can be encoded in real *bulk* observables, due to the induced quasiparticle population inversion [110, 185].

Finally, we note that the quenches studied of  $p + ip$  superfluids in Refs. [110, 111, 127] always assumed an initial nonzero  $p + ip$  order ( $\Delta_i \neq 0$  in Fig. 3). As discussed in Sec. III D, a quench from the normal state requires an analysis of thermal and/or quantum fluctuations. However, even in the superconducting phase it is possible to have an initial combination of both  $p + ip$  (“ $\Delta_+$ ”) and  $p - ip$  (“ $\Delta_-$ ”) orders, given that the natural  $p$ -wave pairing interaction is time-reversal invariant. A very recent study [186] demonstrates that the coherent, topological phase III is replaced by a *chaotic* non-Floquet phase III’, for a quench in such a  $p$ -wave system from any simultaneously initial nonzero combination of  $\{\Delta_+, \Delta_-\}$ . On the other hand, the topological Floquet phase III is recovered

for arbitrarily weak time-reversal symmetry breaking in the Hamiltonian, which favors (e.g.) the development (suppression) of  $p + ip$  ( $p - ip$ ) order [186].

#### IV. DYNAMICAL PHASE TRANSITIONS IN INFINITE DIMENSIONS

For systems which follow a collisionless time evolution, non-thermal dynamical phases can be distinguished in terms of the asymptotic behavior at long times. Beyond this paradigm, a universal understanding of DPTs has yet to emerge. A generic interacting quantum system is expected to thermalize [187], in which case DPTs, such as between phases I to III in the collective spin models of Sec. III, turn into a crossover within the pre-thermal regime. To progress in an understanding of DPTs in non-integrable systems, we can therefore put forward the following questions: (i) How sharp are crossover phenomena which derive from exact mean-field DPTs under experimentally accessible conditions? Are they well-defined even in a realistic solid state setting, and can they be engineered on quantum simulation platforms? (ii) Can one identify different dynamical transitions which are entirely characterized in terms of the short-time dynamics? (iii) Can thermalization be inhibited even in non-integrable systems, so that sharp dynamical transitions exist in the long time behavior?

A challenge in investigating these questions is that the time evolution in non-integrable quantum systems is typically exponentially hard to compute. One limit in which many-body systems can be studied in a numerically controlled way is the limit of infinite dimensions, or infinite lattice connectivity  $Z \rightarrow \infty$  [188]. In contrast to spin models for which mean-field theory becomes exact in this limit (cf. DPTs in Sec. II A and III B), the dynamics of fermionic or bosonic lattice models generally remains non-integrable and ergodic. The limit of infinite dimensions therefore provides a useful setting to investigate the fate of DPTs when the dynamics is no longer collisionless. In the following section we will briefly comment on the solution of lattice models, in particular the Hubbard model, in this limit, and then review two types of DPTs: (i) A crossover in the pre-thermal evolution of symmetry-broken states (Sec. IV B), which is closely related to the mean-field DPTs discussed in the first part of this review, and (ii) DPTs in the short-time evolution (Sec. IV C) which either separate distinct pre-thermal regimes or are related to Bloch oscillations in a time-independent potential gradient.

As a remark we emphasize that the study of non-integrable quantum dynamics is a very active field of research also in the opposite numerically accessible limit, i.e., one-dimensional and finite systems. In particular, many-body localized phases in disordered systems show non-ergodic behavior [189–191], and the separation between non-ergodic many-body localized phases and thermal phases [192] can give rise to dynamical phase trans-

sitions. Weak ergodicity breaking with unusually long relaxation times has also been observed in translationally invariant systems due to dynamical bottlenecks and constraints, somewhat analogous to arrest in glassy dynamics [193–200], and many-body dynamics can remain constrained to atypical eigenstates [201, 202], or quantum many-body scars [203–205]. These settings are naturally interesting for a study of DPTs, but a detailed review of this field of research is beyond the scope of the present work (cf. discussion in Sec. V).

##### A. The Hubbard model in infinite dimensions

A paradigmatic model for strongly interacting fermions is the Hubbard model, given by the Hamiltonian

$$H_{\text{Hub}} = -J \sum_{\langle i,j \rangle, \sigma} c_{i\sigma}^\dagger c_{j\sigma} + U \sum_j n_{j\uparrow} n_{j\downarrow}. \quad (41)$$

Here  $c_{j\sigma}$  ( $c_{j\sigma}^\dagger$ ) is the annihilation (creation) operator for a fermion with spin  $\sigma \in \uparrow, \downarrow$  on a lattice site  $j$ , and  $n_{j\sigma} = c_{j\sigma}^\dagger c_{j\sigma}$  is the onsite number operator. The model describes tunnelling of particles between neighbouring sites  $\langle i,j \rangle$  on a lattice, with a local interaction  $U$ . Depending on interaction and filling, the Hubbard model gives rise to Mott-insulating, magnetically-ordered, and superconducting phases in equilibrium, making it a suitable platform to explore DPTs. A nontrivial solvable limit of the Hubbard model is that of infinite lattice connectivity  $Z \rightarrow \infty$ . For example, the connectivity can be systematically varied on the Bethe lattice, or on the  $D$ -dimensional hypercubic lattice with  $Z = 2D$ . When the tunnelling matrix elements are rescaled like  $J = J_0/\sqrt{Z}$ , with fixed  $J_0$ , interaction and kinetic energy for a system with given nonzero filling fraction (e.g. half filling) remain of the same order, resulting in a meaningful competition of various phases [188]. At the same time, the many-body self-energy  $\Sigma(\mathbf{k}, \omega)$  becomes local in space (independent of momentum  $\mathbf{k}$ ) [206], and the model can be solved exactly within dynamical mean-field theory (DMFT) [207]. Within DMFT, the local self-energy  $\Sigma(\omega)$  is obtained from a quantum impurity model in which one site of the lattice is embedded in a self-consistently determined particle reservoir [208]. Using Keldysh Green's functions, DMFT can be formulated to study lattice models in different non-equilibrium settings [209–211], including the transient dynamics of isolated lattice systems, non-equilibrium steady states of dissipative driven systems [212–214], and periodically driven systems (Floquet DMFT) [215]. The quantum impurity model for the Hubbard model can be solved numerically exactly for short times using real time Quantum Monte Carlo (QMC) [216], or matrix product state (MPS) simulations [217]. Long-time simulations are still exponentially hard due to the dynamical sign problem in case of QMC, and due to the unbounded growth of the entanglement typical for global quenches in many-body systems

in the case of MPS. Nevertheless, diagrammatic expansions on the level of the impurity model both at weak coupling [218] and at strong coupling [219] allow for a solution at long times, and thus provide a unique possibility to achieve a non-perturbative description of the many-body dynamics in a high-dimensional system.

### B. DPTs related to non-thermal symmetry breaking

The half-filled Hubbard model on a bipartite lattice supports antiferromagnetic (AFM) order in the repulsive case  $U > 0$ , and superconductivity as well as charge density wave order in the attractive case  $U < 0$ . In the following, we focus mainly on the repulsive model; the attractive model can be mapped onto the repulsive one by a particle hole transformation. At weak-coupling ( $U \ll J_0$ ), the normal state is metallic and the AFM phase can be understood within mean-field theory. For  $U \gg J_0$ , on the other hand, the normal state is a Mott insulator, and the ordered phase is described by a low-energy Heisenberg model. For  $U < 0$ , the two limits correspond to BCS superconductivity at weak interactions, and a condensate of preformed pairs (BEC) in the Mott regime, respectively. The transition temperature is maximal at the crossover, where  $U$  is comparable to the non-interacting bandwidth  $W$  (which is proportional to the tunneling  $J_0$ ).

The dynamics of the ordered phase after quenches of the interaction has been studied both at weak and at strong interactions. The weak-coupling limit is hereby closely linked to the mean-field models discussed in the first part of this review. To see this, one can choose a unit cell with two sites (corresponding to the two sub-lattices  $A$  and  $B$ ) and define momentum-space spinors  $\hat{\psi}_{\mathbf{k}\sigma} = (c_{\mathbf{k}A\sigma}, c_{\mathbf{k}B\sigma})^T$ ; here  $\mathbf{k}$  is a quasi-momentum in the Brillouin zone of the symmetry-broken state, which has a doubled unit cell with respect to the normal state due to the antiferromagnetic ordering. With this, one can introduce Anderson pseudo-spins  $S_{\mathbf{k}\sigma}^x = \frac{1}{2} \sum_{\sigma} \hat{\psi}_{\mathbf{k}\sigma}^\dagger \hat{\tau}_x \hat{\psi}_{\mathbf{k}\sigma}$ ,  $S_{\mathbf{k}\sigma}^y = \frac{1}{2} \sum_{\sigma} \sigma \hat{\psi}_{\mathbf{k}\sigma}^\dagger \hat{\tau}_y \hat{\psi}_{\mathbf{k}\sigma}$ , and  $S_{\mathbf{k}\sigma}^z = \frac{1}{2} \sum_{\sigma} \sigma \hat{\psi}_{\mathbf{k}\sigma}^\dagger \hat{\tau}_z \hat{\psi}_{\mathbf{k}\sigma}$ , with the Pauli matrices  $\hat{\tau}_{\alpha}$ . The Ne  l order parameter is the sub-lattice magnetization,  $m = \langle n_{A\uparrow} \rangle - \langle n_{B\uparrow} \rangle = \langle n_{B\downarrow} \rangle - \langle n_{A\downarrow} \rangle$ , which becomes  $m = \frac{1}{N_k} \sum_{\mathbf{k}} \langle S_{\mathbf{k}}^z \rangle$  in terms of the pseudo-spins. The mean-field Hamiltonian reads (up to terms which are absorbed in the chemical potential)

$$H_{\text{mf}} = \sum_{\mathbf{k}} \vec{B}_{\mathbf{k}}(t) \cdot \vec{S}_{\mathbf{k}}, \quad (42)$$

with the self-consistent pseudo-magnetic field  $\vec{B}_{\mathbf{k}}(t) = (2\epsilon_{\mathbf{k}}, 0, -Um(t))^T$ ;  $\epsilon_{\mathbf{k}}$  is the dispersion. Equation (42) is a spin model with all-to-all interaction as discussed in Sec. III. Upon a particle-hole transformation it is equivalent to the mean-field models studied for BCS superconductors [107], see also Eq. (12). After an interac-

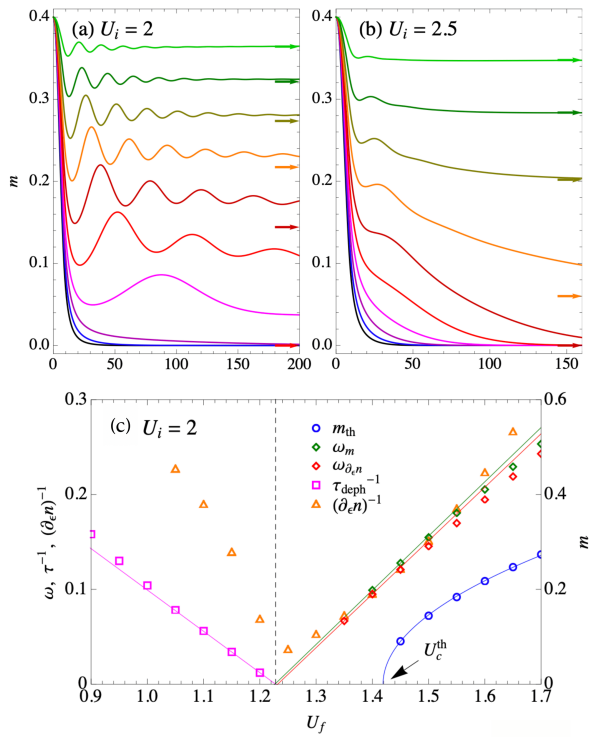


FIG. 7. (a) Antiferromagnetic order  $m$  after an interaction quench in the Hubbard model on the infinitely connected Bethe lattice. All energies (times) are measured in terms of the (inverse) tunneling  $J_0$ , the noninteracting bandwidth is  $W = 4$ . Different curves correspond to different final interactions  $U_f = 1.9, 1.8, \dots, 0.9$  from top to bottom. The arrow indicates the value of the order parameter after thermalization. (b) Analogous to (a), but for a larger initial value of the interaction, and  $U_f = 2.4, 2.3, \dots, 1.4$ . (c) Energy and time scales related to the transition (see text) for the initial interaction  $U_i = 2$ , as function of the quench amplitude  $U_f$ . Figure adapted with permission from Ref. [220].

tion quench starting from the symmetry-broken state, the order parameter  $m$  will therefore either show damped collective oscillations (phase II), an exponential decay (phase I), or self-sustained oscillations (phase III). The solution of the Hubbard model beyond mean field theory allows to investigate the fate of these DPTs outside the collisionless regime.

To study quenches at weak coupling, one can prepare the system in the AFM phase at given interaction  $U = U_i$ , and suddenly decrease  $U$  to a smaller value  $U_f$ . Figure 7 shows the results for a simulation on the infinitely coordinated Bethe lattice. For the smaller value of the initial interaction ( $U_i = 2J_0$ ), one can clearly distinguish two dynamical regimes (Fig. 7a): After weak quenches ( $U_f > 1.2J_0$ ), the order parameter shows a damped oscillatory decay towards a finite value at the longest sim-

ulation times (phase II), while for larger quenches, it follows a monotonous exponential decay (phase I). Similar dynamical transitions related to symmetry broken states in infinite dimensional systems are found in a time-dependent Gutzwiller solution of the Hubbard model [221], and for quenches in an  $O(N)$  model including fluctuations beyond mean field [92], though both approaches cannot describe thermalization. In the DMFT solution, interactions lead to thermalization, and for quenches close to the dynamical critical point  $U_c$  between the two regimes, the order parameter will eventually decay to zero both in phase I and in phase II. However, for sufficiently weak interactions the crossover between the two phases remains remarkably well-defined, and one can even extract the critical behavior close to  $U = U_c$ : The decay time  $\tau_{\text{def}}$  of the order parameter in phase I diverges like  $\tau_{\text{def}} \sim |U - U_c|^{-1}$  and the oscillation frequency  $\omega_m$  in phase II vanishes like  $\omega_m \sim |U - U_c|$ . Even for interactions  $U$  which are half the bandwidth  $W$ , this critical behavior can be observed over an order of magnitude in time (Fig. 7c).

Because of thermalization, the dynamical crossover becomes less well-defined at larger interactions (Fig. 7b). A relevant question is therefore whether one can experimentally distinguish the decay of the order parameter related to phase I from thermalization, although both eventually lead to a vanishing of the order parameter. An indirect evidence would be a crossover in the relaxation time as the system proceeds from the dephasing dynamics to thermalization. More interesting would be a direct measure of the individual momentum-resolved pseudo-spins  $S_{\mathbf{k}}$ : In the dephasing scenario (phase I), the magnitude of  $\langle \vec{S}_{\mathbf{k}} \rangle$  remains nonzero for all  $\mathbf{k}$ , but individual spins oscillate out of phase. In the thermal evolution, in contrast, the magnitude of  $\langle \vec{S}_{\mathbf{k}} \rangle$  for momenta at the Fermi surface decays to zero. Information on the individual pseudo-spins may be obtained by measuring correlations in the momentum occupations  $\langle n_{\mathbf{k}\sigma} n_{\mathbf{k}+\mathbf{Q},\sigma'} \rangle - \langle n_{\mathbf{k}\sigma} \rangle \langle n_{\mathbf{k}+\mathbf{Q},\sigma'} \rangle$  between momenta  $\mathbf{k}$  and  $\mathbf{k} + \mathbf{Q}$  separated by the anti-ferromagnetic nesting vector  $\mathbf{Q}$ . For cold atoms, such quantities could be addressed using noise correlations in time of flight measurements [153–155], while in the solid-state setting intensity correlations in time-resolved photoemission spectroscopy may provide similar access to such higher order correlations in the momentum distribution and thus distinguish the phase I dephasing from thermalization [156].

The findings for weak quenches in the Hubbard model are reminiscent of non-thermal fixed points in bosonic models [4, 222–225]. Non-thermal critical behavior in this case has been linked to an emergent universal form of the momentum distribution function with a steady flow of energy between short and long length scales. To what extent DPTs between phases I and II in mean-field models give rise to non-thermal critical behavior when interactions beyond mean-field are taken into account is still an open question. For the Fermi-Hubbard model, one could look for universal power laws in the momentum-

dependent spin structure factor (antiferromagnetic case) or pair distribution function (superconducting case). A close passage of the non-thermal critical point may moreover lead to a delay in thermalization. For the DMFT simulations, however, the dynamical crossover and subsequent thermalization have so far been seen within the same simulation only for larger interactions, where thermalization is fast, but at the same time the crossover is already relatively broad.

Recent simulations of the long-time dynamics using self-consistent second-order perturbation theory for the  $Z \rightarrow \infty$  Bethe lattice have focused on the thermalization of the order parameter in phase II after the decay of the collective oscillation [226]. The system remains in the non-thermal symmetry broken state for a long period of time, with a slow decay of the order, and a gap separating a valence and conduction band. The transient state in this regime is approximately described by a quasi-steady state with separate chemical potentials in the valence and conduction band. At some point, however, the dynamics speeds up, and the system rapidly approaches the disordered state. This highly non-monotonous decay contrasts the conventional evolution of pre-thermal states, which is expected to be a single exponential relaxation of slow variables (almost conserved quantities) [4, 49, 227–229]. The initial bottleneck against thermalization in the ordered phase may be linked to the gap in the electronic spectrum, so that the non-thermal symmetry-broken phase is somehow self-sustained. Whether such self-sustained relaxation bottlenecks are robust beyond the second order perturbation theory and beyond the infinite dimensional limit is yet to be seen; if so, the prolonged pre-thermal regime would make the dynamical crossover between phase I and II more well-defined.

Next, one can ask for the existence of phase III, i.e., self-sustained oscillations of the order parameter, in the interacting Hubbard model. In the mean-field model (42), phase III would require quenches to larger interaction, for which the mean-field description of the Hubbard model is probably no longer valid. It is nevertheless interesting to see whether phase III can appear in large quenches of the Hubbard model, such as quenches from the Mott AFM to intermediate coupling, where the AFM order is strongest. Even within DMFT, there is at present no approach which provides an unbiased solution to the long-time evolution in both the weak and strong coupling regime. However, one can obtain a numerically exact solution for short times within an MPS-based solution of the DMFT equations, when the initial state of the model is prepared as a perfect Néel AFM, i.e., the mean-field state of the strong-coupling Heisenberg model [230]. In this case, no indications of phase III are found for quenches to arbitrary interactions [230]. For quenches to small  $U$  one finds instead a prompt decay of the order parameter within few hopping times. The experimental realization of this scenario would be the analog of quantum simulation experiments that analyzed the decay of

charge order in a Bose-Hubbard model in one dimension [231].

Quantum quenches in the symmetry broken states have also been performed at large  $U$ , within the Mott phase. In this case, the Mott gap itself provides a dynamical constraint which leads to slow thermalization of the interaction energy (double occupancy  $d = \langle n_{j\uparrow}n_{j\downarrow} \rangle$ ) and the kinetic energy [232, 233]. Relaxation times are found to be exponentially long in the ratio  $U/J_0$  [234, 235], closely related to the slow decay of doublons in cold atom experiments [236, 237]. A quenched state can therefore relax into non-thermal phases in which the density of doublons is fixed as a quasi-conserved quantity. In particular, the repulsive single-band Hubbard model favors superconductivity in the  $\eta$ -pairing channel [238] if the doublon density is sufficiently increased with respect to the equilibrium state at the same effective temperature [233, 239, 240]. Such non-thermal phases in Mott insulators have been discussed in connection to possible light-induced superconductivity [239–243]. Because of the exponentially slow thermalization, dynamical phases which correspond to a relaxation to different ordered or disordered non-thermal states can be well-defined, with a non-thermal critical behavior [244]. However, as long as the non-thermal states are protected by a single or few quasi-conserved quantities, dynamical transitions related to these non-thermal phases should be close to dynamical transitions related to the relaxation to different equilibrium phases in a model which incorporates the constraints. For the Hubbard model at large  $U$ , where the doubly occupancy is the quasi-conserved quantity, the resulting model is a generalized  $t-J$  model, which describes two species of fermions (holes and doubly occupied sites) moving on the background of quantum spins that interact via an antiferromagnetic Heisenberg exchange. The phase diagram of this model has been studied as an approximation of the non-equilibrium phase diagram of the photo-excited Hubbard model for both the infinite-dimensional [239] and the one-dimensional case [240].

### C. DPTs between pre-thermal phases at short-time

A non-perturbative solution of the short time dynamics after an interaction quench in the Hubbard model from the noninteracting Fermi sea has been obtained using DMFT and QMC [245]. The system is initially prepared in the noninteracting Fermi sea, and at time  $t = 0$ , the interaction is suddenly quenched to a value  $U_f > 0$ . The subsequent dynamics can be monitored in terms of various observables, most importantly the momentum occupation  $n_{\mathbf{k}}(t) = \langle c_{\mathbf{k},\sigma}^\dagger c_{\mathbf{k},\sigma} \rangle$  and the doubly occupancy  $d(t) = \langle n_{j\uparrow}n_{j\downarrow} \rangle$ . In the initial state,  $n_{\mathbf{k}}$  shows a unit size discontinuity  $\Delta n_F = n_{\mathbf{k}_F^-} - n_{\mathbf{k}_F^+}$  across the Fermi surface;  $\mathbf{k}_F^\pm$  denotes a momentum infinitesimally above (below) the Fermi momentum. In thermal equilibrium, the discontinuity in the momentum distribution of

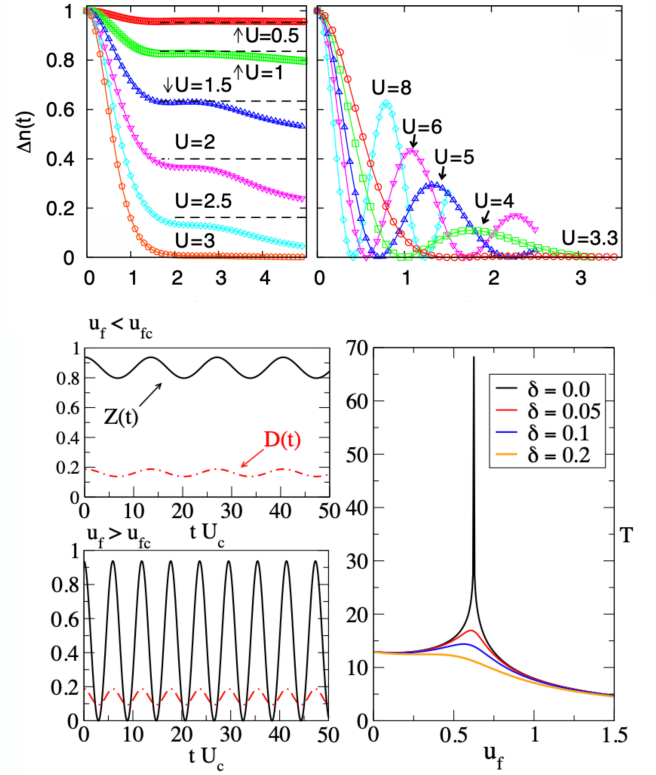


FIG. 8. Upper panels: Fermi surface discontinuity  $\Delta n_F(t)$  for an interaction quench in the Hubbard model on the Bethe lattice (noninteracting bandwidth  $W = 4$ ), from the noninteracting state to interactions  $U$  as indicated. The left and right panel correspond to the different dynamical regimes below and above  $U_{fc} = 3.3$ . Adapted with permission from [245]. Lower panels: Solution of the same model using the time-dependent Gutzwiller approach: Left is the quasiparticle weight ( $Z$ ) and the double occupancy ( $D$ ) for quenches below ( $U_f < U_{fc}$ ) and above ( $U_f > U_{fc}$ ) the DPT, right the period of oscillations for different values of the doping  $\delta$  away from half filling, as function of  $U_f$ . A sharp DPT is observed for  $\delta = 0$  with a divergence of the period. Adapted with permission from [247].

a Fermi liquid exists only at zero temperature. Because a quenched system is excited with respect to the ground state, the existence of a finite jump  $\Delta n_F$  indicates that the system is not yet thermalized. Moreover, one can show that the jump discontinuity is robust: While the magnitude  $\Delta n_F$  can change at  $t > 0$ , there remains an exact step-singularity in the momentum distribution, and the location of the discontinuity is precisely given by the noninteracting Fermi surface [246]. Hence,  $\Delta n_F$  can be taken as an order parameter to distinguish different dynamical regimes.

After the quench, one observes two distinct dynamical regimes, see Fig. 8: For small quenches below a value  $U = U_{fc}$  ( $U_{fc} = 3.3J_0$  for the infinitely connected Bethe lattice), the Fermi surface singularity rapidly decreases to

a value  $\Delta n_F > 0$ . The subsequent slower decay towards the thermal value  $\Delta n_F = 0$  is not resolved within the short time simulations. For quenches above  $U_f = U_{fc}$ , the dynamics features damped oscillations, with zero-crossings of  $\Delta n_F$ . For quenches to an interaction between the two dynamical regimes, the whole momentum distribution thermalizes rapidly. Thermalization is also verified by the fluctuation dissipation relation in dynamical correlation functions [248].

The dynamical transition in the short time evolution is not directly related to the equilibrium Mott transition:  $U_{fc}$  is about a factor two smaller than the equilibrium Mott transition at temperature  $T = 0$ , and the final state, after thermalization to a given temperature  $T^*$ , is in a bad metallic regime far from any known transition in the equilibrium phase diagram. Intriguingly, a singularity in the equilibrium two-particle vertex, which is related to multi-valuedness of self-consistent perturbation theory [249], has been found right at the point  $(U_{cf}, T^*)$  [250]. Whether this is coincidental, or whether such vertex singularities in general are related to DPTs is an open question.

It is useful to note that the two dynamical regimes reflect distinct pre-thermal behavior which can be understood in opposite perturbative limits (although these perturbative limits cannot give a description of the transition itself): Quenches from  $U = 0$  to weak coupling have been studied using perturbative unitary transformations [49] which are accurate for quenches  $U \ll J_0$ , on a timescale  $t \ll J_0/U^2$ . The unitary perturbation theory maps the Hubbard model on a system of non-interacting renormalized quasiparticles; the quasiparticle occupations  $\tilde{n}_k$  are conserved, providing a constraint on the dynamics which prevents the system from reaching a thermal state. For quenches to  $U \gg J_0$ , the effective model that describes the dynamics at least on timescales up to  $U/J_0^2$  can be obtained by unitary perturbation theory, treating  $J_0$  as a small parameter: It is the generalized  $t-J$  model mentioned at the end of Sec. IV B, where the number of doubly occupied sites and holes provides a constraint on the dynamics. The oscillations are well understood in the limit  $J_0 = 0$ , where the dynamics of the system would be  $2\pi/U$ -periodic, because the many-body spectrum is perfectly equidistant (analogous to the collapse and revival oscillations in the bosonic Hubbard model [251, 252]).

While the two dynamical regimes can be understood in a respective perturbative limit, an analytical model of the dynamical transition itself has been observed within time-dependent Gutzwiller theory [247, 253]. The time-dependent Gutzwiller provides a variational approach to the dynamics; for the Hubbard model, one starts from a variational ansatz wave function

$$|\Psi(t)\rangle = \prod_j e^{-iS_j(t)} P_j(t) |\Phi(t)\rangle, \quad (43)$$

where  $|\Phi(t)\rangle$  is a time-dependent Slater determinant,  $P_j(t) = \sum_{n=0,1,2} \lambda_{j,n}(t) P_{j,n}$ , and  $S_j(t) = \sum_n \phi_{j,n}(t) P_{j,n}$

are operators written in terms of variational parameters  $\lambda_{j,n}(t)$  and  $\phi_{j,n}(t)$  and the local projectors  $P_{j,n}$  on the occupation  $n = 0, 1, 2$  on site  $j$ . The time-dependent variational principle  $\delta\langle\Phi(t)|i\partial_t - H|\Phi(t)\rangle = 0$  leads to a set of nonlinearly coupled differential equations for the variational parameters. Within the Gutzwiller approach, an exact dynamical transition is observed, which shares many features with the DMFT results (see Fig. 8, lower panels): For small quenches, the quasiparticle weight  $Z(t)$ , which is proportional to the jump  $\Delta n_F$  defined above, oscillates around a nonzero value. Its time average  $\bar{Z}$  tends to zero as  $U_f$  approaches the dynamical transition. For quenches to the dynamical critical point,  $Z(t)$  exponentially relaxes to its thermal value  $Z = 0$ . The value  $\bar{Z}$  follows the pre-thermal plateau obtained by DMFT with quantitative accuracy [247]. For quenches beyond  $U_c$ ,  $Z(t)$  oscillates with a zero crossing. In contrast to the full solution, the Gutzwiller approach does not describe thermalization, and the dynamical transition therefore distinguishes the dynamics at all times.

Being computationally inexpensive, the Gutzwiller approach has allowed to study the DPT in a wider range of parameters: (i) By varying the initial  $U = U_i$ , one can map out a dynamical phase diagram which connects the dynamical phase transition to the equilibrium Mott transition  $U_c^{eq}$ : For  $U_i = 0$ , the dynamical point  $U_{fc}$  is below  $U_c^{eq}$ , while it approaches  $U_c^{eq}$  as  $U_i$  is increased [247]. (ii) Moreover, the dynamical transition persists if the interaction is ramped up with a nonzero ramp time  $\tau$  instead of a quench [254, 255]. The dynamics after the ramp still distinguishes different dynamical regimes, and the DPT evolves towards the equilibrium phase transition for larger  $\tau$ , as expected for an adiabatic dynamics. (iii) When the system is doped away from half filling, where there is no Mott transition in equilibrium, the dynamical transition turns into a crossover. In particular, time averages of the double occupancy and of  $Z$  evolve smoothly as a function of  $U_f$ . Finally, (iv), time-dependent Gutzwiller simulations have been performed for a multi-orbital Hubbard model [256], which turns out to be different from single-band case due to inter-orbital fluctuations. The dynamical transition is replaced by a broad regime in which the different occupations evolve irregularly, which may be interpreted in terms of long-lived fluctuations between metallic and insulating states.

Unfortunately, DMFT simulations have so far been performed neither away from half filling nor at nonzero  $U_i$ , due to a more severe dynamical sign problem. Hence there are so far no numerically unbiased simulations to support these intriguing observations from the Gutzwiller approach, and a complete picture of the dynamical transition in the Hubbard model is yet to be developed. Another question is the extension of the transition to lower-dimensional systems. In one dimension, the dynamics has been calculated using a systematic solution of the equation of motion for the field operators  $c_{i\sigma}$  in terms of higher order operator products [257]. It is found that the non-equilibrium time-evolution after interaction

quenches exhibits a similar dynamical transition as in the half-filled case, while the transition becomes a crossover upon doping. This may suggest that the dynamical transitions is a general feature of quenches in such models [257]. On the other hand the prethermalization is typically less pronounced in lower dimensions [257, 258].

Finally, a DPT has been found in the Bose-Hubbard model on an infinitely connected lattice [259], for quenches from the superfluid phase towards to Mott phase. A solution of the Bose Hubbard within the non-equilibrium generalization of bosonic DMFT [260] can be done at least for the short time evolution. In this case a single DPT is replaced by a richer dynamical phase diagram, including a non-thermal symmetry broken phase for weak quenches, an extended regime in which the system rapidly for intermediate quenches, and oscillations of the order parameter for quenches deep into the Mott phase.

Alternative to quenches of the interaction, dynamical phase transitions in infinite-dimensional lattice models have also been observed after a sudden switch-on of a potential gradient. In the non-interacting case, this leads to perfect Bloch oscillations if the gradient is aligned with a high-symmetry direction of the lattice. In interacting models, these oscillations will be damped, as the system approaches an infinite temperature state (for ergodic systems) or a non-thermal steady state if the system does behaves ergodic. In infinite dimensions, the latter case is represented by the Falikov-Kimball model, which allows for an exact solution in DMFT [261, 262]. The Falikov-Kimball model describes a Hubbard model in which one species of fermions is frozen. Regarding the mobile species, the dynamics obtained by DMFT in the normal (non-symmetry broken) phase is identical to that of fermions with quenched binary alloy disorder. The model does not thermalize after a quench of the interaction, but instead reaches a non-equilibrium steady state at infinite time [263]. The study of Bloch oscillations in the Hubbard and Falikov Kimball model in infinite dimensions gives a rich dynamical phase diagram [210, 264, 265], with transitions between oscillatory and non-oscillatory regimes.

## V. EXPERIMENTAL OBSERVATION

This Section overviews a broad number of platforms which are currently employed as quantum simulators for the evolution of interacting many-particle systems where DPTs can be hosted. For continuity with the two previous theory sections, we start by overviewing the state of the art in experiments realizing dynamical phases in solid state platforms, and then move to cold atoms experiments.

### A. DPTs in Condensed Matter Systems

The DPT in the integrable BCS model discussed in Section III neglects the retarded character of the dynamical pairing interaction, as typically mediated by phonons [150, 168]. Nevertheless, under specific conditions superconducting materials could be described by the integrable BCS model and display the three distinct dynamical phases I, II, and III discussed in Sec. (III B). For that to happen, the asymptotically exact long-time results obtained from the Richardson-Gaudin model can be relevant to experiments which can access a long prethermalization plateau. For a system of many particles  $N \gg 1$ , this requires that the minimum inelastic lifetime due e.g. to pair-breaking collisions, or inelastic electron-phonon scattering in a superconductor must be much larger than  $t_{\text{dyn}} \simeq 1/\Delta_\infty$ . Here  $t_{\text{dyn}}$  is the timescale for transitioning to the asymptotic regime and  $\Delta_\infty$  is the steady-state value of the order parameter in the prethermalization plateau (phase II) [123].

In the case of two-particle collisions for a quench entirely confined to the weak-pairing BCS regime, the two-particle scattering time can be estimated using Fermi liquid theory [123, 266]  $t_{\text{in}} \sim (\varepsilon_F/\Delta_\infty) t_{\text{dyn}} \gg t_{\text{dyn}}$ , where  $\varepsilon_F$  is the ground-state Fermi energy. This is consistent with simulations for the Hubbard model in infinite dimensions (Sec. IV B), which find a well-defined separation of phase I and phase II even when inelastic collisions are taken into account.

To observe phase III, the period  $\mathcal{T}$  of the quench-induced Floquet oscillation should be much shorter than the minimum inelastic lifetime. For a quench from an initial BCS state with small (but nonzero)  $\Delta_i$ , the Floquet period is of order  $\mathcal{T} = \frac{2}{\Delta_f} \ln \left( \frac{\Delta_f}{\Delta_i} \right) \ll \tau_{\text{in}}$ , where now  $\tau_{\text{in}} \sim (\varepsilon_F/\Delta_f)^2$ , and  $\Delta_f$  denotes the ground-state pairing gap for the post-quench system [106, 107, 111].

In addition to the above requirement, the quench that brings the superconductor out-of-equilibrium must occur on time-scales shorter than the inverse of the quasiparticle gap, to ensure the quasiparticle distribution does not adiabatically follow the variation of the system parameters. At the same time the perturbation has to be weak enough to avoid disrupting the system. The latter has been the most important limitation. Near-visible femtosecond optical pulses, which are used as a non-adiabatic excitation of solid state systems are not compliant since excitations with a frequency higher than the BCS gap can break Cooper pairs into hot quasiparticles, and these can serve as an efficient mechanism for rapid dissipation and thermalization. Nevertheless recent developments in THz technology are allowing now the injection of near monocycle pulses with center frequency close to the BCS gap, opening a window to investigate the coherent transient dynamics of superconductors in the nonadiabatic excitation regime over a window of about 10 picoseconds (ps), well before thermalization occurs on a time scale of 100 ps.

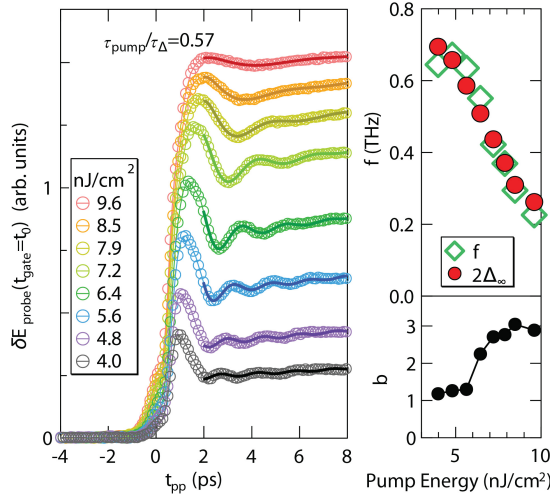


FIG. 9. A possible experimental realization of a phase II quench in a solid-state superconductor by Matsunaga et al., from Ref. [114], see also [115]. This figure shows pump-probe THz spectroscopy data on thin film  $\text{Nb}_{1-x}\text{Ti}_x\text{N}$ . The left panel shows the probe signal oscillations of  $\Delta(t)$ , and implies the approach to a nonequilibrium value  $\Delta_\infty < \Delta_i$  (weak phase II quench). The approach of  $\Delta(t) \rightarrow \Delta_\infty$  is characterized by decaying oscillations with frequency  $2\Delta_\infty$  (top right), consistent with the theory [Eq. (21)] [109, 157].

In particular the experiment done by Matsunaga et al injected an intense, short-duration THz pulse with center frequency  $\omega \simeq \Delta_0$  into a low-temperature NbN thin film *s*-wave superconductor [114, 115]. Since most of the spectral weight of the pulse was below the optical gap edge  $2\Delta_0$ , a weak pulse would not be expected to couple to the system [168]. However, because of the strong character of the injected pulse, it coupled in a nonlinearly fashion and was able to excite the “Higgs” (amplitude) mode of the superconductor. After the application of the pulse, the subsequent free evolution of  $\Delta(t)$  was expected to be described by the *s*-wave Richardson-Gaudin model. The experiment [114] measured the system over a window long enough to observe decaying oscillations as predicted by the Lax method in Eq. (21), as shown in Fig. 9. Despite the different method of initial state preparation (THz pulse versus instantaneous interaction quench), the phase II dynamics was apparently observed.

A THz electric field pulse can be incorporated into the self-consistent solution for the BCS (Bogoliubov-de Gennes) equations. In order to induce a nontrivial evolution of the system, it is necessary to either account for the finite (but very small) photon momentum [116–118, 120], or to include non-quadratic corrections to the band dispersion [119]. Moreover, in order to model the experiment in Ref. [114], a short-duration Gaussian electric pulse  $\mathbf{E}(t)$ , with frequency content mostly below the equilibrium optical gap  $2\Delta_0$ , needs to be fed into the equations of motion for the Anderson pseudospins. The field twists the pseudospins in the *x*-*y* plane, scrambling the ground state order as shown in Fig. 5. Importantly,

the driving of the Higgs mode arises from nonlinear coupling to the field [115, 119]. After the cessation of the pulse, the system is expected to evolve freely according to the Richardson-Gaudin Hamiltonian.

The Richardson-Gaudin calculation [119] predicts a transition to the gapless phase I for sufficiently strong pump energy, as shown in Fig. 6. Indeed a putative gapless phase [with suppressed reactive component of the optical conductivity  $\sigma_2(\omega)$ ] was observed for sufficiently strong pump powers in Ref. [267], potentially consistent with phase I. Strikingly, this experiment also observed extremely slow relaxational dynamics following the quench, on the order of 1000 ps. A subsequent experiment utilizing asymmetric, multicycle pulses exhibited an intervening “gapless” phase with  $\Delta_\infty \neq 0$  [268].

A discrepancy between the collisionless phase II prediction in Eq. (21) and the data in Ref. [114] is the more rapid decay of the oscillating envelope than  $t^{-1/2}$ . This is also consistent with the simulations for the interacting Hubbard model in Sec. IV A. A better theoretical fit can be obtained by employing a phenomenological “ $T_2$ ” dephasing time [269]. Another key question is whether spatial fluctuations (“Cooper pair turbulence” [141]) play an important role in these solid-state experiments [114, 115, 267, 268]. See discussion in Sec. III D.

We finish this section by noting that we have not surveyed here work involving the steady-state driving solid-state materials [147]. In particular, we do not review multipulse THz driving [269] or continuous-wave mid-infrared laser excitation of superconductors. The latter has attracted significant interest as a possible mechanism for enhancing pairing or  $T_c$  far from equilibrium [143–146, 270–275]. Continuous driving has also been discussed in the context of third-harmonic generation via the Higgs mode [115, 276–278]. Although these are certainly interesting developments, our focus here is on the collisionless dynamics of an effectively isolated system, free from external driving (following the quench).

## B. DPTs in Cold Atom Experiments

**DPT in the long-range Ising model.** The first observation and quantitative characterization of a DPT was done in a trapped ion quantum simulator consisting a chain of up to  $N = 53$ , <sup>171</sup>Yb<sup>+</sup> ions trapped in a linear radio-frequency Paul trap [54] (See Fig. 10(a)). Two relevant hyperfine levels were used as a spin 1/2 degree of freedom. Note here we are not accounting for experimental observations of DPTs described in terms of non-analytic behaviors of the Loschmidt echo amplitude which were observed at a similar time [13, 279]. A discussion of these type of experiments can be found in Ref. [14].

In Ref. [54] pairs of laser beams were used to generate an optical dipole force that off resonantly excited vibrational modes of the ion chain. The virtually excited phonon modes in turn mediate tunable spin-spin inter-

actions which lead to long-range Ising couplings in the form of Eq.(1). Explicitly, the engineered Hamiltonian is given by

$$\frac{1}{2} \sum_{i>j} \chi_{ij} \hat{\sigma}_i^x \hat{\sigma}_j^x + \frac{B}{2} \sum_i \hat{\sigma}_i^z, \quad (44)$$

with coupling constants that fall off as  $\chi_{ij} \approx J_0/|i-j|^\alpha$ , i.e, approximately algebraically with the distance between ions in the chain. The power-law exponent  $\alpha$  was set to be between 0.8 and 1.0 in the experiment. Here  $\hat{\sigma}_i^{x,y,z}$  are Pauli matrices acting on the  $i$ th ion. The competing transverse field proportional to  $B$  was generated in the experiment by a controllable Stark shift on the spins from the same laser field that generated the optical dipole force. The transverse field  $B$  was used as the control parameter for crossing the DPT. At time  $t = 0$ , the system was initialized in the state with all the spins pointing along the  $x$  direction of the Bloch sphere and the system was let to evolve under the combined Ising plus transverse field Hamiltonian for some time  $t$  after which the collective magnetization

$$\langle \hat{\sigma}^x(t) \rangle = \frac{1}{N} \sum_i \langle \hat{\sigma}_i^x(t) \rangle, \quad (45)$$

and the corresponding time averaged were measured

$$\overline{\langle \hat{\sigma}^x \rangle}(T) = \frac{1}{T} \int_0^T \langle \hat{\sigma}^x(t) \rangle dt, \quad (46)$$

equivalent to (Eq. 5). At the mean field level the time average magnetization  $\overline{\langle \hat{\sigma}^x \rangle}$  is expected to change, as discussed in Sec. II A, from a finite value to zero as the system crosses between a dynamical ferromagnetic phase ( $B < B^c$ ) to a dynamical paramagnetic phase ( $B > B^c$ ). Nevertheless, as explained in Sec.II B the quantum nature of the model resulted in a direct decay of the order parameter towards a vanishing or non-vanishing expectation value depending on the dynamical phase considered, without the need of long-time averages to classify phases.

To obtain further signatures of the DPT the experiment measured the spatially averaged two-spin correlator

$$C_2(t) = \frac{1}{N^2} \sum_{i,j} \langle \hat{\sigma}_i^x(t) \hat{\sigma}_j^x(t) \rangle \quad (47)$$

This quantity was used as a second order parameters for the DPT. It should cross from 1 (at small  $B$ ) to 1/2 (at large  $B$ ) with a dip at  $B^c$ . However, given the logarithmic scaling of  $C_2$  with  $N$  at the critical point and the limited system size of the systems under consideration, the experiment did not observe sharp signatures in  $C_2$  at the critical point. Nevertheless, measurements of the distribution of domain sizes in the chain (a direct measurement of higher-order correlations) accessible in the experiment allowed it to observe a sharp change of

behavior at the critical point.

**DPT in the Lipkin–Meshkov–Glick model.** After this work a similar type of DPT was observed in two different platforms, more specifically the one in the so called Lipkin–Meshkov–Glick (LMG) model (Eq. (2) in Sec. II A), which corresponds the  $\alpha = 0$  limit of the system described above with an additional longitudinal field, i.e

$$\hat{H} = \chi \hat{S}^+ \hat{S}^- + B \hat{S}^x - \delta \hat{S}^z \quad (48)$$

. Here we have introduced the collective spin operators  $\hat{S}^\alpha = \sum_j \hat{\sigma}_j^\alpha / 2$  and  $\hat{S}^\pm = \hat{S}^x \pm i \hat{S}^y$ . The summation runs over the individual spins  $j = 1, \dots, N$  and the parameter  $\chi$  sets the strength of an infinite-range exchange interaction. To connect with the Hamiltonian, Eq. (2), note that up to  $1/N$  corrections  $\chi \hat{S}^+ \hat{S}^- \approx \chi (\hat{\mathbf{S}} \cdot \hat{\mathbf{S}} - (\hat{S}^z)^2)$ . Since the first term  $\hat{\mathbf{S}} \cdot \hat{\mathbf{S}}$  is a constant when restricted to the fully symmetric spin manifold, which is the case of interest, the Hamiltonian simplifies to  $\hat{H} \rightarrow -\chi \hat{S}_z^2 + B \hat{S}_x - \delta \hat{S}_z$ , which up to an overall  $\pi/2$  rotation along the  $y$  axis of the Bloch sphere, coincides with the one realized in Ref. [54] with an extra term proportional to  $\delta$  which sets the longitudinal field (See Fig. 10(b)).

The observation of a DPT in the Lipkin–Meshkov–Glick model was first achieved in a cavity-QED simulator using ensembles of  $N \approx 10^5\text{--}10^6$  atoms [55]. We note that in the context of cavity QED great deal of experimental progress has been done in the observation of non-equilibrium phases characterized by different steady states which therefore depend on parameters such as pump or loss rates but are independent of the initial conditions [280–287]. We will not further discuss these experiments in the following, as in this review we exclusively focus on DPTs related to the unitary time evolution.

In Ref. [55] the internal spin degree of freedom was encoded in a long lived optical transition (linewidth  $\gamma/2\pi = 7.5$  kHz) between the  $|\downarrow\rangle$  [ ${}^1\text{S}_0$  ( $m_J = 0$ )] and  $|\uparrow\rangle$  [ ${}^3\text{P}_1$  ( $m_J = 0$ )] states of  ${}^{88}\text{Sr}$  atoms. The atoms were confined in a 1D optical lattice and coupled to a single common mode of the optical cavity far detuned from the atomic transition. In this regime the photons can be adiabatically eliminated. As a result their role is reduced to mediate infinite range elastic spin exchange interactions between the atoms, with strength set by  $\chi$ . The transverse field was engineered by pumping the cavity with a laser that generated, at resonance, Rabi flopping at frequency  $B$ . The longitudinal field was simultaneously introduced by detuning the pump laser by a frequency  $\delta$  from the atomic transition.

For this system the time-averaged collective magnetization along  $\hat{z}$  in this case  $\overline{\langle \hat{S}^z \rangle} \equiv \lim_{T \rightarrow \infty} (1/T) \int_0^T \langle \hat{S}^z(t) \rangle dt$  serves as an ideal order parameter as discussed in Sec. II A. This is equivalent to Eq. (5) up to an overall unitary rotation that maps

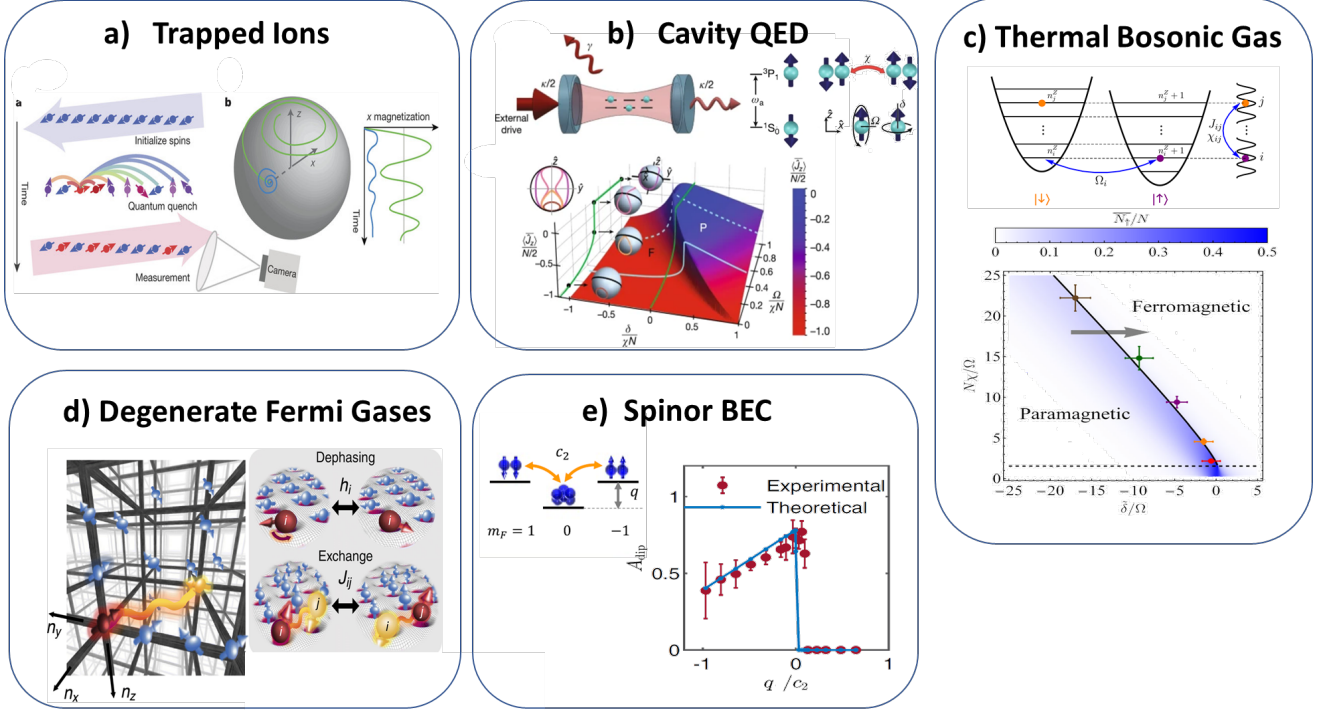


FIG. 10. Dynamical phase transitions (DPTs) observed in ultra-cold atomic gases: a) The first DPT was observed in a trapped ion quantum simulator of the long range Ising model plus transverse field, with up to  $53^{+171}\text{Yb}^+$  ions [54]. b) A similar type of DPT, but in the collective Ising limit plus an additional longitudinal fields (so called LMG model), was also observed in a cavity QED simulator with  $N \approx 10^5\text{-}10^6^{+88}\text{Sr}$  atoms [55], followed up by the observation of a similar DPT in a thermal gas of  $N = 10^4 - 10^5$  bosonic  $^{87}\text{Rb}$  atoms atoms using a sideband transition [56]. d) Using a quantum degenerate trapped Fermi gas of  $N = 10^4^{+40}\text{K}$  atoms the DPT between phase I and phase II predicted to exist in BCS superconductors was observed in Ref. [121]. e) Using three internal levels of  $^{23}\text{Na}$  atoms prepared in a Bose Eisntein Condensate (BEC) with  $N \sim 10^5$  atoms a DPT was observed as the ratio between collective exchange interactions and an effective quadratic magnetic field was tuned from positive to negative [288, 289].

$S^x \leftrightarrow S^z$ . However, in the experiment additional inhomogeneities and other technical imperfections damped the oscillation in the paramagnetic phase. Under these conditions the magnetization  $\langle \hat{S}^z \rangle$  after  $4\mu\text{s}$  of time evolution served as a proxy of the long-term time-averaged magnetization. The experiment observed the DPT in  $\langle \hat{S}^z \rangle$  at  $\delta = 0$  using  $B$  as the control parameter and demonstrated the expected scaling with atom number. The DPT was also probed by varying the longitudinal field for a fixed value of the drive strength  $B$  and by observing a sharp change of behavior of the order parameter at the critical point. The robustness of the DPT was demonstrated by the symmetric response of the magnetization for interaction shift  $\chi N \leftrightarrow -\chi N$ . The experiment also explored the DPT as a function of the initial state. It tracked the variation of the critical point as the system was initialized in a coherent spin state pointing along different directions.

The same LMG Hamiltonian was implemented in an experiment operating with a thermal gas of  $N = 10^4 - 10^5$  bosonic  $^{87}\text{Rb}$  atoms in a 3D harmonic trap using two hyperfine states to set a spin-1/2 degree of freedom [56]. The two internal states were coupled by laser fields tuned

to one of the blue side transitions, i.e the laser not only generated a spin flip but at the same time increased one of the motional quantum numbers in the trap by one unit. As a consequence the two coupled states had different motional eigenstates. Even though the interactions in this system are contact interactions during s-wave collisions, effective long range interactions can due to the delocalized nature of the single particle orbitals when operating in the collisionless regime. This is achieved when the trapping potential is much larger than the interaction strength [290, 291]. In this regime it can be assumed, to an excellent approximation, that each atom is fixed in a mode-space lattice with sites set by the single-particle eigenstates of the 3D harmonic trap. The only relevant process between two colliding atoms is to either remain in the same internal states or to exchange them. Even when dealing with bosonic samples restricting the Hilbert space to include only empty or singly-occupied lattice sites is appropriate when the gas temperature is above quantum degeneracy. Under these conditions the contact interaction term can be mapped to a spin-1/2 long-range XXZ spin model where the indices  $i, j$  run over the occupied

mode-space lattice sites,

$$H_{\text{int}} = \frac{1}{4} \sum_{ij} J_{ij} \vec{\sigma}_i \cdot \vec{\sigma}_j + \frac{1}{4} \sum_{ij} \chi_{ij} \hat{\sigma}_i^z \hat{\sigma}_j^z + \sum_i B_i \hat{\sigma}_i^z. \quad (49)$$

The XXZ couplings depend on the different scattering lengths of the atoms and on the overlap integral of the corresponding 3D harmonic oscillator wave functions. The use of a blue sideband transition that generate mismatched motional states of the coupled internal levels allowed the experiment to generate a finite  $\chi_{ij}$ . Otherwise it would have been negligible for Rb if the experiment had used a carrier transition (when laser only flips the spin). In addition to the interaction term, the interrogating laser generated transverse and longitudinal fields with strengths set by the Rabi frequency, and the laser detuning from the blue sideband transition.

To observe the DPT the atoms were initialized in the  $|\downarrow\rangle$  state. For this initial state, the exchange interaction term not only becomes a constant of motion but also locks the atoms into the fully collective spin manifold reducing the XXZ Hamiltonian to a LMG model with coupling constants replaced by their averaged value. Similar to the cavity experiment, instead of direct measurements of the long-time-averaged excitation which is inevitably limited by technical issues, the order parameter was set to be the excitation fraction at a probe time 0.5s. The entire phase diagram was obtained by scanning the two-photon detuning  $\delta$  for fixed transverse field  $B$  and by varying interactions using different atomic densities (See Fig. 10(c)).

We note that there is a direct connection between the DPT in the LMG model and the phenomena of macroscopic self-trapping and Josephson tunneling observed in coupled atomic condensates [292–295] and in solid state polariton condensates [296]. In this context the ferromagnetic and paramagnetic dynamical phases can be related to the self-trapped and tunneling phases respectively in the corresponding systems. Under this correspondence one can say that self-trapping experiments done years back did observe indications of the distinct dynamical behaviors. However, they did not provide a full characterization of the DPTs.

**DPT in Richardson-Gaudin models.** A similar mapping of the single-particle eigenstates of the harmonic trap onto a lattice in mode space, was used in a trapped gas of  $10^4$  ultracold fermionic potassium atoms. In this case the experiment observed a DPT predicted to exist in quenched s-wave superconductors described by Richardson-Gaudin models as explained in Sec. III. As we will discuss below this DPT has only been indirectly observed in real superconductors (see Sec. V A). The model that was simulated in the experiment [121] was a collective Heisenberg model, in which the non-local spin-spin couplings  $J_{ij}$  compete with an inhomogeneous axial

field set by  $h_i$ :

$$\hat{H} = \sum_i h_i \hat{S}_i^z - \sum_{i,j} J_{ij} \vec{\hat{S}}_i \cdot \vec{\hat{S}}_j. \quad (50)$$

The inhomogeneous axial field in mode space was generated by different harmonic confinement potentials experienced by the two internal hyperfine levels of  $^{40}\text{K}$ . The strength of the inhomogeneity was tuned in two ways. Using the polarization of one of the laser beams forming the optical trap one change the trapping frequency in a spin dependent manner. One can also change the temperature and therefore the distribution of the modes occupied by the atoms. Interatomic collisions were used to generate the exchange term. Due to the extended nature of the motional wave functions, the  $J_{ij}$  were again long-ranged. The mode-dependent coupling factor  $J_{ij}$  was controlled by tuning the s-wave scattering length of the colliding atoms using a magnetic Feshbach resonance [297]. The expected critical behavior was observed in the experiment as a function of the mean and thermally averaged interaction strength  $J = \left\langle \sum_{i,j} J_{ij} / N^2 \right\rangle_T$  and the axial field inhomogeneity  $\tilde{h} = \left\langle \sqrt{\sum_i h_i^2 / N - (\sum_i h_i / N)^2} \right\rangle_T$  where the indices  $i, j$  run over  $N$  populated modes (See Fig. 10d).

In the “all-to-all” limit, in which coupling constants are replaced by their mean value,  $J_{ij} \rightarrow J$ , the Hamiltonian becomes integrable and maps to the Bardeen-Cooper-Schrieffer Hamiltonian for fermionic superconductors expressed in terms of Anderson pseudospin discussed in Eq. (12) with  $h_i \rightarrow 2\varepsilon_i$  and  $J \rightarrow G$ . Note that at the level of mean field the extra term  $(\hat{S}^z) \rightarrow 2\hat{S}^z \langle \hat{S}^z \rangle$  acts as a simple collective rotation along  $z$  which does not modify the dynamics since  $\langle \hat{S}^z \rangle$  is conserved. Moreover this term can be removed by choosing an initial condition with  $\langle \hat{S}^z \rangle = 0$ .

Using the Lax analysis explained in Session IIIB, it is possible to obtain the dynamical phases of this model, characterized by the total transverse magnetization  $\mathcal{S}(t) = 2\sqrt{\langle \hat{S}^x \rangle^2 + \langle \hat{S}^y \rangle^2} / N$ . The initial conditions accessible in experiment, corresponding to a spin polarized state pointing along the  $x$  direction of the Bloch sphere is very similar to the simple example discussed in Sec.III C, but in 3D and with a different dispersion. In this case there is a DPT between the so called “phase I” below a critical coupling strength  $J_c$  where the order parameter quick decays to zero and “phase II” above  $J_c$  where the order parameter  $\mathcal{S}(t)$  exhibits transient oscillations at the frequency  $2|J|\mathcal{S}(\infty)$ , which slowly damp as  $\mathcal{S}(t)$  reaches  $\mathcal{S}(\infty)$  (See Eq. (21)). The oscillation frequency goes to zero at  $J_c$  in a non-analytic manner.

The experimental work described in Ref. [121] not only fully characterized the phase diagram but in addition determined the parameter regime where the spin model was valid. The latter was explicitly demonstrated via a many-body echo sequence that fully reversed the spin Hamiltonian. Terms in the Hamiltonian such as the kinetic

energy, assumed to play no role in the frozen mode approximation, were not reversed. The experiment indeed observed full reversibility of the dynamics in the collisionless regime where the spin model is expected to be valid, and non-reversibility otherwise.

Although the phase diagram was characterized for the first time in Ref. [121], the understanding that exchange interactions can stabilize coherence in a very useful way had been demonstrated experimentally years before. The experiments were carried out using thermal Rb atoms, which feature a very similar Hamiltonian than the potassium fermionic gas. Deep in phase II (dense sample) a coherence time up to 58 s was observed, while in phase I (dilute conditions) the coherence time decreased to at most 3 s [298–300].

Although the Toronto experiment Ref. [121] was able to observe the DPT between phase I and phase II, by simulating a spin model, phase III has not been observed yet.

Fermionic ultracold atomic gas experiments that can actually take advantage of the Fermi statistics of the atoms instead of an indirect mapping to Anderson pseudospins, in principle are an ideal platform for the observation of the dynamical phase diagram. However, unfortunately it has remained a challenge in cold atom experiments to reach conditions required to see BCS pairing. This is because both thermal and quantum fluctuations play a crucial role for quenches from the normal state for systems with a finite number  $N$  of Anderson pseudospins. Moreover, the control and manipulation of interactions in these systems, specially for the  $p$ -wave case, typically require Feshbach resonances. The latter unfortunately introduce strong three-body processes which make the gas unstable and destroy the desired pairing processes [111, 165–167].

Future progress on cooling these systems might allow new opportunities in that direction. An alternative option is the use of an ensemble of cold atoms trapped in an optical cavity. In this case effective Cooper pairs can be encoded in internal states of the atoms and attractive interactions between the internal levels can be realized via the exchange of virtual photons in the cavity. The control of the interaction strength via the parameters of the optical cavity combined with the tunability of the dispersion relation of the effective Cooper pairs via Stark shifts should allow for the near term exploration of the full dynamical phase diagram of the BCS model, as a function of system parameters and the prepared initial state [122]. Ref. [122] discusses a way to prepare the simple toy model discussed in Sec.III C in a cavity setup.

**DPT in multi-level systems.** Beyond two-level systems, DPTs have been also observed in spinor Bose-Einstein condensates (BEC) made of  $N \sim 10^5$   $^{23}\text{Na}$  atoms using the three Zeeman states of the lowest hyperfine level,  $m_F = 1, 0, -1$  [288, 289](See Fig. 10 e). The experiment operated in the regime where to an excel-

lent approximation atoms remained frozen in their single particle motional levels. Motional relaxation was only an issue at long times. Because all atoms in the BEC share the same motional level, in this limit the bosonic statistics enforces atoms to remain in the fully symmetric spin manifold. The Hamiltonian that describes the internal dynamics in the experiment therefore becomes a fully collective spin model:

$$H = \frac{c_2}{2N} \hat{\mathbf{S}} \cdot \hat{\mathbf{S}} + q \sum_i (\hat{S}_i^z)^2. \quad (51)$$

The first term encapsulates the spin dependent interactions, which are infinite-range in mode space even though the atomic collision interaction by itself is fully local. The second term describes a quadratic Zeeman field  $q$  experienced by the atoms from a real magnetic field plus a microwave dressing field. Here  $\hat{S}_{z,i}$  is the spin-1 operator for the  $i$ th particle along the  $z$  component of the Bloch sphere.

To observe the DPT, the experiment prepared the majority of the atoms in the  $m_F = 0$  level and then monitored the number of atoms remaining in that level  $N_0(t)$  as a function of time for different values of the control parameter  $q$ . The order parameter used in the experiment was the quantity  $A_{\text{dip}} \equiv 1 - N_0(t_{\text{dip}})$ , with  $N_0(t_{\text{dip}})$  being the value of  $N_0(t)$  at the first dip of the spin oscillations. For positive  $q > 0$ ,  $A_{\text{dip}}$  was observed to remain almost at 0. Across the DPT transition point of  $q_c = 0$ ,  $A_{\text{dip}}$  was seen to jump to finite value which decreased linearly with  $|q|$  when  $q < 0$  (See Fig. 10 e). Further work in this system was able to connect the DPT to an equilibrium phase transition not for the ground state but for the highest energy level in a subspace with zero spin magnetization [289].

Besides observations of DPT which happened at relatively short times, a follow-up experiment using Rb atoms instead of Na atoms observed another complementary type of universal non-equilibrium behavior associated with the emergence of non-thermal fixed points [224]. This type of behavior was observed at intermediate times satisfying two conditions: i) Times that are long enough to allow the frozen mode approximation used to observe the DPT to become invalid. In this case the system loses the information about the initial conditions due to motional relaxation. ii) Times that are not so long that lead the system to reach a quasi-stationary or an equilibrium situation. In this intermediate regime it was observed that the system develops a universal scaling behaviour in time and space. Physically the emergence of non-thermal fixed points have been attributed to the transport of an emergent collective conserved quantity towards low momentum scales. A similar behavior has been observed by another experiment in a single-component Bose gas [4, 225]. In both of these experiments it was experimentally confirmed (by preparing different initial conditions and obtaining the same scaling behaviour) that the observed non-thermal scaling phenomenon involved no fine-tuning of parameters.

It is clear from all the discussion presented above that ultra-cold atomic system are opening fantastic opportunities to probe DPTs and even more general non-equilibrium universal phenomena in controllable settings. While most of the observations so far have been guided by theory in conditions where either a mean field analysis is sufficient, or when exact calculations are possible, soon experiments will enter regimes intractable to theory. This may lead to the discovery of new forms of non-equilibrium phenomena not yet predicted by theory, pushing the field into even more exciting directions.

## VI. CONCLUSIONS

In this work we reviewed DPTs occurring in the large  $N$ ,  $\mathcal{N}$ , or  $d$  limit of a broad variety of models ranging from statistical mechanics (Ising models,  $\phi^4$  field theories) to condensed matter (Richardson-Gaudin magnets, strongly correlated fermions). We have also discussed numerous experimental platforms where the dynamics of these models can be realized (Sec. V). We have illustrated those regimes where experiments are well fitted by the theory presented in Secs. II and III, as well as the limits where descriptions beyond collision-less regimes may instead be required to describe experiments. Such platforms include trapped ions, cavity QED systems, and ultracold Bose and Fermi systems. They can be employed to demonstrate a broad variety of universality classes of DPTs in isolated quantum systems, and possibly study in the near future operational regimes where DPTs require a full quantum mechanical treatment and cannot be captured by an effective semi-classical description.

There are promising avenues for the future of pre-thermal collisionless DPTs. For instance, Rydberg simulators have been recently shown to be capable to access long-lived athermal states beyond the conventional pre-thermal paradigm [301, 302], referred as quantum scars [303] and defying the eigenstate thermalization hypothesis. This could be potentially employed in the near future to study forms of DPTs which cannot be characterized within a simple semi-classical description. Recent implementations of models with a fragmented Hilbert space using ultracold fermions [304] suggest similar lines of investigation in that context.

Another exciting direction, is the understanding of the fate of the DPTs in systems where quantum fluctuations cannot be ignored. At the theoretical level, it will be crucial to derive new types of order parameters that can describe the distinct dynamical behavior even when quantum effects start to play a role. The order parameters discussed in this review will decay in the ordered phase whenever quantum effects start to play a significant role. Can a properly defined order parameter, genuinely char-

acterize the underlying phases associated with a DPT? It is likely there is an affirmative answer to this question. Feasible candidates are observables that measure the interaction energy of the evolving system and therefore involve at the least two-body correlators, as illustrated by the case of the  $O(\mathcal{N} \rightarrow \infty)$  model in Sec. II C. Closely connected with this question is the robustness of the topological order in non-trivial phases in the presence of quantum effects. Is there a redefinition of the winding number that remains nonzero even in the presence of strong quantum fluctuations?

One of the most important goals of modern quantum science is to learn how to control and entangle many-body systems, and how to use it as a resource in quantum technologies, such as for the development of improved quantum sensors, materials and technologies. A big limitation in this direction comes from the fact that entangled states are difficult to prepare and maintain, since noise and decoherence rapidly collapse them into classical statistical mixtures. In the context of DPTs it is likely that the same parameter regime where interactions stabilize a finite order parameter is also promising for a generation of robust entanglement. In fact, recent investigations have pointed out the generation of robust spin squeezing in phase II [305]. Understanding the dynamics of entanglement across a DPT is a fascinating new direction [306, 307]. Is entanglement maximum at the critical point? What is the best entanglement witness for the state across the DPT?

While all these questions are theoretically extremely challenging, recent experimental advances in synthesizing, manipulating and detecting quantum many-body systems are bringing quantum control into a new paradigm [302, 308]. It is likely that near term experiments will stimulate new theoretical methods, which may provide unprecedented insight into novel classes of DPTs where strong quantum fluctuations play a key role in shaping the dynamical phases. We hope this review will encourage future work and investigations in this direction.

## VII. ACKNOWLEDGEMENTS

This project has been supported by the Deutsche Forschungsgemeinschaft (DFG, German Research Foundation) – Project-ID 429529648 – TRR 306 QuCoLiMa (“Quantum Cooperativity of Light and Matter”), ERC (starting grant No. 716648), AFOSR (FA9550-18-1-0319, FA9550-19-1-027), NSF QLCI OMA-2016244, NSF Phys-1734006, DOE National Quantum Information Science Research Centers (Quantum Systems Accelerator), and NIST.

---

[1] M. Henkel, H Hinrichsen, and S. Lübeck. *Non-Equilibrium Phase Transitions Vol. 1 and 2*. Springer,

Dordrecht, 2008.

- [2] J. Berges. Introduction to nonequilibrium quantum field theory. *AIP Conf. Proc.*, 739(1):3–62, 2005.
- [3] Michael Gring, Maximilian Kuhnert, Tim Langen, Takuya Kitagawa, Bernhard Rauer, Matthias Schreitl, Igor Mazets, D Adu Smith, Eugene Demler, and Jörg Schmiedmayer. Relaxation and prethermalization in an isolated quantum system. *Science*, 337(6100):1318–1322, 2012.
- [4] Tim Langen, Thomas Gasenzer, and Jörg Schmiedmayer. Prethermalization and universal dynamics in near-integrable quantum systems. *J. Stat. Mech.*, 2016(6):064009, 2016.
- [5] Marcus Kollar, F. Alexander Wolf, and Martin Eckstein. Generalized gibbs ensemble prediction of prethermalization plateaus and their relation to nonthermal steady states in integrable systems. *Phys. Rev. B*, 84:054304, Aug 2011.
- [6] F. H. L. Essler, S. Kehrein, S. R. Manmana, and N. J. Robinson. Quench dynamics in a model with tuneable integrability breaking. *Phys. Rev. B*, 89:165104, Apr 2014.
- [7] Bruno Bertini, Fabian H. L. Essler, Stefan Groha, and Neil J. Robinson. Prethermalization and thermalization in models with weak integrability breaking. *Phys. Rev. Lett.*, 115:180601, Oct 2015.
- [8] Matteo Marcuzzi, Jamir Marino, Andrea Gambassi, and Alessandro Silva. Prethermalization from a low-density holstein-primakoff expansion. *Physical Review B*, 94(21):214304, 2016.
- [9] Bruno Bertini, Fabian H. L. Essler, Stefan Groha, and Neil J. Robinson. Thermalization and light cones in a model with weak integrability breaking. *Phys. Rev. B*, 94:245117, Dec 2016.
- [10] Joseph Durnin, M. J. Bhaseen, and Benjamin Doyon. Nonequilibrium dynamics and weakly broken integrability. *Phys. Rev. Lett.*, 127:130601, Sep 2021.
- [11] Cheng-Ju Lin and Olexei I. Motrunich. Quasiparticle explanation of the weak-thermalization regime under quench in a nonintegrable quantum spin chain. *Phys. Rev. A*, 95:023621, Feb 2017.
- [12] Markus Heyl, Anatoli Polkovnikov, and Stefan Kehrein. Dynamical quantum phase transitions in the transverse-field ising model. *Physical review letters*, 110(13):135704, 2013.
- [13] P. Jurcevic, H. Shen, P. Hauke, C. Maier, T. Brydges, C. Hempel, B. P. Lanyon, M. Heyl, R. Blatt, and C. F. Roos. Direct observation of dynamical quantum phase transitions in an interacting many-body system. *Phys. Rev. Lett.*, 119:080501, Aug 2017.
- [14] Markus Heyl. Dynamical quantum phase transitions: A brief survey. *EPL (Europhysics Letters)*, 125(2):26001, 2019.
- [15] Jürgen Berges, Alexander Rothkopf, and Jonas Schmidt. Nonthermal fixed points: Effective weak coupling for strongly correlated systems far from equilibrium. *Physical Review Letters*, 101(4), Jul 2008.
- [16] Boris Nowak, Dénes Sexty, and Thomas Gasenzer. Superfluid turbulence: Nonthermal fixed point in an ultracold bose gas. *Physical Review B*, 84(2), Jul 2011.
- [17] Maximilian Prüfer, Philipp Kunkel, Helmut Strobel, Stefan Lannig, Daniel Linnemann, Christian-Marcel Schmied, Jürgen Berges, Thomas Gasenzer, and Markus K. Oberthaler. Observation of universal dynamics in a spinor bose gas far from equilibrium. *Nature*, 563(7730):217–220, Nov 2018.
- [18] Sebastian Erne, Robert Bücker, Thomas Gasenzer, Jürgen Berges, and Jörg Schmiedmayer. Universal dynamics in an isolated one-dimensional bose gas far from equilibrium. *Nature*, 563(7730):225–229, Nov 2018.
- [19] Christoph Eigen, Jake A. P. Glidden, Raphael Lopes, Eric A. Cornell, Robert P. Smith, and Zoran Hadzibabic. Universal prethermal dynamics of bose gases quenched to unitarity. *Nature*, 563(7730):221–224, Nov 2018.
- [20] Christian-Marcel Schmied, Aleksandr N. Mikheev, and Thomas Gasenzer. Non-thermal fixed points: Universal dynamics far from equilibrium. *International Journal of Modern Physics A*, 34(29):1941006, Oct 2019.
- [21] H. Haken. Cooperative phenomena in systems far from thermal equilibrium and in nonphysical systems. *Rev. Mod. Phys.*, 47:67–121, Jan 1975.
- [22] S. Chandrasekhar. *Hydrodynamic and Hydromagnetic Stability*. Clarendon, Oxford, 1968.
- [23] C. G. Chakrabarti, Sutapa Ghosh, and Syamali Bhadra. Non-equilibrium thermodynamics of lotka-volterra ecosystems: Stability and evolution. *Journal of Biological Physics*, 21(4):273–284, 1995.
- [24] P. Glansdorff and I. Prigogine. *Thermodynamic Theory of Structure, Stability and Fluctuations*. Wiley, New York, 1971.
- [25] LD Landau and EM Lifshitz. Statistical physics, 1969. *Google Scholar*, pages 237–241, 1969.
- [26] PC Hohenberg and AP Krekhov. An introduction to the ginzburg–landau theory of phase transitions and nonequilibrium patterns. *Physics Reports*, 572:1–42, 2015.
- [27] J. Berges, Sz. Borsányi, and C. Wetterich. Prethermalization. *Phys. Rev. Lett.*, 93:142002, Sep 2004.
- [28] J Zinn-Justin. *Quantum Field Theory and Critical Phenomena*. Oxford Clarendon Press, 1989.
- [29] Daniel J. Amit and Victor Martin-Mayor. *Field Theory, the Renormalization Group, and Critical Phenomena*. World Scientific, Singapore, third edition, 2005.
- [30] John Cardy and Uwe C. Täuber. Theory of branching and annihilating random walks. *Phys. Rev. Lett.*, 77:4780–4783, Dec 1996.
- [31] P. C. Hohenberg and B. I. Halperin. Theory of dynamic critical phenomena. *Rev. Mod. Phys.*, 49:435–479, Jul 1977.
- [32] Uwe C Täuber. *Critical Dynamics: a Field Theory Approach to Equilibrium and Non-Equilibrium Scaling Behavior*. Cambridge University Press, 2014.
- [33] A. Kamenev. *Field Theory of Non-Equilibrium Systems*. Cambridge University Press, 2011.
- [34] Pia Gagel, Peter P. Orth, and Jörg Schmalian. Universal postquench prethermalization at a quantum critical point. *Phys. Rev. Lett.*, 113:220401, Nov 2014.
- [35] L M Sieberer, M Buchhold, and S Diehl. Keldysh field theory for driven open quantum systems. *Reports on Progress in Physics*, 79(9):096001, 2016.
- [36] A. J. Glick, H. J. Lipkin, and N. Meshkov. Validity of many-body approximation methods for a solvable model. (III). Diagram summations. *Nuclear Physics*, 62(2):211–224, February 1965.
- [37] H. J. Lipkin, N. Meshkov, and A. J. Glick. Validity of many-body approximation methods for a solvable model. (I). Exact solutions and perturbation theory. *Nuclear Physics*, 62(2):188–198, February 1965.

- [38] N. Meshkov, A. J. Glick, and H. J. Lipkin. Validity of many-body approximation methods for a solvable model. (II). Linearization procedures. *Nuclear Physics*, 62(2):199–210, February 1965.
- [39] Feng Pan and J. P. Draayer. Analytical solutions for the LMG model. *Physics Letters B*, 451(1-2):1–10, April 1999.
- [40] J. Dukelsky, S. Pittel, and G. Sierra. Colloquium: Exactly solvable Richardson-Gaudin models for many-body quantum systems. *Reviews of Modern Physics*, 76(3):643–662, July 2004.
- [41] R. Botet and R. Jullien. Large-size critical behavior of infinitely coordinated systems. *Phys. Rev. B*, 28(7):3955–3967, October 1983.
- [42] Sébastien Dusuel and Julien Vidal. Finite-size scaling exponents and entanglement in the two-level BCS model. *Phys. Rev. A*, 71(6):060304, June 2005.
- [43] Pedro Ribeiro, Julien Vidal, and Rémy Mosseri. Thermodynamical limit of the lipkin-meshkov-glick model. *Phys. Rev. Lett.*, 99:050402, Aug 2007.
- [44] Pedro Ribeiro, Julien Vidal, and Rémy Mosseri. Exact spectrum of the lipkin-meshkov-glick model in the thermodynamic limit and finite-size corrections. *Physical Review E*, 78(2), Aug 2008.
- [45] Nicolò Defenu, Tobias Donner, Tommaso Macrì, Guido Pagano, Stefano Ruffo, and Andrea Trombettoni. Long-range interacting quantum systems. *arXiv preprint arXiv:2109.01063*, 2021.
- [46] José I Latorre, Román Orús, Enrique Rico, and Julien Vidal. Entanglement entropy in the lipkin-meshkov-glick model. *Physical Review A*, 71(6):064101, 2005.
- [47] Román Orús, Sébastien Dusuel, and Julien Vidal. Equivalence of critical scaling laws for many-body entanglement in the lipkin-meshkov-glick model. *Physical review letters*, 101(2):025701, 2008.
- [48] Somnath Maity, Utso Bhattacharya, and Amit Dutta. One-dimensional quantum many body systems with long-range interactions. *Journal of Physics A Mathematical General*, 53(1):013001, January 2020.
- [49] Michael Moekel and Stefan Kehrein. Interaction quench in the hubbard model. *Phys. Rev. Lett.*, 100:175702, May 2008.
- [50] Matteo Marcuzzi, Jamir Marino, Andrea Gambassi, and Alessandro Silva. Prethermalization in a nonintegrable quantum spin chain after a quench. *Physical review letters*, 111(19):197203, 2013.
- [51] N. Nessi, A. Iucci, and M. A. Cazalilla. Quantum quench and prethermalization dynamics in a two-dimensional fermi gas with long-range interactions. *Phys. Rev. Lett.*, 113:210402, Nov 2014.
- [52] Krishnanand Mallayya, Marcos Rigol, and Wojciech De Roeck. Prethermalization and thermalization in isolated quantum systems. *Phys. Rev. X*, 9:021027, May 2019.
- [53] Alessio Lerose, Bojan Žunkovič, Jamir Marino, Andrea Gambassi, and Alessandro Silva. Impact of nonequilibrium fluctuations on prethermal dynamical phase transitions in long-range interacting spin chains. *Physical Review B*, 99(4):045128, 2019.
- [54] J. Zhang, G. Pagano, P. W. Hess, A. Kyprianidis, P. Becker, H. Kaplan, A. V. Gorshkov, Z. X. Gong, and C. Monroe. Observation of a many-body dynamical phase transition with a 53-qubit quantum simulator. *Nature*, 551(7682):601–604, 2017.
- [55] Juan A. Muniz, Diego Barberena, Robert J. Lewis-Swan, Dylan J. Young, Julia R. K. Cline, Ana Maria Rey, and James K. Thompson. Exploring dynamical phase transitions with cold atoms in an optical cavity. *Nature*, 580(7805):602–607, Apr 2020.
- [56] Anjun Chu, Johannes Will, Jan Arlt, Carsten Klempf, and Ana Maria Rey. Simulation of  $xxz$  spin models using sideband transitions in trapped bosonic gases. *Phys. Rev. Lett.*, 125:240504, Dec 2020.
- [57] Anatoli Polkovnikov. Phase space representation of quantum dynamics. *Annals of Physics*, 325(8):1790–1852, 2010.
- [58] Arnab Das, K. Sengupta, Diptiman Sen, and Bikas K. Chakrabarti. Infinite-range ising ferromagnet in a time-dependent transverse magnetic field: Quench and ac dynamics near the quantum critical point. *Phys. Rev. B*, 74:144423, 2006.
- [59] Shane P Kelly, Eddy Timmermans, and S-W Tsai. Detecting macroscopic indefiniteness of cat states in bosonic interferometers. *Physical Review A*, 100(3):032117, 2019.
- [60] Shane P Kelly, Eddy Timmermans, and S-W Tsai. Thermalization and its breakdown for a large nonlinear spin. *Physical Review A*, 102(5):052210, 2020.
- [61] Bruno Scialla and Giulio Biroli. Dynamical transitions and quantum quenches in mean-field models. *Journal of Statistical Mechanics: Theory and Experiment*, 2011(11):P11003, 2011.
- [62] Nicolò Defenu, Tilman Enss, Michael Kastner, and Giovanna Morigi. Dynamical critical scaling of long-range interacting quantum magnets. *Phys. Rev. Lett.*, 121:240403, Dec 2018.
- [63] Tommaso Caneva, Rosario Fazio, and Giuseppe E. Santoro. Adiabatic quantum dynamics of the lipkin-meshkov-glick model. *Phys. Rev. B*, 78:104426, Sep 2008.
- [64] Alessio Lerose, Jamir Marino, Bojan Žunkovič, Andrea Gambassi, and Alessandro Silva. Chaotic dynamical ferromagnetic phase induced by nonequilibrium quantum fluctuations. *Physical review letters*, 120(13):130603, 2018.
- [65] Alessio Lerose, Jamir Marino, Andrea Gambassi, and Alessandro Silva. Prethermal quantum many-body kapitza phases of periodically driven spin systems. *Physical Review B*, 100(10):104306, 2019.
- [66] B. Žunkovič, A. Silva, and M. Fabrizio. Dynamical phase transitions and Loschmidt echo in the infinite-range XY model. *Phil. Trans. R. Soc., A* 374:20150160, 2016.
- [67] A. Gambassi and P. Calabrese. Quantum quenches as classical critical films. *Europhys. Lett.*, 95(6):66007, 2011.
- [68] Alberto Sartori, Jamir Marino, Sandro Stringari, and Alessio Recati. Spin-dipole oscillation and relaxation of coherently coupled bose-einstein condensates. *New Journal of Physics*, 17(9):093036, 2015.
- [69] Bojan Žunkovič, Markus Heyl, Michael Knap, and Alessandro Silva. Dynamical quantum phase transitions in spin chains with long-range interactions: Merging different concepts of nonequilibrium criticality. *Physical review letters*, 120(13):130601, 2018.
- [70] Jad C Halimeh, Valentin Zauner-Stauber, Ian P McCulloch, Ines De Vega, Ulrich Schollwöck, and Michael Kastner. Prethermalization and persistent order in the

- absence of a thermal phase transition. *Physical Review B*, 95(2):024302, 2017.
- [71] Jutho Haegeman, Christian Lubich, Ivan Oseledets, Bart Vandereycken, and Frank Verstraete. Unifying time evolution and optimization with matrix product states. *Physical Review B*, 94(16), Oct 2016.
- [72] Johannes Lang, Bernhard Frank, and Jad C. Halimeh. Concurrence of dynamical phase transitions at finite temperature in the fully connected transverse-field ising model. *Phys. Rev. B*, 97:174401, May 2018.
- [73] Paraj Titum and Mohammad F. Maghrebi. Nonequilibrium criticality in quench dynamics of long-range spin models. *Phys. Rev. Lett.*, 125:040602, Jul 2020.
- [74] Alessio Leroose and Silvia Pappalardi. Origin of the slow growth of entanglement entropy in long-range interacting spin systems. *Phys. Rev. Research*, 2:012041, Feb 2020.
- [75] Jad C. Halimeh, Maarten Van Damme, Lingzhen Guo, Johannes Lang, and Philipp Hauke. Dynamical phase transitions in quantum spin models with antiferromagnetic long-range interactions. *Phys. Rev. B*, 104:115133, Sep 2021.
- [76] Giulia Piccitto and Alessandro Silva. Crossover from fast to slow dynamics in a long range interacting ising chain. *Journal of Statistical Mechanics: Theory and Experiment*, 2019(9):094017, Sep 2019.
- [77] Nicolò Defenu, Tilman Enss, and Jad C. Halimeh. Dynamical criticality and domain-wall coupling in long-range hamiltonians. *Phys. Rev. B*, 100:014434, Jul 2019.
- [78] Steve Campbell. Criticality revealed through quench dynamics in the lipkin-meshkov-glick model. *Phys. Rev. B*, 94:184403, Nov 2016.
- [79] Amit Dutta and JK Bhattacharjee. Phase transitions in the quantum ising and rotor models with a long-range interaction. *Physical Review B*, 64(18):184106, 2001.
- [80] Alessandro Campa, Thierry Dauxois, and Stefano Ruffo. Statistical mechanics and dynamics of solvable models with long-range interactions. *Physics Reports*, 480(3-6):57–159, 2009.
- [81] Mohammad F. Maghrebi, Zhe-Xuan Gong, Michael Foss-Feig, and Alexey V Gorshkov. Causality and quantum criticality in long-range lattice models. *Physical Review B*, 93(12):125128, 2016.
- [82] Anatoli Polkovnikov, Krishnendu Sengupta, Alessandro Silva, and Mukund Vengalattore. *Colloquium : Nonequilibrium dynamics of closed interacting quantum systems*. *Rev. Mod. Phys.*, 83:863–883, Aug 2011.
- [83] T. Barthel and U. Schollwoeck. Dephasing and the steady state in quantum many-particle systems. *Phys. Rev. Lett.*, 100(10):100601, Mar 2008.
- [84] Marcos Rigol, Vanja Dunjko, and Maxim Olshanii. Thermalization and its mechanism for generic isolated quantum systems. *Nature*, 452(7189):854–858, 2008.
- [85] S. Sachdev. *Quantum Phase Transitions*. Cambridge University Press, 2011.
- [86] Shuai Yin and Shao-Kai Jian. Fermion-induced dynamical critical point. *Physical Review B*, 103(12):125116, 2021.
- [87] Shao-Kai Jian, Shuai Yin, and Brian Swingle. Universal prethermal dynamics in gross-neveu-yukawa criticality. *Physical review letters*, 123(17):170606, 2019.
- [88] Anushya Chandran, Arun Nanduri, S. S. Gubser, and S. L. Sondhi. Equilibration and coarsening in the quantum  $o(n)$  model at infinite  $n$ . *Phys. Rev. B*, 88:024306, Jul 2013.
- [89] Anna Maraga, Alessio Chiocchetta, Aditi Mitra, and Andrea Gambassi. Aging and coarsening in isolated quantum systems after a quench: Exact results for the quantum  $O(n)$  model with  $n \rightarrow \infty$ . *Phys. Rev. E*, 92:042151, Oct 2015.
- [90] J. Berges, N. Tetradis, and C. Wetterich. Non-perturbative renormalization flow in quantum field theory and statistical physics. *Phys. Rep.*, 363:223–386, 2002.
- [91] Spyros Sotiriadis and John Cardy. Quantum quench in interacting field theory: A self-consistent approximation. *Phys. Rev. B*, 81:134305, Apr 2010.
- [92] Bruno Sciolla and Giulio Biroli. Quantum quenches, dynamical transitions, and off-equilibrium quantum criticality. *Phys. Rev. B*, 88:201110, Nov 2013.
- [93] Pietro Smacchia, Michael Knap, Eugene Demler, and Alessandro Silva. Exploring dynamical phase transitions and prethermalization with quantum noise of excitations. *Phys. Rev. B*, 91:205136, May 2015.
- [94] Alessio Chiocchetta, Marco Tavora, Andrea Gambassi, and Aditi Mitra. Short-time universal scaling and light-cone dynamics after a quench in an isolated quantum system in  $d$  spatial dimensions. *Phys. Rev. B*, 94:134311, Oct 2016.
- [95] Jad C. Halimeh and Mohammad F. Maghrebi. Quantum aging and dynamical universality in the long-range  $o$  model. *Physical Review E*, 103(5):052142, 2021.
- [96] Gert Aarts, Gian Franco Bonini, and Christof Wetterich. Exact and truncated dynamics in nonequilibrium field theory. *Phys. Rev. D*, 63:025012, Dec 2000.
- S. L. Sondhi, S. M. Girvin, J. P. Carini, and D. Shashar. Continuous quantum phase transitions. *Rev. Mod. Phys.*, 69:315–333, Jan 1997.
- M. Vojta. Quantum phase transitions. *Rep. Prog. Phys.*, 66:2069, 2003.
- [97] Alessio Chiocchetta, Marco Tavora, Andrea Gambassi, and Aditi Mitra. Short-time universal scaling in an isolated quantum system after a quench. *Phys. Rev. B*, 91:220302, Jun 2015.
- [98] H.-K. Janssen, B. Schaub, and B. Schmittmann. New universal short-time scaling behaviour of critical relaxation processes. *Z. Phys. B Cond. Mat.*, 73(4):539–549, 1989.
- [99] Pasquale Calabrese and Andrea Gambassi. Ageing properties of critical systems. *J. Phys. A: Math. Gen.*, 38(18):R133, 2005.
- [100] L. M. Sieberer, M. Buchhold, and S. Diehl. Keldysh Field Theory for Driven Open Quantum Systems. *arXiv:1512.00637*, 2015.
- [101] Alessio Chiocchetta, Andrea Gambassi, Sebastian Diehl, and Jamir Marino. Dynamical crossovers in prethermal critical states. *Physical review letters*, 118(13):135701, 2017.
- [102] Alan J Bray. Theory of phase-ordering kinetics. *Adv. Phys.*, 43(3):357–459, 1994.
- [103] G. Biroli. Slow Relaxations and Non-Equilibrium Dynamics in Classical and Quantum Systems. *arXiv:1507.05858*, 2015.
- [104] Leticia F. Cugliandolo. Coarsening phenomena. *C. R. Phys.*, 16(3):257 – 266, 2015.
- [105] Anna Maraga, Pietro Smacchia, and Alessandro Silva. Linear ramps of the mass in the  $o(n)$  model: Dynamical transition and quantum noise of excitations. *Physical*

- Review B*, 94(24):245122, 2016.
- [106] R. A. Barankov, L. S. Levitov, and B. Z. Spivak. Collective rabi oscillations and solitons in a time-dependent bcs pairing problem. *Phys. Rev. Lett.*, 93:160401, Oct 2004.
- [107] R. A. Barankov and L. S. Levitov. Synchronization in the bcs pairing dynamics as a critical phenomenon. *Phys. Rev. Lett.*, 96:230403, Jun 2006.
- [108] Emil A. Yuzbashyan and Maxim Dzero. Dynamical vanishing of the order parameter in a fermionic condensate. *Phys. Rev. Lett.*, 96:230404, Jun 2006.
- [109] Emil A. Yuzbashyan, Oleksandr Tsypliyatayev, and Boris L. Altshuler. Relaxation and persistent oscillations of the order parameter in fermionic condensates. *Phys. Rev. Lett.*, 96:097005, Mar 2006.
- [110] Matthew S. Foster, Maxim Dzero, Victor Gurarie, and Emil A. Yuzbashyan. Quantum quench in a  $p + ip$  superfluid: Winding numbers and topological states far from equilibrium. *Phys. Rev. B*, 88:104511, Sep 2013.
- [111] Matthew S. Foster, Victor Gurarie, Maxim Dzero, and Emil A. Yuzbashyan. Quench-induced floquet topological  $p$ -wave superfluids. *Phys. Rev. Lett.*, 113:076403, Aug 2014.
- [112] Jason Alicea. New directions in the pursuit of majorana fermions in solid state systems. *Reports on Progress in Physics*, 75(7):076501, Jun 2012.
- [113] Qijin Chen, Jelena Stajic, Shina Tan, and K. Levin. Bcs–bec crossover: From high temperature superconductors to ultracold superfluids. *Physics Reports*, 412(1):1–88, 2005.
- [114] Ryusuke Matsunaga, Yuki I. Hamada, Kazumasa Makise, Yoshinori Uzawa, Hirotaka Terai, Zhen Wang, and Ryo Shimano. Higgs amplitude mode in the bcs superconductors  $nb_{1-x}ti_xN$  induced by terahertz pulse excitation. *Phys. Rev. Lett.*, 111:057002, Jul 2013.
- [115] Ryo Shimano and Naoto Tsuji. Higgs mode in superconductors. *Annual Review of Condensed Matter Physics*, 11(1):103–124, 2020.
- [116] T. Papenkort, V. M. Axt, and T. Kuhn. Coherent dynamics and pump-probe spectra of bcs superconductors. *Phys. Rev. B*, 76:224522, Dec 2007.
- [117] T. Papenkort, T. Kuhn, and V. M. Axt. Coherent control of the gap dynamics of bcs superconductors in the nonadiabatic regime. *Phys. Rev. B*, 78:132505, Oct 2008.
- [118] H. Krull, D. Manske, G. S. Uhrig, and A. P. Schnyder. Signatures of nonadiabatic bcs state dynamics in pump-probe conductivity. *Phys. Rev. B*, 90:014515, Jul 2014.
- [119] Yang-Zhi Chou, Yunxiang Liao, and Matthew S. Foster. Twisting anderson pseudospins with light: Quench dynamics in terahertz-pumped bcs superconductors. *Phys. Rev. B*, 95:104507, Mar 2017.
- [120] T Papenkort, T Kuhn, and V M Axt. Nonequilibrium dynamics and coherent control of BCS superconductors driven by ultrashort THz pulses. *Journal of Physics: Conference Series*, 193:012050, Nov 2009.
- [121] Scott Smale, Peiru He, Ben A Olsen, Kenneth G Jackson, Haile Sharum, Stefan Trotzky, Jamir Marino, Ana Maria Rey, and Joseph H Thywissen. Observation of a transition between dynamical phases in a quantum degenerate fermi gas. *Sci. Adv.*, 5(8):eaax1568, 2019.
- [122] Robert J. Lewis-Swan, Diego Barberena, Julia R. K. Cline, Dylan J. Young, James K. Thompson, and Ana Maria Rey. Cavity-qed quantum simulator of dynamical phases of a bardeen-cooper-schrieffer superconductor. *Phys. Rev. Lett.*, 126:173601, Apr 2021.
- [123] E. A. Yuzbashyan, M. Dzero, V. Gurarie, and M. S. Foster. Quantum quench phase diagrams of an  $s$ -wave bcs–bec condensate. *Phys. Rev. A*, 91:033628, Mar 2015.
- [124] V. Gurarie and L. Radzhikovsky. Resonantly paired fermionic superfluids. *Annals of Physics*, 322(1):2–119, 2007. January Special Issue 2007.
- [125] V. Gurarie. Nonequilibrium dynamics of weakly and strongly paired superconductors. *Phys. Rev. Lett.*, 103:075301, Aug 2009.
- [126] Maxim Dzero, Maxim Khodas, and Alex Levchenko. Amplitude modes and dynamic coexistence of competing orders in multicomponent superconductors. *Phys. Rev. B*, 91:214505, Jun 2015.
- [127] Yunxiang Liao and Matthew S. Foster. Spectroscopic probes of isolated nonequilibrium quantum matter: Quantum quenches, floquet states, and distribution functions. *Phys. Rev. A*, 92:053620, Nov 2015.
- [128] R.W. Richardson and N. Sherman. Exact eigenstates of the pairing-force hamiltonian. *Nuclear Physics*, 52:221–238, 1964.
- [129] R.W. Richardson and N. Sherman. Pairing models of pb206, pb204 and pb202. *Nuclear Physics*, 52:253–268, 1964.
- [130] Michel Gaudin. *The Bethe Wavefunction*. Cambridge University Press, 2014.
- [131] J. Dukelsky, S. Pittel, and G. Sierra. Colloquium: Exactly solvable Richardson-Gaudin models for many-body quantum systems. *Rev. Mod. Phys.*, 76:643–662, 2004.
- [132] R.W. Richardson. New class of solvable and integrable many-body models, 2002.
- [133] T. Skrypnik. Non-skew-symmetric classical r-matrices, algebraic bethe ansatz, and bardeen–cooper–schrieffer-type integrable systems. *Journal of Mathematical Physics*, 50(3):033504, 2009.
- [134] Miguel Ibañez, Jon Links, Germán Sierra, and Shao-You Zhao. Exactly solvable pairing model for superconductors with  $p_x + ip_y$ -wave symmetry. *Phys. Rev. B*, 79:180501, May 2009.
- [135] Clare Dunning, Miguel Ibañez, Jon Links, Germán Sierra, and Shao-You Zhao. Exact solution of the  $p + ip$  pairing hamiltonian and a hierarchy of integrable models. *Journal of Statistical Mechanics: Theory and Experiment*, 2010(08):P08025, Aug 2010.
- [136] Stefan M. A. Rombouts, Jorge Dukelsky, and Gerardo Ortiz. Quantum phase diagram of the integrable  $p_x + ip_y$  fermionic superfluid. *Phys. Rev. B*, 82:224510, Dec 2010.
- [137] Emil A Yuzbashyan, Boris L Altshuler, Vadim B Kuznetsov, and Victor Z Enolskii. Solution for the dynamics of the BCS and central spin problems. *Journal of Physics A: Mathematical and General*, 38(36):7831–7849, Aug 2005.
- [138] Emil A. Yuzbashyan, Boris L. Altshuler, Vadim B. Kuznetsov, and Victor Z. Enolskii. Nonequilibrium cooper pairing in the nonadiabatic regime. *Phys. Rev. B*, 72:220503, Dec 2005.
- [139] R. A. Barankov and L. S. Levitov. Excitation of the dissipationless higgs mode in a fermionic condensate, 2007.
- [140] Emil A. Yuzbashyan and Oleksandr Tsypliyatayev. Dynamics of emergent cooper pairing at finite temperatures. *Phys. Rev. B*, 79:132504, Apr 2009.

- [141] M. Dzero, E. A. Yuzbashyan, and B. L. Altshuler. Cooper pair turbulence in atomic fermi gases. *EPL (Europhysics Letters)*, 85(2):20004, jan 2009.
- [142] Jasen A. Scaramazza, Pietro Smacchia, and Emil A. Yuzbashyan. Consequences of integrability breaking in quench dynamics of pairing hamiltonians. *Phys. Rev. B*, 99:054520, Feb 2019.
- [143] Yonah Lemonik and Aditi Mitra. Time-resolved spectral density of interacting fermions following a quench to a superconducting critical point. *Phys. Rev. B*, 96:104506, Sep 2017.
- [144] Yonah Lemonik and Aditi Mitra. Model predictions for time-resolved transport measurements made near the superfluid critical points of cold atoms and  $k_3c_{60}$  films. *Phys. Rev. Lett.*, 121:067001, Aug 2018.
- [145] Yonah Lemonik and Aditi Mitra. Quench dynamics of superconducting fluctuations and optical conductivity in a disordered system. *Phys. Rev. B*, 98:214514, Dec 2018.
- [146] Yonah Lemonik and Aditi Mitra. Transport and spectral signatures of transient fluctuating superfluids in the absence of long-range order. *Phys. Rev. B*, 100:094503, Sep 2019.
- [147] Takashi Oka and Sota Kitamura. Floquet engineering of quantum materials. *Annual Review of Condensed Matter Physics*, 10(1):387–408, 2019.
- [148] Xiao-Liang Qi and Shou-Cheng Zhang. Topological insulators and superconductors. *Rev. Mod. Phys.*, 83:1057–1110, Oct 2011.
- [149] Fenner Harper, Rahul Roy, Mark S. Rudner, and S.L. Sondhi. Topology and broken symmetry in floquet systems. *Annual Review of Condensed Matter Physics*, 11(1):345–368, 2020.
- [150] J.R. Schrieffer. *Theory Of Superconductivity*. CRC Press, 2018.
- [151] P. W. Anderson. Random-phase approximation in the theory of superconductivity. *Phys. Rev.*, 112:1900, 1958.
- [152] Instead of an  $N$ -fold spin product (spin coherent) state, one can also consider a state with  $P \leq N$  “blocked” levels. These are states that possess a single fermion occupying one state of a Cooper pair. For the reduced BCS Hamiltonian in Eq. (12), blocked levels completely decouple from the time-evolution of the pseudospins (which are superpositions of doubly empty and occupied states of a Cooper pair).
- [153] Ehud Altman, Eugene Demler, and Mikhail D. Lukin. Probing many-body states of ultracold atoms via noise correlations. *Phys. Rev. A*, 70:013603, Jul 2004.
- [154] Simon Fölling, Fabrice Gerbier, Artur Widera, Olaf Mandel, Tatjana Gericke, and Immanuel Bloch. Spatial quantum noise interferometry in expanding ultracold atom clouds. *Nature*, 434(7032):481–484, 2005.
- [155] T. Rom, Th Best, D. van Oosten, U. Schneider, S. Fölling, B. Paredes, and I. Bloch. Free fermion antibunching in a degenerate atomic fermi gas released from an optical lattice. *Nature*, 444(7120):733–736, 2006.
- [156] Christopher Stahl and Martin Eckstein. Noise correlations in time- and angle-resolved photoemission spectroscopy. *Phys. Rev. B*, 99:241111, Jun 2019.
- [157] A. F. Volkov and Sh. M. Kogan. Collisionless relaxation of the energy gap in superconductors. *JETP*, 38:1018, 1974. [Russian original - Zh. Eksp. Teor. Fiz. **65**, 2038 (1973)].
- [158] Francesco Peronaci, Marco Schiró, and Massimo Capone. Transient dynamics of  $d$ -wave superconductors after a sudden excitation. *Phys. Rev. Lett.*, 115:257001, Dec 2015.
- [159] X. Zhang, V. Gurarie, and M. S. Foster. *unpublished*.
- [160] M. Dzero, E. A. Yuzbashyan, B. L. Altshuler, and P. Coleman. Spectroscopic signatures of nonequilibrium pairing in atomic fermi gases. *Phys. Rev. Lett.*, 99:160402, Oct 2007.
- [161] D. M. Kennes, E. Y. Wilner, D. R. Reichman, and A. J. Millis. Nonequilibrium optical conductivity: General theory and application to transient phases. *Phys. Rev. B*, 96:054506, Aug 2017.
- [162] Emil A. Yuzbashyan. Normal and anomalous solitons in the theory of dynamical cooper pairing. *Phys. Rev. B*, 78:184507, Nov 2008.
- [163] M. Mootz, J. Wang, and I. E. Perakis. Lightwave terahertz quantum manipulation of nonequilibrium superconductor phases and their collective modes. *Phys. Rev. B*, 102:054517, Aug 2020.
- [164] Gia-Wei Chern and Kipton Barros. Nonequilibrium dynamics of superconductivity in the attractive hubbard model. *Phys. Rev. B*, 99:035162, Jan 2019.
- [165] J. Zhang, E. G. M. van Kempen, T. Bourdel, L. Khaykovich, J. Cubizolles, F. Chevy, M. Teichmann, L. Tarruell, S. J. J. M. F. Kokkelmans, and C. Salomon.  $p$ -wave feshbach resonances of ultracold  ${}^6\text{Li}$ . *Phys. Rev. A*, 70:030702, Sep 2004.
- [166] M. Jona-Lasinio, L. Pricoupenko, and Y. Castin. Three fully polarized fermions close to a  $p$ -wave feshbach resonance. *Phys. Rev. A*, 77:043611, Apr 2008.
- [167] J. Levinsen, N. R. Cooper, and V. Gurarie. Stability of fermionic gases close to a  $p$ -wave feshbach resonance. *Phys. Rev. A*, 78:063616, Dec 2008.
- [168] M. Tinkham. *Introduction to Superconductivity: Second Edition*. Dover Books on Physics. Dover Publications, 2004.
- [169] Chetan Nayak, Steven H. Simon, Ady Stern, Michael Freedman, and Sankar Das Sarma. Non-abelian anyons and topological quantum computation. *Rev. Mod. Phys.*, 80:1083–1159, Sep 2008.
- [170] G.E Volovik. *The Universe in a Helium Droplet*. International Series of Monographs on Physics. Clarendon Press, 2003.
- [171] Takeshi Mizushima, Yasumasa Tsutsumi, Takuto Kawakami, Masatoshi Sato, Masanori Ichioka, and Kazushige Machida. Symmetry-protected topological superfluids and superconductors —from the basics to  ${}^3\text{He}$ —. *Journal of the Physical Society of Japan*, 85(2):022001, 2016.
- [172] Luca D’Alessio and Marcos Rigol. Dynamical preparation of floquet chern insulators. *Nature Communications*, 6:8336, Oct 2015.
- [173] M. D. Caio, N. R. Cooper, and M. J. Bhaseen. Quantum quenches in chern insulators. *Phys. Rev. Lett.*, 115:236403, Dec 2015.
- [174] A Bermudez, L Amico, and M A Martin-Delgado. Dynamical delocalization of majorana edge states by sweeping across a quantum critical point. *New Journal of Physics*, 12(5):055014, may 2010.
- [175] E. Perfetto. Dynamical formation and manipulation of majorana fermions in driven quantum wires in contact with a superconductor. *Phys. Rev. Lett.*, 110:087001, Feb 2013.

- [176] P. D. Sacramento. Fate of majorana fermions and chern numbers after a quantum quench. *Phys. Rev. E*, 90:032138, Sep 2014.
- [177] G. Kells, D. Sen, J. K. Slingerland, and S. Vishveshwara. Topological blocking in quantum quench dynamics. *Phys. Rev. B*, 89:235130, Jun 2014.
- [178] Justin H. Wilson, Justin C. W. Song, and Gil Refael. Remnant geometric hall response in a quantum quench. *Phys. Rev. Lett.*, 117:235302, Nov 2016.
- [179] Ying Hu, Peter Zoller, and Jan Carl Budich. Dynamical buildup of a quantized hall response from nontopological states. *Phys. Rev. Lett.*, 117:126803, Sep 2016.
- [180] Wei Sun, Chang-Rui Yi, Bao-Zong Wang, Wei-Wei Zhang, Barry C. Sanders, Xiao-Tian Xu, Zong-Yao Wang, Joerg Schmiedmayer, Youjin Deng, Xiong-Jun Liu, Shuai Chen, and Jian-Wei Pan. Uncover topology by quantum quench dynamics. *Phys. Rev. Lett.*, 121:250403, Dec 2018.
- [181] N. R. Cooper, J. Dalibard, and I. B. Spielman. Topological bands for ultracold atoms. *Rev. Mod. Phys.*, 91:015005, Mar 2019.
- [182] Deepak Iyer and Matthew S. Foster. Topological quantum control: Edge currents via floquet depinning of skyrmions in the  $\nu = 0$  graphene quantum hall antiferromagnet. *Phys. Rev. B*, 101:241403, Jun 2020.
- [183] Ying Dong, Lin Dong, Ming Gong, and Han Pu. Dynamical phases in quenched spin-orbit-coupled degenerate fermi gas. *Nature Communications*, 6:6103, Jan 2015.
- [184] Maxim Dzero, Ammar A. Kirmani, and Emil A. Yuzbashyan. Nonadiabatic dynamics of superfluid spin-orbit-coupled degenerate fermi gas. *Phys. Rev. A*, 92:053626, Nov 2015.
- [185] Ezyo Stouten, Pieter W. Claeys, Jean-Sébastien Caux, and Vladimir Gritsev. Integrability and duality in spin chains. *Phys. Rev. B*, 99:075111, Feb 2019.
- [186] Aidan Zabalo and Emil A. Yuzbashyan. Time reversal symmetry protected chaotic fixed point in the quench dynamics of a topological  $p$ -wave superfluid, 2021.
- [187] Anatoli Polkovnikov, Krishnendu Sengupta, Alessandro Silva, and Mukund Vengalattore. Colloquium: Nonequilibrium dynamics of closed interacting quantum systems. *Rev. Mod. Phys.*, 83:863–883, Aug 2011.
- [188] Walter Metzner and Dieter Vollhardt. Correlated lattice fermions in  $d = \infty$  dimensions. *Phys. Rev. Lett.*, 62:324–327, Jan 1989.
- [189] Fabien Alet and Nicolas Laflorencie. Many-body localization: An introduction and selected topics. *Comptes Rendus Physique*, 19(6):498–525, 2018.
- [190] Rahul Nandkishore and David A. Huse. Many-body localization and thermalization in quantum statistical mechanics. *Annual Review of Condensed Matter Physics*, 6(1):15–38, 2015.
- [191] Dmitry A. Abanin, Ehud Altman, Immanuel Bloch, and Maksym Serbyn. Colloquium: Many-body localization, thermalization, and entanglement. *Rev. Mod. Phys.*, 91:021001, May 2019.
- [192] S. A. Parameswaran, A. C. Potter, and R. Vasseur. Eigenstate phase transitions and the emergence of universal dynamics in highly excited states. *Ann. Phys. (Berlin)*, 529:1600302, 2017.
- [193] Giuseppe Carleo, Federico Becca, Marco Schiró, and Michele Fabrizio. Localization and glassy dynamics of many-body quantum systems. *Scientific Reports*, 2(1):243, 2012.
- [194] A. Smith, J. Knolle, R. Moessner, and D. L. Kovrizhin. Absence of ergodicity without quenched disorder: From quantum disentangled liquids to many-body localization. *Phys. Rev. Lett.*, 119:176601, Oct 2017.
- [195] A. Smith, J. Knolle, D. L. Kovrizhin, and R. Moessner. Disorder-free localization. *Phys. Rev. Lett.*, 118:266601, Jun 2017.
- [196] N. Y. Yao, C. R. Laumann, J. I. Cirac, M. D. Lukin, and J. E. Moore. Quasi-many-body localization in translation-invariant systems. *Phys. Rev. Lett.*, 117:240601, Dec 2016.
- [197] Alexios A. Michailidis, Marko Žnidarič, Mariya Medvedyeva, Dmitry A. Abanin, Tomaž Prosen, and Z. Papić. Slow dynamics in translation-invariant quantum lattice models. *Phys. Rev. B*, 97:104307, Mar 2018.
- [198] Zhihao Lan, Merlijn van Horssen, Stephen Powell, and Juan P. Garrahan. Quantum slow relaxation and metastability due to dynamical constraints. *Phys. Rev. Lett.*, 121:040603, Jul 2018.
- [199] Merlijn van Horssen, Emanuele Levi, and Juan P. Garrahan. Dynamics of many-body localization in a translation-invariant quantum glass model. *Phys. Rev. B*, 92:100305, Sep 2015.
- [200] Sebastian Scherg, Thomas Kohlert, Pablo Sala, Frank Pollmann, Bharath Hebbe Madhusudhana, Immanuel Bloch, and Monika Aidelsburger. Observing non-ergodicity due to kinetic constraints in tilted fermi-hubbard chains. *Nature Communications*, 12(1):4490, 2021.
- [201] Thomas Iadecola and Marko Žnidarič. Exact localized and ballistic eigenstates in disordered chaotic spin ladders and the fermi-hubbard model. *Phys. Rev. Lett.*, 123:036403, Jul 2019.
- [202] Oskar Vafek, Nicolas Regnault, and B. Andrei Bernevig. Entanglement of Exact Excited Eigenstates of the Hubbard Model in Arbitrary Dimension. *SciPost Phys.*, 3:043, 2017.
- [203] C. J. Turner, A. A. Michailidis, D. A. Abanin, M. Serbyn, and Z. Papić. Weak ergodicity breaking from quantum many-body scars. *Nature Physics*, 14(7):745–749, 2018.
- [204] Soonwon Choi, Christopher J. Turner, Hannes Pichler, Wen Wei Ho, Alexios A. Michailidis, Zlatko Papić, Maksym Serbyn, Mikhail D. Lukin, and Dmitry A. Abanin. Emergent su(2) dynamics and perfect quantum many-body scars. *Phys. Rev. Lett.*, 122:220603, Jun 2019.
- [205] Wen Wei Ho, Soonwon Choi, Hannes Pichler, and Mikhail D. Lukin. Periodic orbits, entanglement, and quantum many-body scars in constrained models: Matrix product state approach. *Phys. Rev. Lett.*, 122:040603, Jan 2019.
- [206] E. Müller-Hartmann. Correlated fermions on a lattice in high dimensions. *Zeitschrift für Physik B Condensed Matter*, 74(4):507–512, 1989.
- [207] Antoine Georges, Gabriel Kotliar, Werner Krauth, and Marcelo J. Rozenberg. Dynamical mean-field theory of strongly correlated fermion systems and the limit of infinite dimensions. *Rev. Mod. Phys.*, 68:13–125, Jan 1996.
- [208] Antoine Georges and Gabriel Kotliar. Hubbard model in infinite dimensions. *Phys. Rev. B*, 45:6479–6483, Mar 1992.

- [209] Schmidt P. and Monien H. Nonequilibrium dynamical mean-field theory of a strongly correlated system.
- [210] J. K. Freericks, V. M. Turkowski, and V. Zlatić. Nonequilibrium dynamical mean-field theory. *Phys. Rev. Lett.*, 97:266408, Dec 2006.
- [211] Hideo Aoki, Naoto Tsuji, Martin Eckstein, Marcus Kollar, Takashi Oka, and Philipp Werner. Nonequilibrium dynamical mean-field theory and its applications. *Rev. Mod. Phys.*, 86:779–837, Jun 2014.
- [212] Enrico Arrigoni, Michael Knap, and Wolfgang von der Linden. Nonequilibrium dynamical mean-field theory: An auxiliary quantum master equation approach. *Phys. Rev. Lett.*, 110:086403, Feb 2013.
- [213] A. V. Joura, J. K. Freericks, and Th. Pruschke. Steady-state nonequilibrium density of states of driven strongly correlated lattice models in infinite dimensions. *Phys. Rev. Lett.*, 101:196401, Nov 2008.
- [214] Orazio Scarlattella, Aashish A. Clerk, Rosario Fazio, and Marco Schiró. Dynamical mean-field theory for markovian open quantum many-body systems. *Phys. Rev. X*, 11:031018, Jul 2021.
- [215] Naoto Tsuji, Takashi Oka, and Hideo Aoki. Correlated electron systems periodically driven out of equilibrium: Floquet + DMFT formalism. *Phys. Rev. B*, 78:235124, Dec 2008.
- [216] Philipp Werner, Takashi Oka, and Andrew J. Millis. Diagrammatic monte carlo simulation of nonequilibrium systems. *Phys. Rev. B*, 79:035320, Jan 2009.
- [217] F. Alexander Wolf, Ian P. McCulloch, and Ulrich Schollwöck. Solving nonequilibrium dynamical mean-field theory using matrix product states. *Phys. Rev. B*, 90:235131, Dec 2014.
- [218] Naoto Tsuji and Philipp Werner. Nonequilibrium dynamical mean-field theory based on weak-coupling perturbation expansions: Application to dynamical symmetry breaking in the hubbard model. *Phys. Rev. B*, 88:165115, Oct 2013.
- [219] Martin Eckstein and Philipp Werner. Nonequilibrium dynamical mean-field calculations based on the non-crossing approximation and its generalizations. *Phys. Rev. B*, 82:115115, Sep 2010.
- [220] Naoto Tsuji, Martin Eckstein, and Philipp Werner. Nonthermal antiferromagnetic order and nonequilibrium criticality in the hubbard model. *Phys. Rev. Lett.*, 110:136404, Mar 2013.
- [221] Matteo Sandri and Michele Fabrizio. Nonequilibrium dynamics in the antiferromagnetic hubbard model. *Phys. Rev. B*, 88:165113, Oct 2013.
- [222] Jürgen Berges, Alexander Rothkopf, and Jonas Schmidt. Nonthermal fixed points: Effective weak coupling for strongly correlated systems far from equilibrium. *Phys. Rev. Lett.*, 101:041603, Jul 2008.
- [223] Boris Nowak, Jan Schole, and Thomas Gasenzer. Universal dynamics on the way to thermalization. *New Journal of Physics*, 16(9):093052, 2014.
- [224] Maximilian Prüfer, Philipp Kunkel, Helmut Strobel, Stefan Lannig, Daniel Linnemann, Christian-Marcel Schmied, Jürgen Berges, Thomas Gasenzer, and Markus K. Oberthaler. Observation of universal dynamics in a spinor bose gas far from equilibrium. *Nature*, 563(7730):217–220, 2018.
- [225] Sebastian Erne, Robert Bücker, Thomas Gasenzer, Jürgen Berges, and Jörg Schmiedmayer. Universal dynamics in an isolated one-dimensional bose gas far from equilibrium. *Nature*, 563(7730):225–229, 2018.
- [226] Antonio Picano and Martin Eckstein. Accelerated gap collapse in a slater antiferromagnet. *Phys. Rev. B*, 103:165118, Apr 2021.
- [227] M. Stark and M. Kollar. Kinetic description of thermalization dynamics in weakly interacting quantum systems. *arXiv:1308.1610*, 2013.
- [228] Luca D’Alessio, Yariv Kafri, Anatoli Polkovnikov, and Marcos Rigol. From quantum chaos and eigenstate thermalization to statistical mechanics and thermodynamics. *Adv. Phys.*, 65(3):239–362, 2016.
- [229] Krishnanand Mallayya, Marcos Rigol, and Wojciech De Roeck. Prethermalization and thermalization in isolated quantum systems. *Phys. Rev. X*, 9:021027, May 2019.
- [230] Karsten Balzer, F. Alexander Wolf, Ian P. McCulloch, Philipp Werner, and Martin Eckstein. Nonthermal melting of néel order in the hubbard model. *Phys. Rev. X*, 5:031039, Sep 2015.
- [231] S. Trotzky, Y-A. Chen, A. Flesch, I. P. McCulloch, U. Schollwöck, J. Eisert, and I. Bloch. Probing the relaxation towards equilibrium in an isolated strongly correlated one-dimensional bose gas. *Nature Physics*, 8(4):325–330, 2012.
- [232] Corinna Kollath, Andreas M. Läuchli, and Ehud Altman. Quench dynamics and nonequilibrium phase diagram of the bose-hubbard model. *Phys. Rev. Lett.*, 98:180601, Apr 2007.
- [233] Achim Rosch, David Rasch, Benedikt Binz, and Matthias Vojta. Metastable superfluidity of repulsive fermionic atoms in optical lattices. *Phys. Rev. Lett.*, 101:265301, Dec 2008.
- [234] Martin Eckstein and Philipp Werner. Thermalization of a pump-excited mott insulator. *Phys. Rev. B*, 84:035122, Jul 2011.
- [235] Rajdeep Sensarma, David Pekker, Ehud Altman, Eugene Demler, Niels Strohmaier, Daniel Greif, Robert Jördens, Leticia Tarruell, Henning Moritz, and Tilman Esslinger. Lifetime of double occupancies in the fermi-hubbard model. *Phys. Rev. B*, 82:224302, Dec 2010.
- [236] Niels Strohmaier, Daniel Greif, Robert Jördens, Leticia Tarruell, Henning Moritz, Tilman Esslinger, Rajdeep Sensarma, David Pekker, Ehud Altman, and Eugene Demler. Observation of elastic doublon decay in the fermi-hubbard model. *Phys. Rev. Lett.*, 104:080401, Feb 2010.
- [237] W. Morong, S. R. Muleady, I. Kimchi, W. Xu, R. M. Nandkishore, A. M. Rey, and B. DeMarco. Disorder-controlled relaxation in a three-dimensional hubbard model quantum simulator. *Phys. Rev. Research*, 3:L012009, Jan 2021.
- [238] Chen Ning Yang.  $\eta$  pairing and off-diagonal long-range order in a hubbard model. *Phys. Rev. Lett.*, 63:2144–2147, Nov 1989.
- [239] Jiajun Li and Martin Eckstein. Nonequilibrium steady-state theory of photodoped mott insulators, 2020.
- [240] Yuta Murakami, Shintaro Takayoshi, Tatsuya Kaneko, Zhiyuan Sun, Denis Golež, Andrew J. Millis, and Philipp Werner. Emergent nonequilibrium phases in the photo-doped one-dimensional mott insulator, 2021.
- [241] Tatsuya Kaneko, Tomonori Shirakawa, Sandro Sorella, and Seiji Yunoki. Photoinduced  $\eta$  pairing in the hubbard model. *Phys. Rev. Lett.*, 122:077002, Feb 2019.

- [242] Francesco Peronaci, Olivier Parcollet, and Marco Schiró. Enhancement of local pairing correlations in periodically driven mott insulators. *Phys. Rev. B*, 101:161101, Apr 2020.
- [243] J. Tindall, F. Schlawin, M. Buzzi, D. Nicoletti, J. R. Coulthard, H. Gao, A. Cavalleri, M. A. Sentef, and D. Jaksch. Dynamical order and superconductivity in a frustrated many-body system. *Phys. Rev. Lett.*, 125:137001, Sep 2020.
- [244] Philipp Werner, Naoto Tsuji, and Martin Eckstein. Nonthermal symmetry-broken states in the strongly interacting hubbard model. *Phys. Rev. B*, 86:205101, Nov 2012.
- [245] Martin Eckstein, Marcus Kollar, and Philipp Werner. Thermalization after an interaction quench in the hubbard model. *Phys. Rev. Lett.*, 103:056403, Jul 2009.
- [246] Götz S. Uhrig. Interaction quenches of fermi gases. *Phys. Rev. A*, 80:061602, Dec 2009.
- [247] Marco Schiró and Michele Fabrizio. Time-dependent mean field theory for quench dynamics in correlated electron systems. *Phys. Rev. Lett.*, 105:076401, Aug 2010.
- [248] Martin Eckstein, Marcus Kollar, and Philipp Werner. Interaction quench in the hubbard model: Relaxation of the spectral function and the optical conductivity. *Phys. Rev. B*, 81:115131, Mar 2010.
- [249] O. Gunnarsson, G. Rohringer, T. Schäfer, G. Sangiovanni, and A. Toschi. Breakdown of traditional many-body theories for correlated electrons. *Phys. Rev. Lett.*, 119:056402, Aug 2017.
- [250] T. Schäfer, G. Rohringer, O. Gunnarsson, S. Ciuchi, G. Sangiovanni, and A. Toschi. Divergent precursors of the mott-hubbard transition at the two-particle level. *Phys. Rev. Lett.*, 110:246405, Jun 2013.
- [251] Markus Greiner, Olaf Mandel, Theodor W. Hänsch, and Immanuel Bloch. Collapse and revival of the matter wave field of a bose-einstein condensate. *Nature*, 419(6902):51–54, 2002.
- [252] Sebastian Will, Thorsten Best, Ulrich Schneider, Lucia Hackermüller, Dirk-Sören Lühmann, and Immanuel Bloch. Time-resolved observation of coherent multi-body interactions in quantum phase revivals. *Nature*, 465(7295):197–201, 2010.
- [253] Marco Schiró and Michele Fabrizio. Quantum quenches in the hubbard model: Time-dependent mean-field theory and the role of quantum fluctuations. *Phys. Rev. B*, 83:165105, Apr 2011.
- [254] Matteo Sandri, Marco Schiró, and Michele Fabrizio. Linear ramps of interaction in the fermionic hubbard model. *Phys. Rev. B*, 86:075122, Aug 2012.
- [255] Felix Hofmann, Martin Eckstein, and Michael Potthoff. Nonequilibrium self-energy functional approach to the dynamical mott transition. *Phys. Rev. B*, 93:235104, Jun 2016.
- [256] Malte Behrmann, Michele Fabrizio, and Frank Lechermann. Extended dynamic mott transition in the two-band hubbard model out of equilibrium. *Phys. Rev. B*, 88:035116, Jul 2013.
- [257] Simone A. Hamerla and Götz S. Uhrig. Dynamical transition in interaction quenches of the one-dimensional hubbard model. *Phys. Rev. B*, 87:064304, Feb 2013.
- [258] Naoto Tsuji, Peter Baromettler, Hideo Aoki, and Philipp Werner. Nonequilibrium dynamical cluster theory. *Phys. Rev. B*, 90:075117, Aug 2014.
- [259] Bruno Sciolla and Giulio Biroli. Quantum quenches and off-equilibrium dynamical transition in the infinite-dimensional bose-hubbard model. *Phys. Rev. Lett.*, 105:220401, Nov 2010.
- [260] Hugo U. R. Strand, Martin Eckstein, and Philipp Werner. Nonequilibrium dynamical mean-field theory for bosonic lattice models. *Phys. Rev. X*, 5:011038, Mar 2015.
- [261] U. Brandt and C. Mielsch. Thermodynamics and correlation functions of the falicov-kimball model in large dimensions. *Zeitschrift für Physik B Condensed Matter*, 75(3):365–370, 1989.
- [262] J. K. Freericks and V. Zlatić. Exact dynamical mean-field theory of the falicov-kimball model. *Rev. Mod. Phys.*, 75:1333–1382, Oct 2003.
- [263] Martin Eckstein and Marcus Kollar. Nonthermal steady states after an interaction quench in the falicov-kimball model. *Phys. Rev. Lett.*, 100:120404, Mar 2008.
- [264] Martin Eckstein and Philipp Werner. Damping of bloch oscillations in the hubbard model. *Phys. Rev. Lett.*, 107:186406, Oct 2011.
- [265] H. Fotso, K. Mikelsons, and J. K. Freericks. Thermalization of field driven quantum systems. *Scientific Reports*, 4(1):4699, 2014.
- [266] V.P. Galaiko. Kinetic equations for relaxation processes in superconductors. *JETP*, 34:203, 1972. [Russian original - Zh. Eksp. Teor. Fiz. **61**, 382 (1971)].
- [267] X. Yang, C. Vaswani, C. Sundahl, M. Mootz, P. Gagel, L. Luo, J. H. Kang, P. P. Orth, I. E. Perakis, C. B. Eom, and J. Wang. Terahertz-light quantum tuning of a metastable emergent phase hidden by superconductivity. *Nature Materials*, 17:586–591, 2018.
- [268] X. Yang, C. Vaswani, C. Sundahl, M. Mootz, L. Luo, J. H. Kang, I. E. Perakis, C. B. Eom, and J. Wang. Lightwave-driven gapless superconductivity and forbidden quantum beats by terahertz symmetry breaking. *Nature Photonics*, 13:707–713, 2019.
- [269] Tianbai Cui, Xu Yang, Chirag Vaswani, Jigang Wang, Rafael M. Fernandes, and Peter P. Orth. Impact of damping on the superconducting gap dynamics induced by intense terahertz pulses. *Phys. Rev. B*, 100:054504, Aug 2019.
- [270] D. Fausti, R. I. Tobey, N. Dean, S. Kaiser, A. Dienst, M. C. Hoffmann, S. Pyon, T. Takayama, H. Takagi, and A. Cavalleri. Light-induced superconductivity in a stripe-ordered cuprate. *Science*, 331(6014):189–191, 2011.
- [271] W. Hu, S. Kaiser, D. Nicoletti, C. R. Hunt, I. Gierz, M. C. Hoffmann, M. Le Tacon, T. Loew, B. Keimer, and A. Cavalleri. Optically enhanced coherent transport in  $yba_2cu_3o_6.5$  by ultrafast redistribution of interlayer coupling. *Nature Materials*, 13:705–711, 2014.
- [272] M. Mitrano, A. Cantaluppi, D. Nicoletti, S. Kaiser, A. Perucchi, S. Lupi, P. Di Pietro, D. Pontiroli, M. Ricc'o, Clark S. R., D. Jaksch, and A. Cavalleri. Possible light-induced superconductivity in  $k_3c60$  at high temperature. *Nature*, 530:461–464, 2016.
- [273] Michael Knap, Mehrash Babadi, Gil Refael, Ivar Martin, and Eugene Demler. Dynamical cooper pairing in nonequilibrium electron-phonon systems. *Phys. Rev. B*, 94:214504, Dec 2016.
- [274] D. M. Kennes, E. Y. Wilner, D. R. Reichman, and A. J. Millis. Transient superconductivity from electronic squeezing of optically pumped phonons. *Nature Physics*,

- 13:479–483, 2017.
- [275] Giuliano Chiriacò, Andrew J. Millis, and Igor L. Aleiner. Transient superconductivity without superconductivity. *Phys. Rev. B*, 98:220510, Dec 2018.
- [276] Ryusuke Matsunaga, Naoto Tsuji, Hiroyuki Fujita, Arata Sugioka, Kazumasa Makise, Yoshinori Uzawa, Hirotaka Terai, Zhen Wang, Hideo Aoki, and Ryo Shimanono. Light-induced collective pseudospin precession resonating with Higgs mode in a superconductor. *Science*, 345(6201):1145–1149, 2014.
- [277] Naoto Tsuji and Hideo Aoki. Theory of anderson pseudospin resonance with higgs mode in superconductors. *Phys. Rev. B*, 92:064508, Aug 2015.
- [278] T. Cea, C. Castellani, and L. Benfatto. Nonlinear optical effects and third-harmonic generation in superconductors: Cooper pairs versus higgs mode contribution. *Phys. Rev. B*, 93:180507, May 2016.
- [279] N. Fläschner, D. Vogel, M. Tarnowski, B. S. Rem, D. S. Lühmann, M. Heyl, J. C. Budich, L. Mathey, K. Sengstock, and C. Weitenberg. Observation of dynamical vortices after quenches in a system with topology. *Nature Physics*, 14(3):265–268, 2018.
- [280] Renate Landig, Lorenz Hruby, Nishant Dogra, Manuele Landini, Rafael Mottl, Tobias Donner, and Tilman Esslinger. Quantum phases from competing short- and long-range interactions in an optical lattice. *Nature*, 532(7600):476–479, 2016.
- [281] M. Landini, N. Dogra, K. Kroeger, L. Hruby, T. Donner, and T. Esslinger. Formation of a spin texture in a quantum gas coupled to a cavity. *Phys. Rev. Lett.*, 120:223602, May 2018.
- [282] Ronen M. Kroese, Yudan Guo, Varun D. Vaidya, Jonathan Keeling, and Benjamin L. Lev. Spinor self-ordering of a quantum gas in a cavity. *Phys. Rev. Lett.*, 121:163601, Oct 2018.
- [283] Ronen M. Kroese, Yudan Guo, and Benjamin L. Lev. Dynamical spin-orbit coupling of a quantum gas. *Phys. Rev. Lett.*, 123:160404, Oct 2019.
- [284] Markus P. Baden, Kyle J. Arnold, Arne L. Grimsmo, Scott Parkins, and Murray D. Barrett. Realization of the dicke model using cavity-assisted raman transitions. *Phys. Rev. Lett.*, 113:020408, Jul 2014.
- [285] Kristian Baumann, Christine Guerlin, Ferdinand Brennecke, and Tilman Esslinger. Dicke quantum phase transition with a superfluid gas in an optical cavity. *Nature*, 464(7293):1301, Apr 2010.
- [286] Helmut Ritsch, Peter Domokos, Ferdinand Brennecke, and Tilman Esslinger. Cold atoms in cavity-generated dynamical optical potentials. *Rev. Mod. Phys.*, 85:553–601, Apr 2013.
- [287] Jens Klinder, Hans Keßler, Matthias Wolke, Ludwig Mathey, and Andreas Hemmerich. Dynamical phase transition in the open dicke model. *Proceedings of the National Academy of Sciences*, 112(11):3290–3295, 2015.
- [288] H-X Yang, T Tian, Y-B Yang, L-Y Qiu, H-Y Liang, A-J Chu, C B Da $\uparrow$  g, Y Xu, Y Liu, and L-M Duan. Observation of dynamical quantum phase transitions in a spinor condensate. *Phys. Rev. A*, 100(1):013622, 2019.
- [289] T. Tian, H.-X. Yang, L.-Y. Qiu, H.-Y. Liang, Y.-B. Yang, Y. Xu, and L.-M. Duan. Observation of dynamical quantum phase transitions with correspondence in an excited state phase diagram. *Phys. Rev. Lett.*, 124:043001, Jan 2020.
- [290] A M Rey, A V Gorshkov, C V Kraus, M J Martin, M Bishop, M D Swallows, X Zhang, C Benko, J Ye, N D Lemke, and A D Ludlow. Probing many-body interactions in an optical lattice clock. *Ann. Phys.*, 340(1):311, 2014.
- [291] J. N. Fuchs, D. M. Gangardt, and F. Laloë. Internal state conversion in ultracold gases. *Phys. Rev. Lett.*, 88:230404, May 2002.
- [292] Michael Albiez, Rudolf Gati, Jonas Fölling, Stefan Hunsmann, Matteo Cristiani, and Markus K. Oberthaler. Direct observation of tunneling and nonlinear self-trapping in a single bosonic Josephson junction. *Phys. Rev. Lett.*, 95:010402, 2005.
- [293] Th. Anker, M. Albiez, R. Gati, S. Hunsmann, B. Eiermann, A. Trombettoni, and M. K. Oberthaler. Nonlinear self-trapping of matter waves in periodic potentials. *Phys. Rev. Lett.*, 94:020403, 2005.
- [294] Aaron Reinhard, Jean-Félix Riou, Laura A. Zundel, David S. Weiss, Shuming Li, Ana Maria Rey, and Rafael Hipolito. Self-trapping in an array of coupled 1D Bose gases. *Phys. Rev. Lett.*, 110:033001, 2013.
- [295] S. Levy, E. Lahoud, I. Shomroni, and J. Steinhauer. The a.c. and d.c. Josephson effects in a bose-einstein condensate. *Nature*, 449:579, 2007.
- [296] M. Abbarchi, A. Amo, V. G. Sala, D. D. Solnyshkov, H. Flayac, L. Ferrier, I. Sagnes, E. Galopin, A. Lemaître, G. Malpuech, and J. Bloch. Macroscopic quantum self-trapping and Josephson oscillations of exciton polaritons. *Nat. Phys.*, 9:275, 2013.
- [297] Cheng Chin, Rudolf Grimm, Paul Julienne, and Eite Tiesinga. Feshbach resonances in ultracold gases. *Rev. Mod. Phys.*, 82:1225–1286, 2010.
- [298] C. Deutsch, F. Ramirez-Martinez, C. Lacroûte, F. Reinhard, T. Schneider, J. N. Fuchs, F. Piéchon, F. Laloë, J. Reichel, and P. Rosenbusch. Spin self-rephasing and very long coherence times in a trapped atomic ensemble. *Phys. Rev. Lett.*, 105:020401, 2010.
- [299] C Solaro, A Bonnin, F Combes, M Lopez, X Alauze, J N Fuchs, F Piéchon, and F Pereira Dos Santos. Competition between spin echo and spin self-rephasing in a trapped atom interferometer. *Phys. Rev. Lett.*, 117:163003, 2016.
- [300] F. Piéchon, J. N. Fuchs, and F. Laloë. Cumulative identical spin rotation effects in collisionless trapped atomic gases. *Phys. Rev. Lett.*, 102:215301, 2009.
- [301] Hannes Bernien, Sylvain Schwartz, Alexander Keesling, Harry Levine, Ahmed Omran, Hannes Pichler, Soonwon Choi, Alexander S Zibrov, Manuel Endres, Markus Greiner, et al. Probing many-body dynamics on a 51-atom quantum simulator. *Nature*, 551(7682):579–584, 2017.
- [302] Sepehr Ebadi, Tout T Wang, Harry Levine, Alexander Keesling, Giulia Semeghini, Ahmed Omran, Dov Bluvstein, Rhine Samajdar, Hannes Pichler, Wen Wei Ho, et al. Quantum phases of matter on a 256-atom programmable quantum simulator. *Nature*, 595(7866):227–232, 2021.
- [303] Maksym Serbyn, Dmitry A Abanin, and Zlatko Papić. Quantum many-body scars and weak breaking of ergodicity. *Nature Physics*, 17(6):675–685, 2021.
- [304] Thomas Kohlert, Sebastian Scherg, Pablo Sala, Frank Pollmann, Bharath Hebbe Madhusudhana, Immanuel Bloch, and Monika Aidelsburger. Experimental realization of fragmented models in tilted fermi-hubbard

- chains. *arXiv preprint arXiv:2106.15586*, 2021.
- [305] P. He, M. A. Perlin, S. R. Muleady, R. J. Lewis-Swan, R. B. Hutson, J. Ye, and A. M. Rey. Engineering spin squeezing in a 3d optical lattice with interacting spin-orbit-coupled fermions. *Phys. Rev. Research*, 1:033075, Nov 2019.
- [306] M. Foss-Feig, P. Niroula, J. T. Young, M. Hafezi, A. V. Gorshkov, R. M. Wilson, and M. F. Maghrebi. Emergent equilibrium in many-body optical bistability. *Phys. Rev. A*, 95:043826, Apr 2017.
- [307] R. J. Lewis-Swan, S. R. Muleady, D. Barberena, J. J. Bollinger, and A. M. Rey. Characterizing the dynamical phase diagram of the dicke model via classical and quantum probes. *Phys. Rev. Research*, 3:L022020, Jun 2021.
- [308] Christian Gross and Immanuel Bloch. Quantum simulations with ultracold atoms in optical lattices. *Science*, 357(6355):995–1001, 2017.